Coordinated regulation of glycolysis and the folate one-carbon cycle

by

Brian Prescott Fiske

A.B., Harvard College (2007)

Submitted to the Department of Biology
in Partial Fulfillment of the Requirements for the Degree of

Doctor of Philosophy

at the

MASSACHUSETTS INSTITUTE OF TECHNOLOGY

June 2015

Signature of Author ..... Signature redacted
Department of Biology
January 22, 2015

Certified by ..... Signature redacted
Matthew Vander Heiden
Associate Professor of Biology
Thesis Supervisor

Accepted by ..... Signature redacted
David Sabatini
Chairman, Professor of Biology

Coordinated regulation of glycolysis and the folate one-carbon cycle

by

Brian Prescott Fiske

Submitted to the Department of Biology on January 22, 2015
in Partial Fulfillment of the Requirements for the
Degree of Doctor of Philosophy in Biology

ABSTRACT

Rapid cell proliferation is characteristic of many biological systems, including cancer, normal development, and immune responses. At a basic level, proliferation requires that a cell synthesize a new copy of itself, with cell metabolism supplying the building blocks for new proteins, nucleic acids and lipids. Cancer and other proliferating cell types exhibit "aerobic glycolysis" characterized by elevated glucose uptake and conversion of glucose to lactate even in the presence of oxygen. Aerobic glycolysis is associated with anabolic reactions to generate new cellular material, but how aerobic glycolysis supports proliferative metabolism is not well understood. Pyruvate kinase (PK) catalyzes the last step in glycolysis, and while there is no evidence that PK activity is limiting for glycolysis, all proliferating cells express the PKM2 isoform of PK that is unique in having regulated activity which is decreased in the context of cellular proliferation. The simultaneous requirement for increased aerobic glycolysis and expression of the PKM2 isoform that is inhibited by growth signaling is a paradox, and it is unclear how elevated glucose metabolism enables rapid proliferation yet also requires decreased PKM2 activity. This thesis will explore two potential explanations for this paradox. The first hypothesizes the existence of an undiscovered enzyme that catalyzes a PK-like reaction, resolving the paradox by aligning increased flux through glycolysis with increased or unchanged activity of the PK step. The second hypothesis explores how PKM2 expression and PK inhibition supports proliferation by increasing serine synthesis from upstream glycolytic intermediates. This diverts one-carbon units into the folate pool to generate nucleotides via phosphoserine inhibition of SHMT1-mediated serine synthesis and one-carbon “wasting” in some cancer cells. We will also consider the reciprocal question of how folate one-carbon pool status in turn may regulate both PKM2 activity and glycolytic serine biosynthesis. The ability of PKM2 regulation to control folate metabolism for nucleotide synthesis explains for the first time at a mechanistic level one way that aerobic glycolysis promotes proliferative metabolism.

Thesis Supervisor: Matthew Vander Heiden
Title: Associate Professor of Biology

ACKNOWLEDGEMENTS

This thesis would not have been possible without the support of a number of people over the last 5½ years. I would like to start by thanking my advisor, Matt Vander Heiden, for his constant guidance and support, as well as for comments which greatly improved this thesis. Matt has taught me an enormous amount about science and the importance of having strong beliefs to drive work forward. I will very much miss working as a graduate student with him in lab.

My committee members David Sabatini, Barbara Imperiali, and Phillip Sharp were always well-prepared and had very helpful advice during and outside of committee meetings. Special thanks are also due to David Fisher for taking the time to serve as an outside member for the defense.

Thank you to my undergraduate students Alice Chen and especially my current student Mitali Kini for believing in our work and excelling under the sometimes difficult circumstances of science. Thank you also to current and former members of the Vander Heiden group for making lab an engaging and fun work environment: Will Israelsen, Katie Mattiani, Amelia (Yimin) Yu, Caroline Lewis, Dan Gui, Aaron Hosios, Shawn Davidson, Jared Mayers, Mark Sullivan, Ben Olenchock, Sophia Lunt, Anna Nguyen, Lucas Sullivan, Alba Luengo, Margaret Torrence, Andrea Howell, Vivan Liu, Kali Xu, Amy Liu, Natalie Vokes, Vinayak Murilander, Thasin Khan, and Zachary Johnson

Thank you also to outside collaborators for entrusting me with your work and assisting me with my own: Dohoon Kim, Natalia Drosu, Michael Pacold, Lisa Freinkman, Mark Keibler, Eric Bell, Talya Dayton, Jana Hersch, Christian Metallo, Byron DeLaBarre, Kelly Marsh, Jeff Simpson, Yoav Shaul, Luke Berchowitz, Daniel Dadon, Eric Wang, Elanor Cameron, Thales Papagiannakopoulos, Clary Clish, Scott Malstrom, Matt Demers, and Craig Thomas.

Thank you also to Professors David Housman, Paul Chang, and Frank Solomon. I could not have asked for a better source of sage advice right on my floor. I also frequently turned to my copy of *The Eighth Day of Creation* by Horace Judson as another source of wisdom.

Thank you to my amazing and supportive roommates Valerie Belinson, Adrian Randall, and Sophia Lunt. Thank you to members of the MIT Biology and CSBi entering classes of 2009, especially Vikram Agrawal and Chris Smilie. Thank you also to my friends Robert Rogers, Jonathan Loch, and Stephen Norberg for support.

Most importantly, thank you to my wife Anna Podgornaia for continuous love and support. Lastly, thank you to my parents Phil and Linda for providing me with the opportunity to be where I am today.

TABLE OF CONTENTS

Chapter 1 – Introduction

Authorship Statement

Some passages have been adapted or quoted verbatim from the following sources:
Preliminary Exam Proposal, Brian Fiske, 5/20/11
Thesis Committee Research Summaries and Presentations, Brian Fiske, 2010-2014
Poitras Fellowship Proposal, Brian Fiske, 4/21/14

The paradox of proliferative metabolism - increased glycolysis and reduced pyruvate kinase activity

Rapid cellular proliferation is characteristic of many biological systems, including cancer, normal development, and immune responses. At a basic level, proliferation requires that a cell synthesize a new copy of itself, with cell metabolism supplying the building blocks for new proteins, nucleic acids and lipids. Remarkable advances have been made in the past thirty years in our understanding of how cells "decide" to grow by integrating the status of multiple signaling pathways. However, only recently have biologists begun to explore the molecular basis of the metabolic changes that accompany rapid proliferation and enable cells to synthesize new cellular material.

The observation that cancer exhibits an altered metabolism is older than molecular biology. Over 90 years ago, Otto Warburg observed that cancer cells exhibit "aerobic glycolysis" characterized by elevated glucose uptake and conversion of glucose to lactate even in the presence of oxygen (Warburg, 1924). It is now clear that aerobic glycolysis is a phenomenon associated with proliferation of cancer cells, immune cells, and normal developing tissues (Fiske, 2012 and Macintyre, 2013). In addition, cancer cell proliferation in culture is sensitive to inhibitors of glucose uptake (Ralser, 2008) and the ability of therapies to decrease glucose

uptake in patient tumors is correlated with response (Ben-Haim, 2009). On a molar basis, glucose is the most-consumed metabolite of cancer cells in culture (Jain, 2012 and Figure 1). However, despite decades of study, how aerobic glycolysis supports proliferative metabolism is not well understood.

Pyruvate kinase (PK) catalyzes the last step in glycolysis, a phosphoryl transfer from PEP to ADP to form pyruvate and ATP. While there is no evidence that PK activity is limiting for glycolysis in cancer cells, all proliferating cells, including all cancer cells, express a specific isoform of PK, PKM2, which is subject to allosteric activity regulation by metabolites and pro-growth signals (Mazurek, 2011 and Gui, 2013). Expression of the constitutively active PKM isoform, PKM1, is associated with proliferative arrest in tumor models (Israelsen, 2013 and Anastasiou, 2012). Alternative splicing of the PKM2 isoform is controlled by expression of the splicing repressors PTB, hnRNPA1, and hnRNPA2 that bind to the PKM1-specific exon under transcriptional control of c-Myc (David, 2010 and Clower, 2010). Furthermore, PKM2 is inactivated when phosphotyrosine-containing proteins, generated by pro-growth signaling in mammalian cells, promote the release of Fructose 1,6-Bisphosphate (FBP) from its allosteric activating site on PKM2 (Christofk, 2008a). PKM2 differs from PKM1 in having a less stable subunit interface such that FBP-binding is required to stabilize the active tetrameric enzyme (Anastasiou, 2012 and Figure 2). Other signaling events such as acetylation can also disrupt formation of active PKM2 tetramers (Lv, 2011) illustrating that proliferating cells have several mechanisms to shut off PKM2, which via an unknown mechanism is necessary to support proliferation.

The simultaneous requirement for increased aerobic glycolysis and expression of the PKM2 pyruvate kinase isoform that is inhibited by growth signaling is a paradox, and it is unclear how elevated glucose metabolism enables rapid proliferation yet also requires decreased PKM2

activity. This thesis will explore two potential explanations for this paradox. The first hypothesizes the existence of an undiscovered enzyme that catalyzes a PK-like reaction, resolving the paradox by aligning increased flux through glycolysis with increased or unchanged activity of the PK step. Although we were unable to clone an alternative PK-like activity, its potential existence is unfalsifiable and by presenting our data we will define the space of potential future directions to clone such an activity. The second hypothesis explores how PKM2 expression and PK inhibition supports proliferation by increasing glycolytic serine synthesis and diverting folate one-carbon units to generate nucleotides in some cancer cells. We will also consider the reciprocal question of how folate one-carbon pool status in turn may regulate both PKM2 activity and glycolytic serine biosynthesis. The second mechanism proposed is the first to explain at a mechanistic level one way that aerobic glycolysis promotes proliferative metabolism.

History of glycolysis and aerobic glycolysis

In order to consider potential alternative PK activities it is important to consider how traditional biochemical methods discovered PK, and review early work in metabolic biochemistry to understand why such an activity might have remained unidentified. Canonical pyruvate kinase was discovered in 1934 (Parnas, 1934), enabled by the work of early biochemists who laid the foundations for our modern understanding of biochemistry (Figure 3). These foundations are:

- Live cells carry out and catalyze chemical reactions
- The reactants and products of those chemical reactions are the same as those that can be made synthetically
- Enzymes are the non-living components excreted by, or contained in, cells that are responsible for catalysis
- Enzymes are chemicals, specifically high molecular weight protein "macromolecules"

These advances in understanding biochemistry predate the elucidation of glycolysis (Figure 4), and surprisingly most enzymatic activities in glycolysis were discovered using knowledge of both chemically isolated and hypothetical metabolic intermediates involved in glucose fermentation, without separately purifying the enzymes involved (Florkin, 1972-83, Barnett, 2003, and Barnett, 2005). The only exception to this was the discovery of GAPDH and PGK, the enzymes that bracket the unstable 1,3-DPG. There, the discovery of 1,3-DPG as the intermediate between glyceraldehyde-3-phosphate to 3-phosphoglycerate (Negelein, 1939) necessitated the purification of GAPDH from yeast (Warburg, 1939).

When glycolytic enzymes from animal tissues were finally purified (Figure 5), the source tissue was usually a large, non-proliferating adult organ such as liver, muscle, or brain, making it plausible that a pathway specific to proliferating cells could still be undiscovered. In addition, from the early 1930s when biochemists began to understand that ATP could serve as an energy currency in the cell (Lipmann F, 1941 and Kalckar, 1941), up until the 1970s when Peter Mitchell's chemiosmotic hypothesis (Mitchell, 1961) gained broad acceptance, a major question in metabolism was how ATP was generated via metabolic pathways. This ATP-centric view of metabolism could have biased researchers against looking for an alternative glycolytic pathway that does not produce ATP. In fact, canonical PK was discovered by Jakub Parnas in 1934 as a phosphoenolpyruvate (PEP)-dependent activity that, together with Adenylate Kinase, which catalyzes conversion of AMP and ATP to two ADP, preserved AMP from degradation to ammonia and IMP by AMP deaminase (Parnas, 1934) (Figure 6).[1] It is therefore plausible that early metabolic biochemists, focused on an ATP-centric chemistry of metabolism, may have failed to isolate alternative PK enzymes associated with proliferative metabolism.

[1] Parnas' original discovery was of a phosphoglycerate-dependent activity, which we know now can be converted to PEP via PGAM and Enolase. PK was shown a year later (Lehmann, 1935) to be dependent on PEP as the substrate for the enzyme.

Otto Warburg described aerobic glycolysis in proliferating cancer tissue simultaneous with these discoveries related to the mechanism of glycolysis in yeast and non-proliferating tissues. Warburg and his later colleagues including Hans Krebs, Fritz Lipmann, and Peter Mitchell presided over a golden age of metabolic biochemistry from 1920-1970. However, soon after, as the majority of metabolic pathways became well defined and scientists began to understand the genetic basis of cancer, interest in cancer metabolism waned for several decades.

A resurgence of interest in cancer metabolism

Three reasons stand out for the resurgent interest in cancer metabolism. First, the ability to measure metabolism directly has grown exponentially with advances in mass spectrometry and NMR technology. Second, various cancer genome sequencing projects identified recurrent mutations (isocitrate dehydrogenase, Parsons, 2008) and copy number variations (phosphoglycerate dehydrogenase, Locasale, 2011 and Possemato, 2011) in metabolic genes, in addition to enzymes already known to be alternatively spliced (pyruvate kinase M2, Christofk, 2008b) or deleted (fumarate hydratase, Tomlinson, 2002). Lastly and most importantly, while we now understand much better than in 1970 how proliferation is dysregulated via altered signaling pathways and gene expression, there remain many unanswered questions as to how altered metabolism supports the biomass accumulation that defines cancer.

Mass-spectrometry based metabolomics provides new insight into metabolism

Mass-spectrometry based metabolomics is critical to many of the experiments presented in this thesis and so merits a brief overview. Any accurate metabolite measurement requires

consideration of three main steps: sample preparation, sample extraction, and metabolite measurement.

Samples can be prepared for steady-state metabolomics experiments that involve measurement of relative metabolite levels in a sample, or that involve absolute quantitation of metabolite levels. The latter requires knowing the sample volume and availability of a set of standards for each metabolite to be quantified to generate a standard curve. The absolute level of metabolites in the original samples can then be calculated. Samples can also be prepared for stable isotope tracing experiments, which measure both the levels of metabolites as well as allow estimation of flux through metabolic pathways. All stable isotope tracing experiments involve use of a suitable tracer. In cell culture, tracer can be added one of two ways. In one method, the media can be changed to fresh media with tracer, however, this can change steady state by substituting fresh media for conditioned media. Alternatively, the tracer can be introduced directly into conditioned media, which will disrupt steady state to a lesser extent but result in less than 100% isotopic enrichment of the nutrient being traced if unlabeled metabolites species already exist in the conditioned media. Analysis of isotope-labeled metabolites also requires correction for natural abundance of the isotope, particularly when ^{13}C is traced since this isotope of carbon is ~1% of the carbon present without tracer addition (Fernandez, 1996). Additionally, tracing of labels can either involve long term exposure to reach steady-state (>24h) and employ metabolic flux analysis (Zamboni, 2009), or short term assessment of labeling over time for kinetic tracing experiments (Yuan, 2008). Kinetic tracing has the advantage of directly measuring flux without additional assumptions, although it requires a timecourse of measurements and is only possible across slow steps in a given pathway. Fortunately, PK is one such slow step that is amenable to kinetic tracing as discussed in Chapter 4.

Once the biologic sample is prepared, metabolites must be extracted in a manner that quenches metabolism at a given moment in time. This step is critical as methods of cell lysis employed for analysis of relatively stable molecules such as nucleic acids and proteins disrupt many metabolic reactions that can alter the levels of metabolites in a sample post-lysis. Preparation also is necessary to clear the sample of debris that might otherwise clog the chromatography system. Gas chromatography (GC) is much more tolerant in this regard than liquid chromatography (LC) since non-volatile debris is adsorbed in the disposable liner without much increase in pressure or leakage into the column. Guard columns for LC also provide a second chance to remove debris but can easily overpressure the system. Free metabolites, for example in cell culture media, can be extracted with monophasic organic solvent systems (typically 80% methanol), although highly charged free metabolites such as phosphoryl esters in cellular samples are more efficiently extracted from cellular debris when one equivalent of chloroform is added to form a biphasic system. Acid can also be used to extract highly charged free metabolites more efficiently, although this may cause degradation of some metabolites in the sample.

Macromolecular polymers can also be extracted and hydrolysed to their constituent monomers. Proteins can be broken down to amino acids by acid hydrolysis and then extracting with monophasic organic solvent (usually 80% methanol). DNA/RNA can be extracted with phenol/chloroform, then hydrolysed with nucleases, and monophosphoryl nucleotides extracted with biphasic organic solvent (e.g. methanol/chloroform). Following extraction, samples are best preserved by drying immediately under N_2 and storing at -80°C. Lastly, preparing metabolite samples for GC involves derivitization with alkyl groups before loading onto the column in order to lower the boiling point below about 300°C. A common derivitization involves adding tert-butyl dimethyl silyl (TBDMS) groups to polar hydroxyl, amine, and thiol functional groups, which normally mediate strong ionic and dipole interactions between molecules.

Sample measurement involves the sequential chromatographic separation of compounds, followed by ionization, and then measurement of the ion's mass-to-charge (m/z) ratio in a mass analyzer. For most small metabolites, the charge (z) is usually -1 or +1 and therefore m/z is equal to the mass (m) of the ion. Each instrument differs in how it achieves each of the three steps. As examples, I will briefly detail the specific instruments that were used in this thesis.

Chromatographic separation can be achieved in either liquid or gas phase. For GC, the sample is first vaporized in the injector and introduced into the column. The column then separates the derivatized metabolites by boiling point inside an oven that increases with temperature with time. The separation is achieved as individual derivatized metabolites dynamically partition between condensing on a solid stationary phase and boiling off into a mobile gas phase. Helium is commonly used as the mobile phase for GC including in the experiments reported here. Post-column, the separated derivatized metabolites are ionized while in the gas phase, in our case using electron ionization, which generates positively charged (+1) ions and fragments of those ions. In the GC-MS experiments described here, intact and fragmented ions are fed into a single-quadrupole mass analyzer with unit mass resolution. A quadrupole is a mass filter that only allows a given range of m/z at any given time. A particle detector then counts particles over time as the quadrupole scans over the mass range, in our case only with unit mass resolution, to generate the mass spectrum at any given time. The many mass spectra (in our case sampled at 4Hz) obtained during the chromatographic run then form a two-dimensional spectrum along the dimensions of time and m/z, which after reference to known standard compounds is sufficient for compound identification and quantification. Occasionally, when used for stable isotope tracing, a given metabolite has multiple known fragments representing the labeling at different individual atoms and the % labeling as well as the abundance of isotopomers of equal mass can be calculated.

In the case of LC, both small molecule chromatography and mass analyzers have made great strides in recent years. Improvements in chromatography have allowed for separation of polar metabolites without the use of ion pairing reagents in reverse phase (i.e. load with an ion-pairing molecule in polar solvent, elute in gradient to non-polar solvent). While ion-pairing reverse phase chromatography can be useful for separation of polar compounds using C18 and C8 reverse-phase columns, these ion pairing reagents, such as tributylammonium acetate, tend to clog the ion source. They can also suppress ionization of sample ions and reduce sensitivity if their resultant ions are not filtered out of the mass spectra, such as when using an orbitrap detector in "full scan" mode. Using hydrophilic interaction (HILIC) or amino (NH_2) columns in normal phase (i.e. load in non-polar solvent, elute in gradient to polar solvent) occasionally gives broader peaks than ion-pairing reverse phase but eliminates a need for ion pairing reagents in order to separate polar compounds. However, these silica-based columns are run at high pH, conditions where the silica tends to dissolve and 90% of the collected spectra is related to this column bleed when these masses are not filtered out. In our experience, therefore, the ideal chromatography solution for metabolomics of polar metabolites, especially when using an orbitrap in "full scan" mode, is normal phase at high pH on a PEEK-based HILIC column ("pHILIC"). The pHILIC provides the benefits of no ion pairing and low column bleed at high pH, although the gradients tend to be long (~1hr).

After LC-based chromatography, the liquid effluent is fed into the ion source, usually based on electrospray ionization (ESI), which vaporizes the solvent and ionizes the separated metabolites. In our work, the ions are then fed into either a triple-quadrupole (QQQ) mass analyzer similar to the GC-MS single-quadrupole, or a Thermo QExactive, which consists at its core of an orbitrap mass analyzer behind a single quadrupole. The orbitrap is a spindle-shaped ion trap that measures the linear oscillation parallel to the spindle of packets of injected ions

over time. Each ion's oscillation frequency is related to its m/z ratio, and by Fourier transforming the time-domain oscillations, a m/z spectrum is obtained. The major advantages of an orbitrap over a quadrupole-only instrument are twofold: it measures ions of all m/z ratios simultaneously without reconfiguring the instrument, and its high resolution allows three- to four-decimal exact mass determination. Exact mass resolution is useful in distinguishing compounds with different empirical formulas but the same unit mass, such as Lysine ($C_6H_{14}N_2O_2$, 146.1882 g/mol) and Glutamine ($C_5H_{10}N_2O_3$, 146.1451 g/mol). It is also useful in stable isotope tracing, as different isotopomers of the same compound can have different exact masses, such as ^{13}C (1.00335 g/mol heavier than ^{12}C), ^{15}N (0.99703 g/mole heavier than ^{14}N), and ^{2}H (1.00628 g/mol heavier than ^{1}H). Exact mass resolution also enables untargeted metabolomics, which allows for unbiased identification of altered metabolites across samples. Untargeted metabolomics played a role in the discovery of 2-HG as an "oncometabolite" (Dang, 2009), and enabled portions of this thesis as well.

There are other types of mass analyzers and ion sources that can be used for metabolomics, such as time of flight (TOF) mass analyzers, fourier transform ion cyclotron resonance (FT-ICR) mass analyzers, chemical ionization (CI) sources, and atmospheric pressure chemical ionization (APCI) sources, which each have their own advantages but are not covered here. Metabolomics can also be performed with NMR (Kim, 2011), although this will not be covered here either, as this technology did not enable the work presented in this thesis.

The role of metabolic enzymes in cancer

Two genes associated with altered metabolism in cancer, one discovered through the cancer genome project, Isocitrate Dehydrogenase (IDH), and another discovered in a rare familial cancer, Fumarate Hydratase (FH), have provided insight into how altered metabolism can

impact cancer. IDH mutations in cancer were discovered in 2008 from a glioblastoma exome sequencing study (Parsons, 2008), with gain of function mutations now also associated with AML (Mardis, 2009) and other cancers (Cairns, 2013). FH is a tumor suppressor discovered in 2002 as the causative gene deleted in familial multiple leiomyomatosis, which also predisposes for renal cell carcinoma (Tomlinson, 2002). Interestingly, in both cases a metabolite, R-2-hydroxyglutarate (R-2HG) for IDH mutant cancers, and fumarate as well as succinate for FH null cancers, accumulates to extremely high levels in the tumor (Dang, 2009 and Pollard, 2005). And in both cases, a plausible explanation for how these metabolites promote cancer involves high steady-state levels of these "oncometabolites" having effects on other proteins and pathways involved in signaling or epigenetics.

IDH is a TCA cycle enzyme that catalyzes the decarboxylation/oxidation of isocitrate to alpha-ketoglutarate (aKG). Mutations in IDH are now known to occur in over 80% of secondary grade II/III gliomas, as well as around 20% of normal karyotype AMLs. While IDH mutations were initially thought to be loss-of-function (Zhao, 2009), it was later shown that almost all functional mutations in both the mitochondrial (IDH2) and cytosolic (IDH1) $NADP^+$-dependent IDHs cause enzymatic gain of function for reduction of alpha-ketoglutarate to R-2-HG (Dang, 2009). R-2-HG accumulates to very high levels in tumors as it does not occur naturally except as an error product of metabolism and therefore has a small capacity to be broken down in cells. Importantly, exogenously added cell-permeable R-2-HG can recapitulate the biology of IDH mutations in several systems (Lu, 2012 and Losman, 2013a), further suggesting that high levels of R-2-HG up to 30mM are necessary and sufficient for the cancer-promoting mechanism of IDH mutations. Several mechanisms have been proposed for how 2HG promotes tumorigenesis, but the most advanced hypotheses all involve antagonism of enzymes that require aKG, such as the TET2 5-methylcytosine hydroxylase, JmjC histone demethylases, and EglN prolyl

hydroxylases (Losman 2013b). Lastly, IDH inhibitors have recently shown promise in Phase I trials for treatment of IDH-mutant leukemia (Stein, 2014).

Fumarate hydratase, which catalyzes the hydration of fumarate to malate, is another TCA cycle enzyme altered in cancer metabolism. FH was originally identified as a tumor suppressor in familial multiple leiomyomatosis, which predisposes for renal cell cancer (RCC). One defining hallmark of these rare FH null RCC tumors is that they overexpress the HIF family oncogenes, a property in common with other forms of RCC, such as tumors with VHL mutations, normally present in 50% or more of RCC (Cowey, 2009, Linehan, 2010, and Issacs, 2005). It is thought that increased fumarate and succinate in FH null tumors stabilizes HIF by inhibiting prolyl hydroxylases that normally promote HIF degradation (Pollard, 2005). An alternative hypothesis states that fumarate causes accumulation of NRF2, an oncogenic transcription factor, via succination of KEAP1, which promotes NRF2 degradation. In the end, both mechanisms as well as the proposed IDH mechanism contend that genetic changes drive an "oncometabolite" to high steady state levels, which then affects the function of other proteins not directly related to metabolism. While these findings define how metabolism might be a driver of malignancy, they fail to address how metabolism is rewired in cancer cells to support increased flux to biomass.

The search for an alternative PK-like activity

As noted earlier, glucose is the major nutrient consumed by cancer cells yet the pyruvate kinase step of glycolysis is inhibited by growth signaling and spliced to a less active form, PKM2, across many cancers. One explanation could be the existence of an "alternative" pyruvate kinase, expressed in proliferating cells and supportive of biomass accumulation by converting PEP to pyruvate via enzyme(s) that differ from canonical PK. This hypothesis is plausible

considering that the ATP-centric view of metabolism that dominated when glycolytic enzymes were purified from non-proliferating organs in the 1930s may have prevented the discovery of an alternative non-ATP-producing PK selected for in proliferating cells.

This "alternative" PK hypothesis motivated the discovery of a PEP-dependent PGAM1 histidine kinase activity, which could be involved in an alternative pathway to PK (Vander Heiden, 2010). Cancer cell lines contain an activity that transfers the phosphoryl group of phosphoenolpyruvate (PEP) to the catalytic histidine, His11, of Phosphoglycerate Mutase 1 (PGAM1), and this activity is further associated with the conversion of PEP to pyruvate (Figure 7). This PEP-dependent PGAM1 histidine kinase activity could be important in enabling the proliferative metabolism of cancer in two distinct ways. First, as only His11 phosphorylated PGAM1 (P-PGAM1) is active (Rose, 1976), the activity could serve to activate PGAM1. Phenotypically, PGAM1 is ten to one-hundred times more phosphorylated in PKM2-expressing cancer cells and tumors than in PKM1-expressing cells and normal tissue (Vander Heiden, 2010). Additionally, computational modeling (M Vander Heiden, Unpublished) predicts that a PEP-dependent activation of PGAM1 would lead to accumulation of 3-Phosphoglycerate (3-PG), an important precursor for amino acid and nucleotide biosynthesis (Snell, 1990). Second, if the PEP-dependent PGAM1 kinase activity results in the conversion of PEP to pyruvate without the production of ATP, this could allow cancer cells to simultaneously consume large amounts of glucose while producing less ATP during the PK step of glycolysis. Production of too much ATP has been hard to reconcile with the high rates of glycolysis in cancer cells, and the recent discovery that an ATP-to-AMP converting activity is upregulated in PTEN-/- cells suggests that it may be advantageous for cancer cells to lower ATP levels in vivo (Fang, 2010). A non-ATP producing PK activity would prevent ATP-mediated inhibition of upstream glycolysis (Gevers, 1966). In addition, by activating PGAM1, a PEP-dependent PGAM1 kinase activity might also represent an important metabolic regulatory node in proliferating cells.

While evidence for a PEP-dependent PGAM1 histidine kinase activity is recent, aspects of PGAM and PEP-dependent histidine kinase biology have been studied for decades. PGAMs are biochemically divided into two classes based on their dependence on 2,3-DPG as a cofactor for mutase activity. Humans have two 2,3-DPG dependent PGAMs: the ubiquitously expressed PGAM1, and a muscle-specific PGAM2 (Sakoda, 1988). PGAM1 and PGAM2 assemble into homodimers in most tissues, but can form heterodimers in muscle cells that express both isoforms (Sakoda, 1988). The mechanism of the 2,3-DPG dependent PGAMs involves substrate phosphorylation of 2-Phosphoglycerate (2-PG) or 3-PG by the phosphohistidine residue (H11 in the case of human PGAM1) on P-PGAM to form 2,3-DPG, which then donates a phosphoryl group back to the same histidine residue to form 3-PG or 2-PG and regenerate the active P-PGAM (Rose, 1976). 2,3-DPG is required not as a true cofactor, but rather to provide the initial phosphoryl group to "prime" the catalytic histidine residue. The two other human PGAM family members, PGAM4 and PGAM5, may have important cellular functions but are unlikely to contribute significantly to total phosphoglycerate mutase activity. PGAM4 is an intronless gene recently evolved in primates that was likely derived from a retroduplication event of PGAM1 (Betran, 2002). While PGAM4 shows low but detectable expression in lymphocytes, its catalytic properties or function remain obscure (Betran, 2002). PGAM5 is localized to the mitochondria, where it interacts with BCL-X_L and exhibits serine/threonine phosphatase activity towards the ASK1 MAP-kinase; however, it does not have phosphoglycerate mutase activity (Takeda, 2009). Given the nonexistent catalytic activity of PGAM5 and the low and/or tissue-specific expression patterns of PGAM4 and PGAM2, it is likely that PGAM1 provides the majority of the phosphoglycerate mutase activity in non-muscle cells.

While a PGAM-phosphorylating activity would be the first known PEP-dependent histidine kinase activity in animals, PEP-dependent histidine kinases play essential metabolic roles in

both bacteria and plants. Instead of using ATP as a phosphoryl donor for glucose phosphorylation after import, as in humans, the phosphotransferase system (PTS) in bacteria utilizes PEP as a phosphoryl donor to couple sugar transport with phosphorylation. In the first step of the PTS pathway, Enzyme I (PTS-EI) autophosphorylates on a histidine residue using PEP as the phosphoryl donor. This phosphoryl group then shuttles along a sequence of histidine residues on proteins Hpr and then Enzyme II, which spans the membrane and transfers the phosphoryl to sugar after it has been transported into the cytoplasm (Deutscher, 2006). Other examples of PEP-dependent histidine phosphorylation include PEP synthetase in bacteria and pyruvate phosphate dikinase (PPDK) in C_4 plants. Both PEP synthetase and PPDK couple the conversion of ATP to AMP and pyruvate to PEP, and in both cases the reverse reaction involves a PEP-dependent histidine phosphorylation (Wang, 1988 and Narindrasorasak, 1977).

The utilization of PEP as a substrate for protein kinases in bacteria and plants, combined with the original paradox of low PK activity in proliferative cells motivated the search for a PEP-dependent kinase activity in proliferating cells using [^{32}P]PEP labeling of the kinase target (Vander Heiden, 2010). Following biochemical purification and identification by peptide mass spectrometry of the major band observed upon [^{32}P]PEP incubation with cell lysate as [^{32}P]His11 PGAM1, the authors fractionated lysate tracking the activity responsible for the PGAM1 phosphorylation on a DEAE cellulose (D) column and locate it in the D150-500 fraction. Western blotting and activity assays suggested that this D fraction does not contain enolase or ATP-dependent pyruvate kinase, the only two glycolytic enzymes known to act on PEP in mammalian cells (Figure 7). It was also suggested that the D150-500 fraction contains an ATP-independent PK activity, as shown by ^{1}H-^{13}C HSQC NMR detection of [2,3-^{13}C]pyruvate upon incubation of [2,3-^{13}C]PEP with the D150-500 fraction. Lastly, metabolite mass spectrometry on cells engineered to express either PKM1 or PKM2 showed dramatic (~30-fold) elevation of 2,3-

DPG and 2-fold elevation of PEP in PKM2-expressing cells and little change in PKM1-expressing cells upon stimulation with pervanadate, a pan-phosphatase inhibitor which causes an increase in phosphotyrosine peptides that results in inhibition of PKM2 but not PKM1 (Christofk, 2008a). Combined with the observation that PKM2-expressing cells and Brca-/- murine breast tumor samples show elevated levels of phospho-PGAM1 versus PKM1-expressing cells and normal murine breast tissue, respectively, the authors' work correlates cancer with the molecular phenotypes of elevated PGAM1-phosphorylating activity, elevated P-PGAM1, and elevated PEP and 2,3-DPG levels in vivo.

In chapter two of this thesis, I will demonstrate via biochemical fractionation that the majority of the PEP-dependent PGAM1 phosphoryl transfer activity found in proliferating cell lysates can be accounted for by reverse glycolysis (Figure 8). Enolase and 2,3-DPG are necessary and sufficient components in the D150-500 fraction that mediate [^{32}P]PEP phosphoryltransfer to PGAM1. A related activity that originally appeared to be an ATP-independent PK activity using an NADH-oxidation-linked assay for pyruvate is also accounted for by reverse glycolysis. This time, the necessary and sufficient components are enolase, PGAM, PGK, and GAPDH, which utilize contaminating ATP in commercially available NADH, resulting in NADH oxidation via GAPDH. However, the hypothesis that an alternative PK exists in proliferating cells is unfalsifiable, and I will conclude by summarizing the prospects and next steps for finding such an enzymatic system as well as some related outstanding questions about the lower part of glycolysis. The same methods developed for this work were used to show that PKM2 is likely not a protein kinase (Hosios, 2015). This work appears as an appendix at the end of this thesis.

A new direction, starting with canonical PK

Despite all the reasons to search for an alternative pyruvate kinase, solid evidence for its existence proved elusive. We therefore sought a new approach to solve the paradox of low PK activity in cancer. We began by asking two fundamental questions. What is known about the role of PK activity regulation in cancer? And, what changes in metabolism are controlled by modulation of PK activity? With these questions as a starting point, we were able to explain for the first time how PK inhibition enables high glycolytic flux to support biomass accumulation.

Regulation of canonical PK activity in cancer

Two pyruvate kinase genes exist in mammals, PKLR and PKM. PKLR is alternatively spliced to PKL in the liver by exclusion of exon 1 and PKR in erythrocytes by inclusion of exon 1. PKLR expression is restricted to the liver, kidney and red blood cells and has not been found in tumors (Israelsen, 2013 and Imamura, 1972). In contrast, PKM is widely expressed throughout the body and in tumors. The PKM message is alternatively spliced to select mutually exclusive exons that produce either PKM1 in tissues such as muscle and brain, or PKM2 in tissues such as kidney, lung, white fat, the choroid plexus, and the early embryo (Talya Dayton, unpublished). PKM2 is ubiquitously expressed in proliferating tumors and tissues, including all tumors and cell lines (Israelsen, 2013 and Mazurek, 2011). Splicing repressors (PTB, hnRNPA1 and hnRNPA2) under control of c-myc bind to the PKM1-specific exon (David, 2010 and Clower, 2010), providing a mechanistic explanation for PKM2 isoform selection in proliferating tissues.

PK is a homotetrameric enzyme, and is only active as a tetramer (Mazurek, 2011). PKM1 and PKM2 differ by only 22 of 531 amino acids, and these amino acids form the dimer-dimer interface of the PK tetramer (Figure 2). This small difference allows PKM1 to assemble as a stable tetramer, whereas binding of several metabolites, including FBP, SAICAR, and serine

help stabilize PKM2 as an active tetramer (Christofk, 2008a, Keller, 2012, Eigenbrodt, 1983). FBP binding is particularly essential for PKM2 tetramerization and activity (Anastasiou et al, 2012), but can be removed from its binding site by phosphotyrosine peptides (Christofk, 2008a). In addition, PKM2 but not PKM1 activity is downregulated by oxidative stress (Anastasiou, 2011), lysine acetylation (Lv, 2011), and tyrosine phosphorylation (Hitosugi, 2009). In addition, the regulatory properties of PKM2 are ancestral to many bacteria and yeast, while the constitutively high activity of PKM1 is a newly evolved function in multicellular animals, consistent with a hypothesis that PKM1 evolved to control proliferation in differentiated tissues. Expression of PKM2 in tumors enables reversible downregulation of PK activity versus the constitutively high activity of PKM1.

What is the adaptive significance of PKM2 expression and reversible downregulation in tumors? Given the complex allosteric regulation of PKM2, it is not surprising that knockdown experiments of PKM2 in xenograft tumors (Cortes-Cros, 2013 and Goldberg, 2012) have yielded variable results. Loss of the PKM2-specific exon in a mouse model of breast cancer accelerates tumor progression, and some human cancers show decreased PKM2 expression or genetic inactivation of PKM2 (Israelsen, 2013). However, one consistent result has been that PKM1 expression suppresses the growth of tumor cells in several systems: xenografts, primary MEFs, and tissue culture cells under hypoxia (Christofk, 2008b; Israelsen, 2013; Lunt, 2014). In addition, small molecule activators of PKM2 that stabilize PKM2 into a PKM1-like constitutive tetramer are also tumor suppressive under the same conditions (Anastasiou, 2012). Most surprisingly, growth suppression in PKM1 expressing primary, but not transformed, MEFs can be rescued by adding thymidine to the media (Lunt, 2014). However, it remains unclear why downregulation of pyruvate kinase activity under these conditions is necessary for proliferation, or why thymidine rescues the ability of high PK activity to suppress proliferation.

Changes in metabolism caused by modulation of PK activity

One answer to why constitutively high PK activity suppresses proliferation may lie in understanding the metabolomic changes that occur upon PK activation and PKM1 expression. PKM1 expression or administration of PKM2 activators causes a 20-30% decrease in lactate production in standard cell culture (Christofk, 2008b and Kung, 2012). PKM2 activators have also been shown to decrease glycolytic serine biosynthesis by 60% in cell culture at the in vitro EC50 for PKM2 (Kung, 2012), and PKM1 expression decreases new serine production from glucose (Anastasiou et al, 2012, Lunt et al., 2014). The resulting decrease in serine biosynthesis is severe enough to make some cell lines auxotrophic for serine when treated with PKM2 activators. It is worth noting that while several studies suggest that this change in serine synthesis is due to "backing up" of glycolytic intermediates (Ye, 2012), evidence for decreased glycolytic intermediate upstream of PEP upon PKM1 expression or PKM2 activation is lacking (Lunt et al, 2014). In addition, decreased glycolytic serine biosynthesis caused by increased and constitutive PK activity is especially interesting given other recent discoveries about the importance of this branch-point in glycolysis.

Glycolytic serine biosynthesis

As mentioned above, interest in cancer metabolism was rekindled in no small part due to the discovery of genetic changes in metabolic genes uncovered by the cancer genome atlas. Besides IDH mutations, it was also discovered that 70% of ER-negative breast cancers and melanomas amplified a region of the genome containing phosphoglycerate dehydrogenase (PHGDH), the first step of glycolytic serine biosynthesis (Figure 9) (Locasale, 2011 and Possemato, 2011). These PHGDH-amplified tumors and cell lines are dependent on PHGDH expression and also exhibit increased glycolytic serine synthesis. However, modulation of

PHGDH expression in either direction does not influence serine levels in cell culture (Possemato, 2011), and at most glycolytic serine biosynthesis contributes 30-40% of total serine. In addition, serine is unable to rescue PHGDH knockdown (Possemato, 2011 and Locasale, 2011), suggesting that glycolytic serine biosynthesis is important for proliferative metabolism but confers an advantage beyond the production of serine

PHGDH catalyzes the oxidation of 3-PG to phosphohydroxypyruvate (PHP), a highly unstable intermediate which is transaminated by phosphoserine aminotransferase (PSAT) using glutamate as an amino donor to produce phosphoserine. Phosphoserine is then converted to serine by phosphoserine phosphatase (PSPH), which removes the phosphoryl group via an unusual mechanism which involves a phosphoenzyme intermediate instead of direct hydrolysis of the substrate phosphoryl group. PSPH-bound phosphoserine first donates its phosphoryl group to PSPH, forming a phosphoenzyme intermediate and bound serine. Next, serine leaves the active site and is replaced by water, which cleaves the phosphoenzyme intermediate and releases free phosphate, regenerating the enzyme (Collet, 1999 and Neuhaus, 1959a, 1959b, 1960). This unique mechanism has three important consequences. First, because the phosphoryl transfer from phosphoserine to PSPH is reversible, serine can inhibit PSPH forward flux not only by product inhibition, but also by binding to the phosphoenzyme intermediate and re-forming phosphoserine. For the same reason, isotopically labeled serine can easily bind to the reversible phosphoenzyme intermediate to create isotopically labeled phosphoserine. This impairs the ability to isotopically trace whether glycolytically synthesized serine is channeled to a different metabolic fate than exogenous serine because pool mixing across what is a net irreversible step. Lastly, unlike many metabolic pathways which are inhibited by their products at the first committed step, PHGDH in animals is not inhibited by serine. This is not true for PHGDH from several other organisms (Fell, 1988). The glycolytic serine biosynthesis pathway in animals is therefore relatively unique in being product-regulated at its last step, meaning all

the pathway intermediates will accumulate when serine is abundant and glycolytic serine synthesis is favored.

The unusual regulatory properties of the glycolytic serine biosynthesis pathway combined with the seeming paradox that serine biosynthesis is important for proliferation but not to simply produce serine itself led us to investigate the biological rationale behind this regulation and consider alternative benefits of glycolytic serine biosynthesis for proliferating cells. Four possibilities exist:

1. PHGDH, PSAT, or PSPH has an alternative function that is distinct from their known enzymatic activities
2. Flux through the glycolytic serine biosynthesis pathway is important for proliferation to convert NAD(P)+ to NAD(P)H and/or glutamate to aKG, with flux from 3-PG to serine facilitating these reactions (Figure 9)
3. Glycolytically synthesized serine is channeled to a different metabolic fate than exogenous serine
4. Steady state levels of one or more pathway intermediates is important for supporting proliferative metabolism

The first explanation is unattractive because catalytically dead PHGDH does not rescue PHGDH knockdown (Mattaini, 2015). The second is a plausible explanation, although at least in cell culture, we find glycolytic serine transamination to be a small percentage of total glutamate transamination, even in PHGDH-dependent cells. The third is not readily testable in vivo with isotopic tracing due to the unique mechanism of PSPH as discussed. However, this isotope exchange potentially opens up an opportunity to find previously characterized serine-dependent reactions including some where phosphoserine might be a substrate, as isotopically

labeled serine can exchange with phosphoserine. For any serine-dependent enzyme cloned from mammalian cells, phosphoserine could be the preferred substrate since isotopic equilibration across PSPH would make use of serine or phosphoserine indistinguishable as substrates in vivo. This possibility motivated us to test phosphoserine as a substrate for serine-dependent enzymes, including SHMT1, which provides the specific folate necessary for de novo thymidine synthesis. Contrary to our initial hypothesis, we find that phosphoserine is instead an inhibitor of the serine-dependent SHMT1 reaction. Interestingly, preliminary results suggest that this property is not found in SHMT2, the mitochondrial enzyme that catalyzes the identical reaction. To explore why SHMT1 inhibition might be important to proliferative metabolism, we examine the directionality and compartmentalization of folate one-carbon metabolism. In this thesis, we show that phosphoserine inhibition of SHMT1 supports proliferative metabolism via diversion of one-carbon folate pool flux towards de novo nucleotide biosynthesis, and this explains both why high PK activity is tumor suppressive as well as why glycolytic serine biosynthesis is critical independent of a need for additional serine.

Directionality, compartmentalization, and the role of phosphoserine in regulating folate one-carbon metabolism

The directionality and compartmentalization of one-carbon metabolism explains how phosphoserine inhibition of SHMT1 could support proliferation by modulating flux through the compartmentalized one-carbon folate pathways in cells (Figure 10). Folates are a series of related compounds that carry both redox equivalents and one-carbon units. Folates consist of a modified pteridine group linked to para-amino benzoic acid and a glutamic acid, which can then be polyglutamated on the gamma carboxyl group (Figure 11). Polyglutamylation promotes intracellular accumulation of folates and modulates binding to folate-dependent enzymes (Shane, 2010). Folate is transported in the blood as 5-methyl-tetrahydrofolate (5-methyl-THF),

although folic acid can also be found in vivo after high doses of the vitamin (National Academy of Sciences, 1998 and Bailey, 2010). Folic acid is the vitamin supplemented in the diet because it is more stable. The one-carbon pool can be charged by histidine breakdown as well as exogenous formate, but is physiologically buffered primarily by serine/glycine metabolism, which can interconvert in the cell via serine hydroxymethyltransferase (SHMT), and methionine/homocysteine, which can interconvert in the cell via methionine synthase. Once charged, the one-carbon units on various folate species are used to synthesize the nucleosides adenosine, guanosine, and thymidine (Figure 12), and are interconvertible with the other one-carbon pool in cells including the methionine cycle involved in methylation reactions (Stover, 2010). Many successful cancer chemotherapies have targeted folates and one-carbon metabolism using folate and nucleic acid antimetabolites (Zhao, 2003), with activity attributed to impaired nucleotide synthesis (Vander Heiden, 2011).

Folate species are not able to cross the mitochondrial inner membrane in appreciable quantities to directly transfer one-carbon units (Tibbetts, 2010). Serine is transported across mitochondrial membranes and by interconversion with glycine can serve to move one-carbon units between these intracellular compartments. The direction of serine-glycine interconversion, as well as the oxidation/reduction reactions that interconvert folate species may have different directionality in the mitochondria and cytosol (Figure 13). More specifically, both the cytosolic (SHMT1) and mitochondrial (SHMT2) forms of SHMT can interconvert serine and tetrahydrofolate (THF) to glycine and 5,10-methylenetetrahydrofolate (5,10-methylene-THF). In addition, both cytosolic (MTHFD1) and mitochondrial (MTHFD2, MTHFD1L, MTHFD2L) isoforms exist for interconverting 5,10-methylene-THF and NAD(P)+ to NAD(P)H and 5,10-methenyl-THF. MTHFD1 is a trifunctional NADP+-dependent enzyme that also includes a 5,10-methenyl-THF cyclohydrolase activity, which interconverts 5,10-methenyl-THF and water to 10-formyltetrahydrofolate (10-formyl-THF) as well as a 10-formyl-THF synthetase activity, which

interconverts 10-formyl-THF, ADP, and phosphate with formate, ATP, and THF. MTHFD2 and MTHFD2L are bifunctional NAD+-dependent enzymes with 5,10-methenyl-THF cyclohydrolase activity. MTHFD1L is a monofunctional 10-formyl-THF synthetase. Lastly, the 10-formyl-THF dehydrogenases ALDH1L2 (mitochondrial) and ALDH1L1 (cytosolic) may also release formate from 10-formyl-THF by direct hydrolysis (Tibbetts, 2010). Formate is transported across mitochondrial membranes. Thus, considering activities in both compartments, this metabolic pathway simplifies as the breakdown of serine to glycine and 5,10-methylene-THF, which can be oxidized to 10-formyl-THF, which is effectively permeable across the mitochondrial inner membrane as formate. 5,10-methylene-THF is used to synthesize dTMP from dUMP via thymidylate synthetase (TYMS), while 10-formyl-THF is used twice in de novo purine synthesis to make adenosine and guanosine. These steps of nucleotide synthesis are thought to occur primarily in the cytosol and nucleus (An, 2008 and Anderson, 2012). In addition, the mitochondria has a unique activity, the glycine cleavage system, that can break down glycine to ammonia, carbon dioxide, and 5,10-methylene-THF. Regardless, since serine can be reversibly broken down to glycine, formate and reducing equivalents in both compartments, all of which can be transported across the inner mitochondrial membrane (reducing equivalents as NAD(P)(H) are not directly permeable, but those electrons can be transported via other shuttles), this portion of folate one-carbon metabolism forms a metabolic cycle that can transport redox equivalents across the mitochondrial membrane and burn ATP. In fact, the cytosolic portion of this shuttle has been proposed to be a major source of redox equivalents in the cytosol (Fan, 2014), however, the directionality of the folate one-carbon cycle remains controversial.

Stable isotope tracing experiments have been used to determine the directionality of folate one-carbon metabolism in the cytosol and mitochondria. The directionality of the redox steps could be determined by utilizing [3,3-^{2}H]serine to label the NAD(P)H produced by MTHFD in a

compartment specific manner. While assaying each pool separately is not directly possible, expressing a compartment-specific isoform of mutant IDH that transfers compartmentalized redox equivalents to produce 2-HG can report on where the labeled NADPH was made (Lewis, 2014). As mentioned above, the 2-HG produced by mutant IDH accumulates to high levels in cells due to lack of an efficient breakdown system. Therefore, by measuring 2-HG deuteration, we can determine the contribution of folate oxidation to compartmentalized NAD(P)H pools, and therefore the extent of folate flux through MTHFD in the oxidative direction. In another experiment, we can measure the directionality of compartmentalized SHMTs using the same [3,3-^{2}H]serine tracer, this time measuring deuterium incorporation into dTMP monomers in DNA. Mitochondrial processing of serine to formate necessarily results in a loss of a deuteron via MTHFD oxidation, meaning at most one deuteron survives in m+1 dTMP. Cytosolic processing of serine to glycine, without equilibration of the resulting 5,10-methylene-THF across cytosolic MTHFD will result in survival of both deuterons in m+2 dTMP (Herbig, 2002). Therefore, the ratio of m+2 to m+1 dTMP in DNA from [3,3-^{2}H]serine tracer can inform the relative flux from serine to glycine through SHMT1 or SHMT2 to generate one-carbon units in thymidine. Lastly, flux from [^{13}C]formate to m+1 serine can inform flux through MTHFD and SHMT to generate serine from glycine and formate-derived folate species. Using these tracing tools, we will show in this thesis that serine is net broken down to formate in the mitochondria, where it is exported and reduced to support nucleotide biosynthesis in the cytosol (Figure 13).

What about the directionality of SHMT1? In the glycine to serine direction, SHMT1 has the potential to "waste" one-carbon equivalents and complete a futile cycle that deprives the cell of one-carbon equivalents for nucleotide biosynthesis. We propose that reversible inhibition of SHMT1 but not SHMT2 by phosphoserine breaks this cycle. Phosphoserine was previously not known to be an inhibitor of SHMT1, so it is worth considering why this aspect of SHMT1 enzymology was missed despite extensive study (Blakley, 1953, 1954, 1955, 1957a, 1957b).

One explanation may lie in the assay used for SHMT activity. SHMT was originally purified as a folate-dependent activity that interconverted serine and glycine, however, once it was found that SHMT also could catalyze the cleavage of beta-hydroxyamino acids, such as threonine, many SHMT assays were done without folates using beta-hydroxyamino acid cleavage as a readout for convenience (Schirch, 1968). In addition, it was shown that the folate-dependent SHMT reaction is not dependent on divalent metal cations (Blakley, 1954, 1955), and so assays of folate-dependent SHMT assay often included EDTA or were performed in a buffer without any such ions. Originally we hypothesized that phosphoserine could be a substrate for SHMT, an idea that has been proposed previously (Neuhaus, 1959a). Contrary to our expectations, we preliminarily found phosphoserine inhibition of SHMT1 but not SHMT2 that may be magnesium-dependent using a folate-dependent reaction. Importantly, this provides a mechanism for increased serine synthesis to support proliferative metabolism by reducing the "wasting" of folate one-carbon units, and instead directs them towards nucleotide biosynthesis.

Of note, phosphoserine inhibition of serine synthesis via SHMT1 is also consistent with the regulation of serine biosynthesis. Low serine levels not only favor dephosphorylation of newly produced phosphoserine by allowing hydrolysis of PSPH phosphoenzyme intermediate, but also increase serine synthesis from glycine via SHMT1 by reducing phosphoserine levels. Furthermore, because glucose is also necessary for the ribose portion of nucleotides, it may be that phosphoserine inhibition of SHMT1 signals to the cell the availability of both glucose for ribose and serine for one-carbon units in nucleotide biosynthesis.

Reciprocal regulation - folate one-carbon metabolism modulates glycolysis

In addition to our proposal that a glycolytic branchpoint intermediate, phosphoserine, regulates folate one-carbon metabolism, we propose that folate one-carbon metabolism can regulate

glycolysis. It has been reported that the purine biosynthetic intermediate SAICAR (Figure 12) is an activator of PKM2 (Keller, 2012). SAICAR is one step upstream of AICAR formyltransferase, which adds the second 10-formyl-THF unit for de novo purine biosynthesis. We find that some cells are dependent on SHMT2 to keep cellular formate levels high and reduce levels of SAICAR such that PKM2 activity remains low (Kim, 2015). These data are presented in Chapter 4. Together this allows glycolysis and folate one-carbon metabolism be coordinately regulated to support cell proliferation.

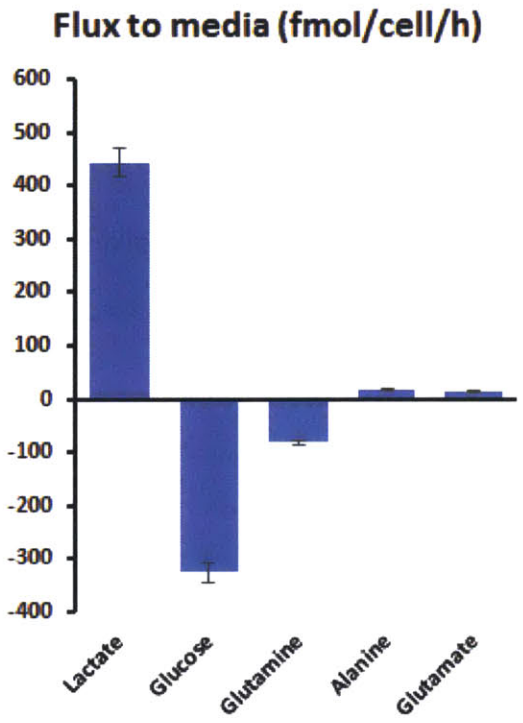

Figure 1 - Media flux of top 5 metabolites in cell culture across NCI-60 cell lines. Error bars are SEM. Data from (Jain, 2012)

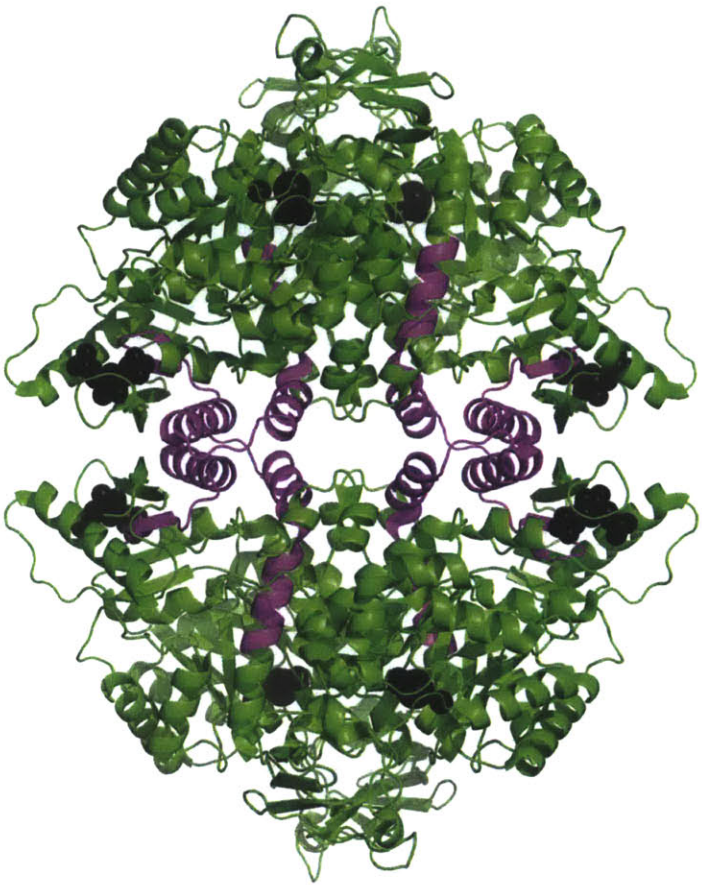

FIGURE 2 - Structure of PKM2 tetramer. PKM2 is viewed here as a tetramer parallel to the dimer-dimer interface. Residues contained in the PKM2-specific exon are highlighted in purple, near the dimer-dimer interface. FBP is shown bound in black, also near the dimer-dimer interface. Used with permission from William Israelsen.

1810 - Louis Planche (1776-1840) describes the first enzyme assay, of horseradish peroxidase oxidizing alpha-guaiaconic acid found in wood to guaiacum blue (Planche, 1810)
1828 - Friedrich Wohler (1800-1882) synthesizes urea, an organic compound, from inorganic ammonium cyanate (Wohler, 1828). He later mocked Pasteur for the idea that yeast were alive (Anonymous, 1839).
1833 - Anselme Payen (1795-1871) and Jean Persoz (1805-1868) purify the first enzyme, the starch breakdown enzyme diastase, by ethanol precipitation from germinating barley (Payen, 1833)
1847 - Adolph Kolbe (1818-1884) completes the chemical synthesis of acetic acid by synthesizing tricholoracetic acid (Chlorkohlenoxalsäure) from chlorine, water, and carbon disulfide, demonstrating that Wohler's synthesis is a general phenomenon (Kolbe, 1845)
1857 - Louis Pasteur (1822-1895) proposes that lactic acid fermentation is caused by a microorganism rather than a chemical process (Pasteur, 1857)
1858 - Moritz Traube (1826-1894) proposes that enzymes are "definite chemical compounds", despite little evidence to support this theory (Traube, 1858).
1877 - Felix Hoppe-Seyler (1825-1895) coins the term "biochemistry" ("biochemie") in his foreward to the first issue of Zeitschrift fur Physiologische Chemie, the first dedicated journal of biochemistry (Hoppe-Seyler, 1877)
1917 - SPL Sørensen (1868-1939) measures ovalbumin molecular weight by osmotic pressure as 34kDa, the first evidence that macromolecules exist (Sørensen, 1917)
1927 - James Sumner (1887-1955) crystallizes Urease from jack bean, proving Traube correct in demonstrating that enzymes are chemicals (Sumner, 1927)

Figure 3 - Timeline of early discoveries in biochemistry

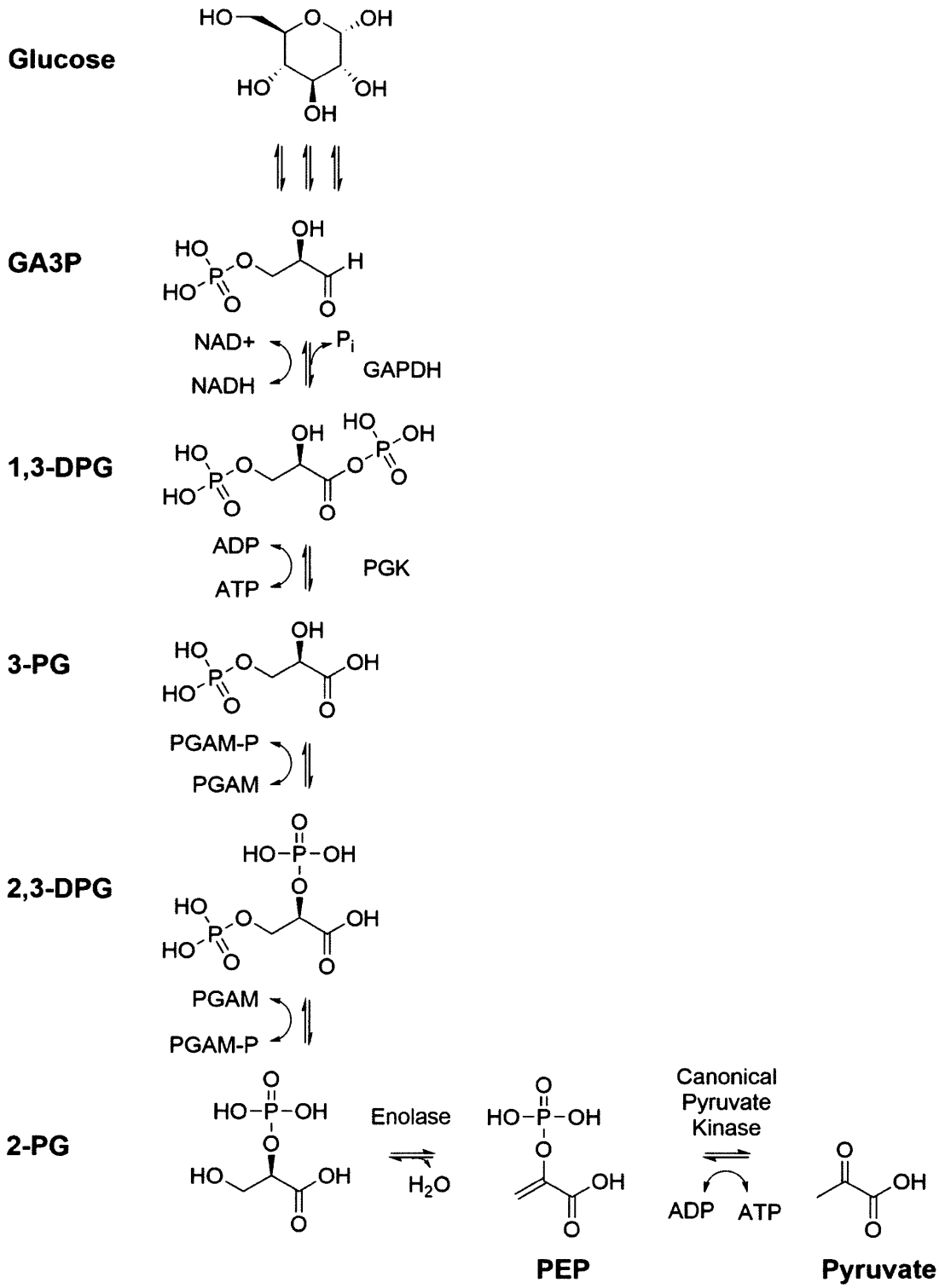

Figure 4 - Lower portion of classic "Embden–Meyerhof–Parnas" glycolytic pathway in mammalian cells.

1909 – Alcohol Dehydrogenase
1911 – Pyruvate Decarboxylase
1927 – Hexokinase
1933 – LDH
1933 – GPI
1934 – PK
1935 – PGAM
1935 – Enolase
1936 – PFK1
1936 – Aldolase
1936 – TPI
1936 – Glycogen Phosphorylase
1936 – Phosphoglucomutase
1939 – GAPDH
1942 – PGK
1980 – PFK2

Figure 5 - Timeline of the discovery of enzymes in glycolysis (Adapted from Florkin, 1972-83)

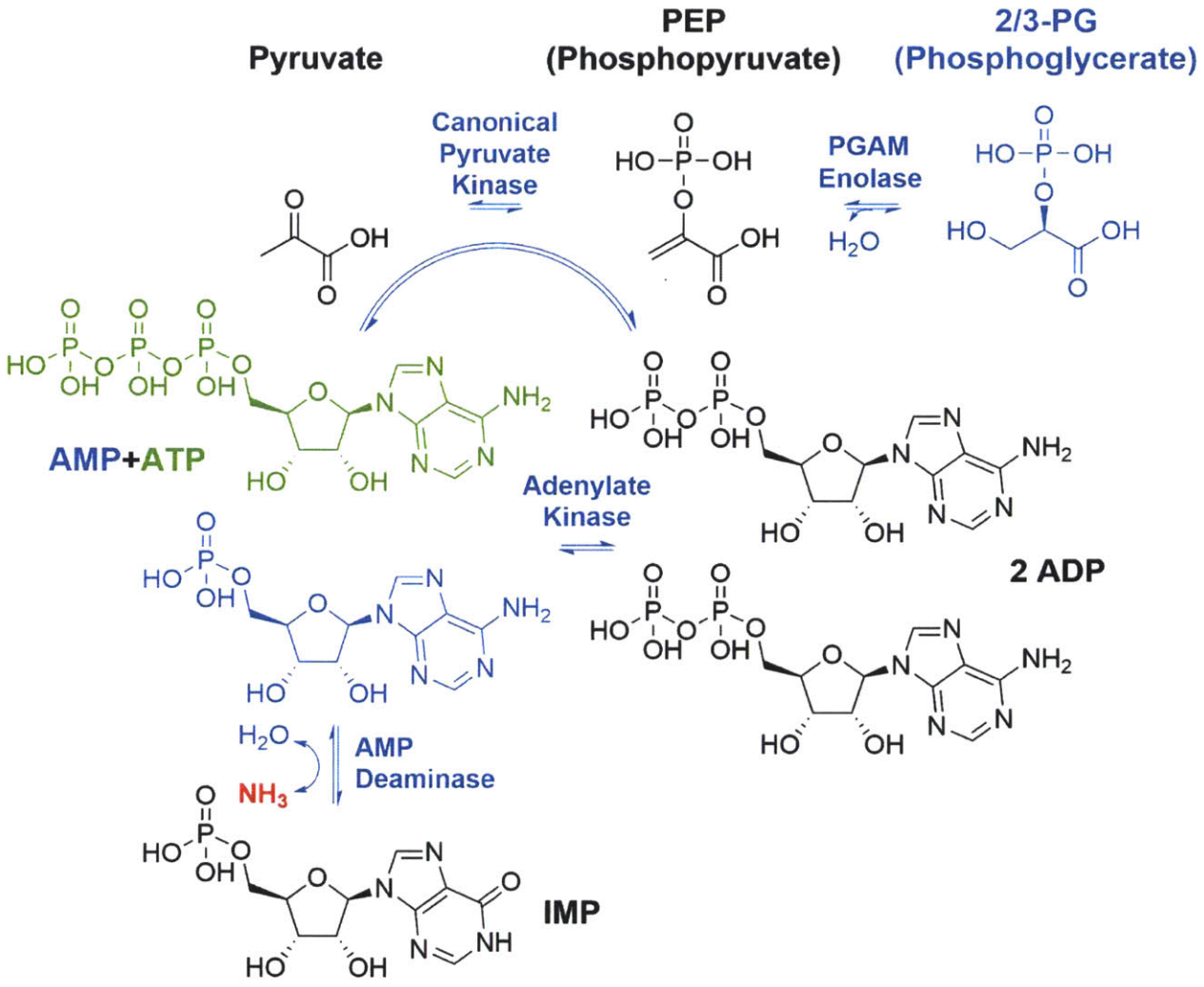

Figure 6 - The discovery of canonical ADP-dependent Pyruvate Kinase in 1934 by Jakub Parnas. Pyruvate kinase was discovered as an activity that inhibited ammonia (in red) formation from AMP in the presence of phosphoglycerate (a mixture of 2-PG and 3-PG), forming ATP (in green) instead (Parnas, 1934). The exact chemical structure of PEP, the discovery of 2-PG, and consequently Enolase and PGAM were unpublished as of the time of Parnas' publication. The discovery of PEP was published in the next volume of Biochemische Zeitschrift after the discovery of pyruvate kinase (Lohmann, 1934).

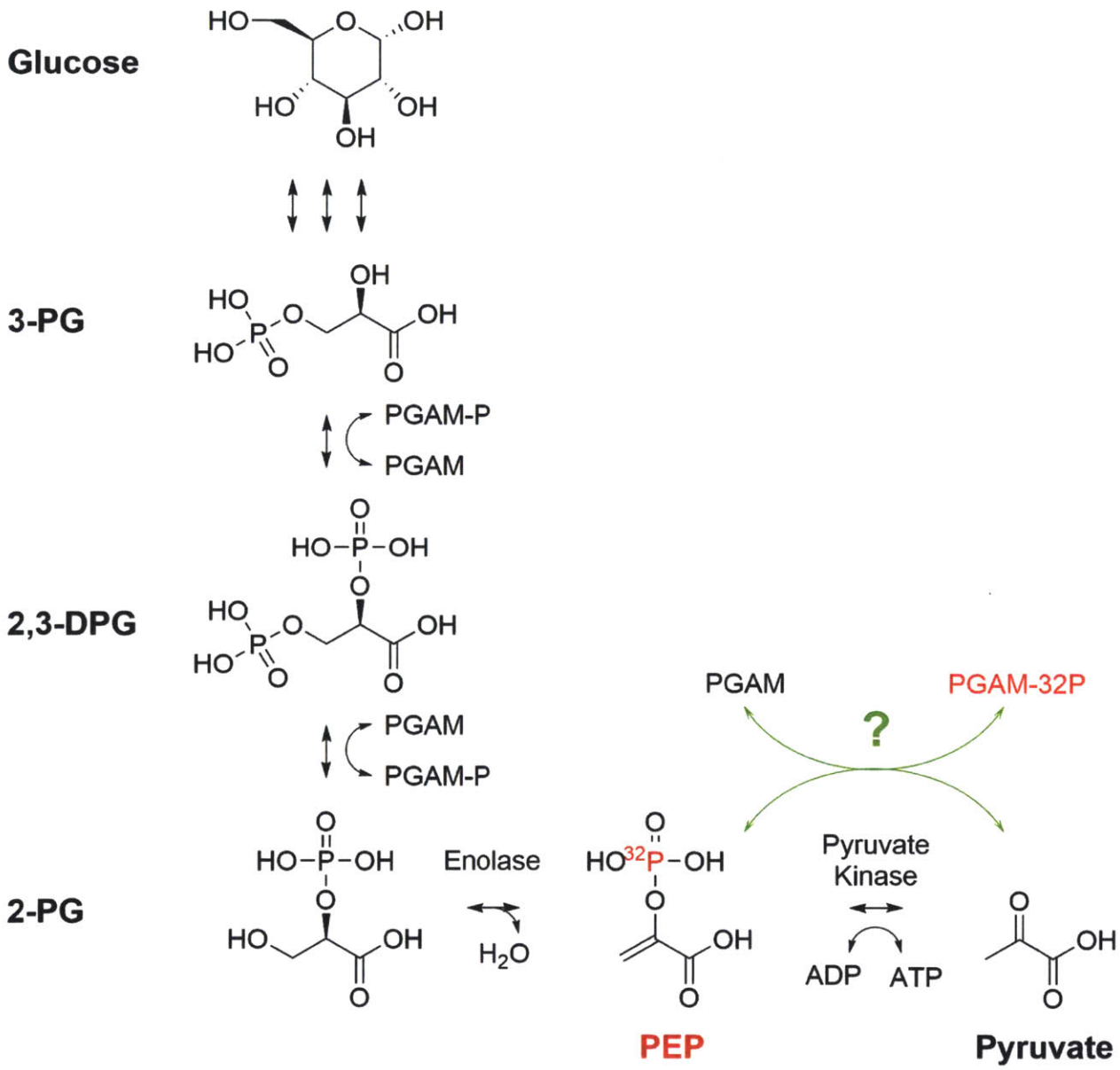

Figure 7 - The unknown PEP-dependent PGAM kinase activity in the context of lower glycolysis. If enolase is not involved in PGAM labeling, the activity must represent a novel pathway (shown in green). Radioactively labeled species are shown in red.

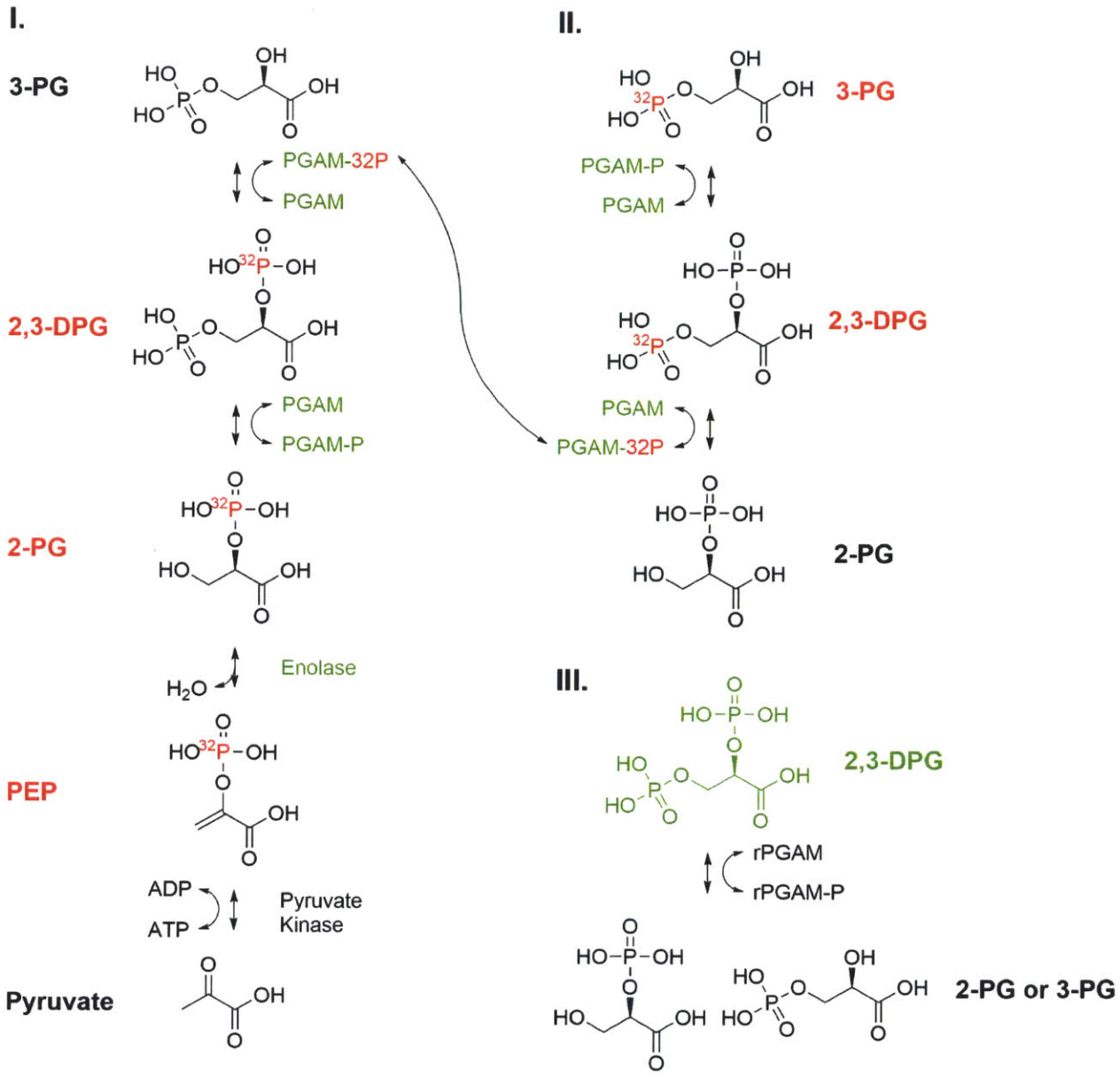

Figure 8 - Reverse glycolysis is responsible for the PEP-dependent PGAM labeling activity. Radioactively labeled species are shown in red, components of the PEP-dependent PGAM labeling activity are shown in green. In (I), labeled PEP is converted to labeled 2-PG or 2,3-DPG via enolase and phosphoryl transfer can occur to produce labeled endogenous PGAM. Labeled endogenous PGAM can transfer label to 3-PG as shown in (II). Recombinant PGAM (rPGAM), which is initially dephosphorylated, can be phosphorylated by the second activity, 2,3-DPG, as shown in (III). Phosphorylated rPGAM can then be labeled by many species as in (I) and (II).

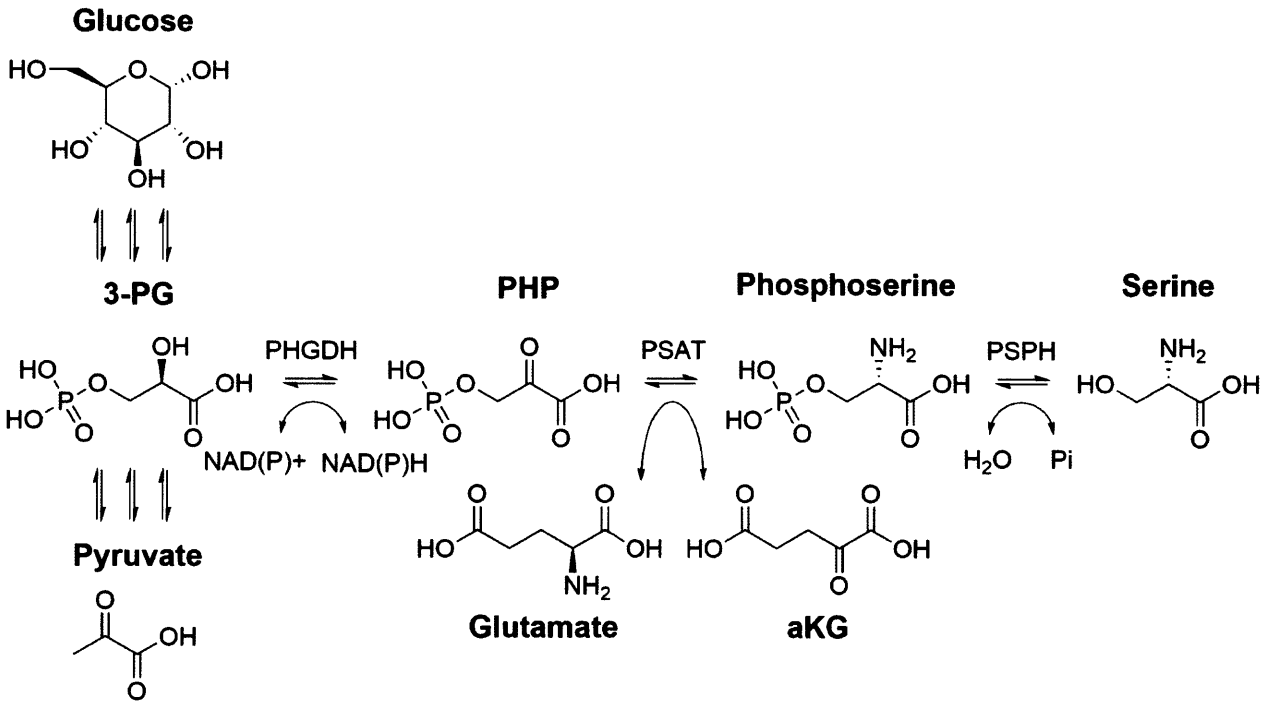

Figure 9 - Glycolytic serine biosynthesis in the context of glycolysis.

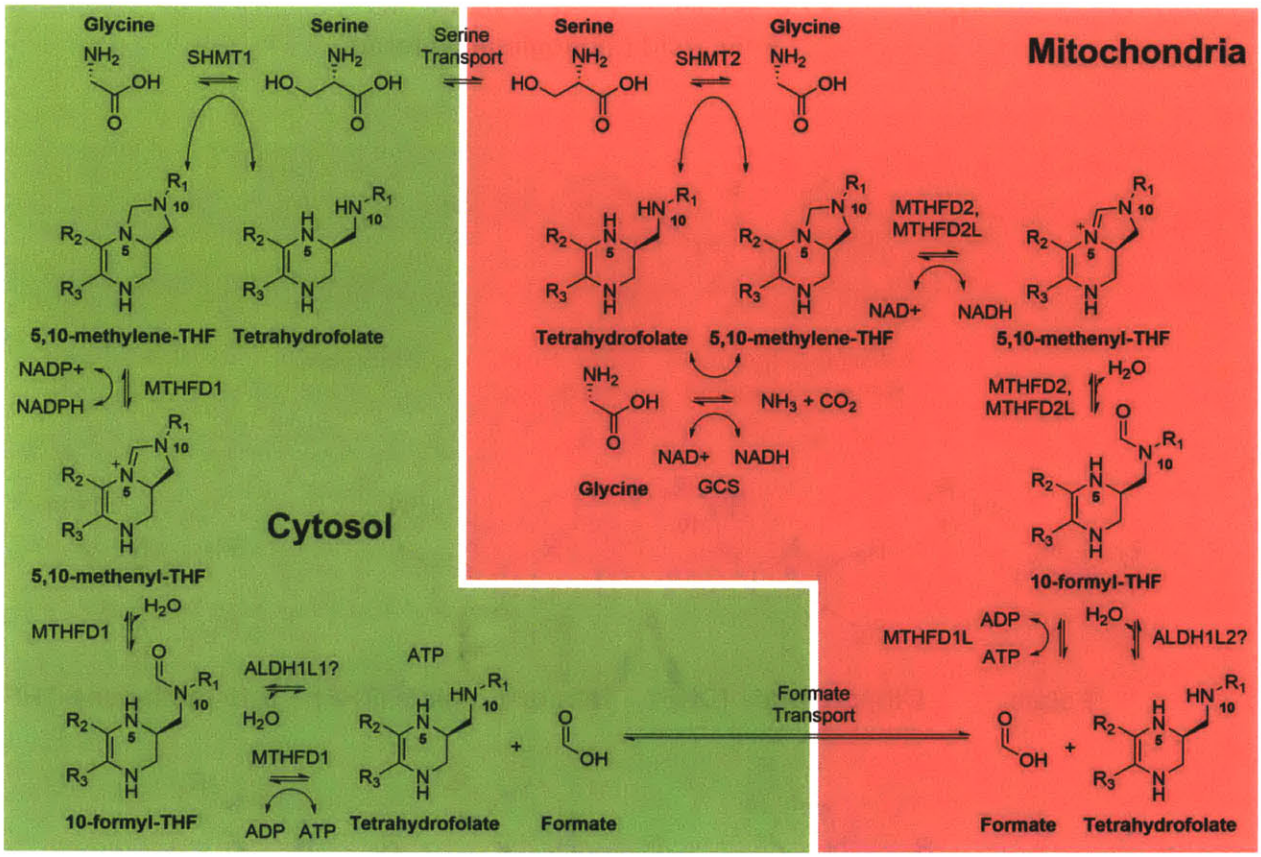

Figure 10 - Compartmentalization of folate one-carbon metabolism. GCS = "glycine cleavage system".

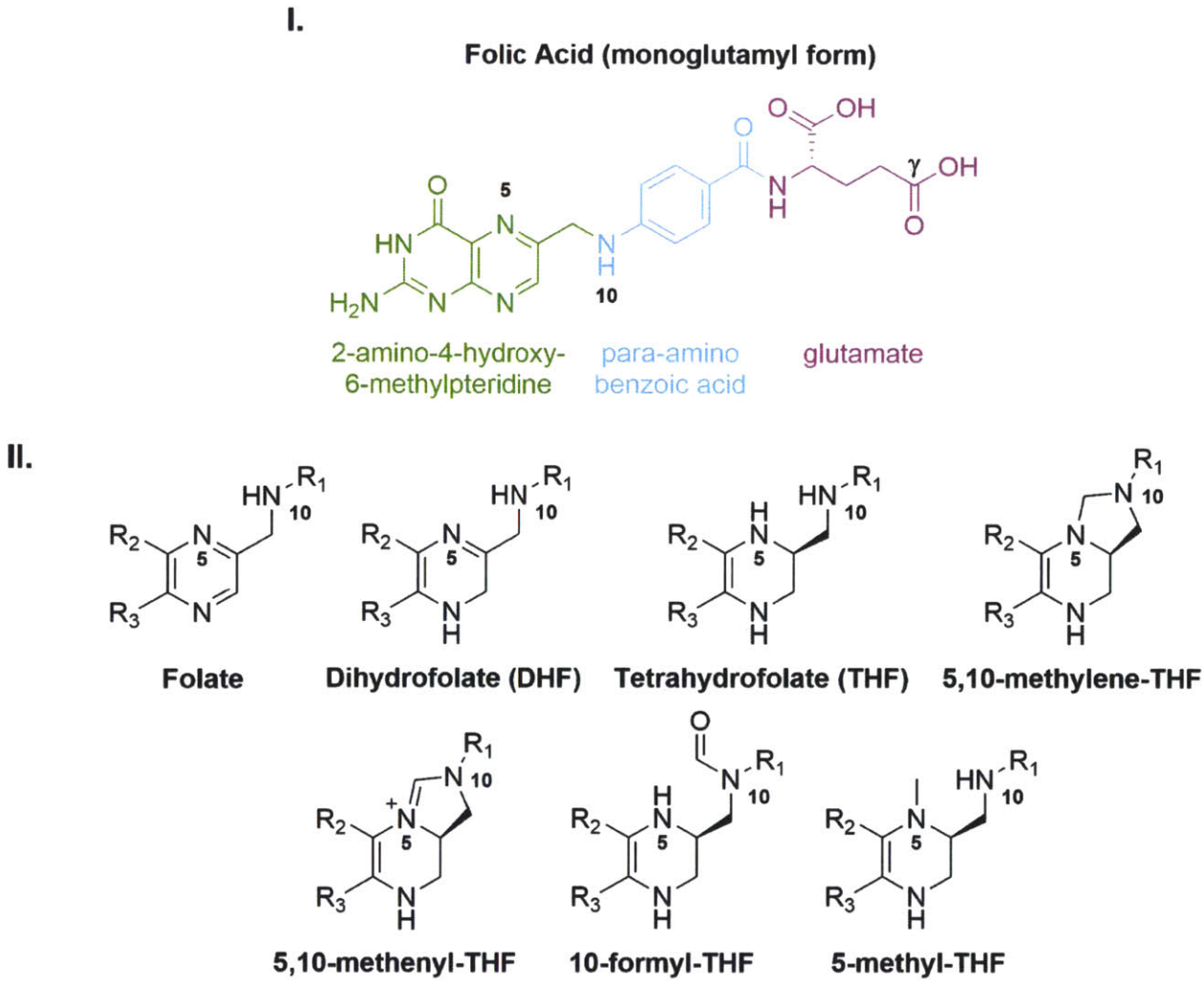

Figure 11 - Folate chemical structure. Folic acid in (I) and constituent pteridine, PABA, and glutamate moieties, 5 and 10 nitrogen positions (site of one-carbon attachment), and gamma carboxyl group (site of gamma-polyglutamylation). Different oxidation and one-carbon species of folate in (II).

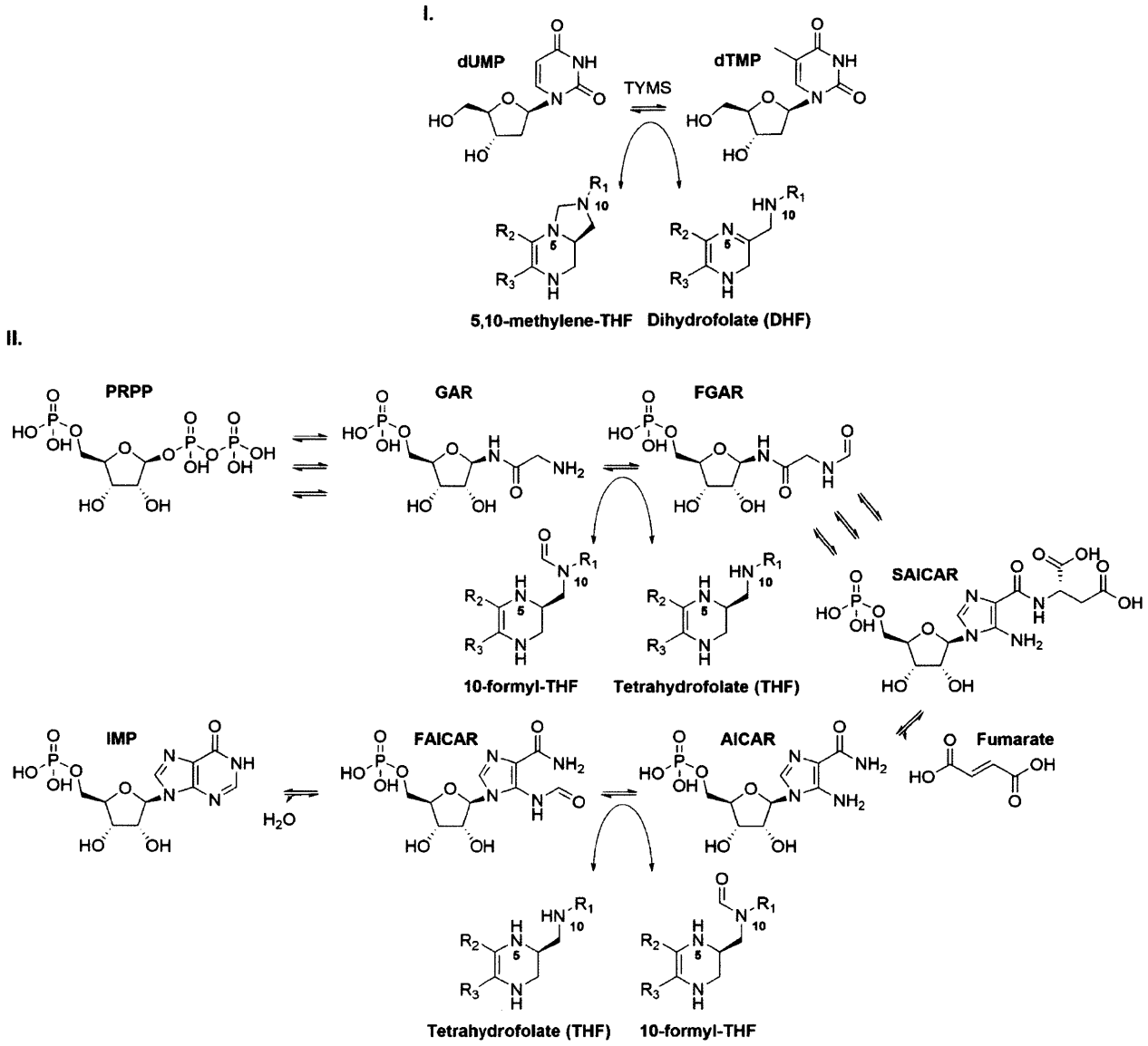

Figure 12 - Folate-dependent de novo nucleotide biosynthesis. Pyrimidine de novo synthesis of dTMP via thymidylate synthase (TYMS) shown in (I). Abbreviated purine de novo synthesis highlighting both steps that use 10-formyl-THF shown in (II).

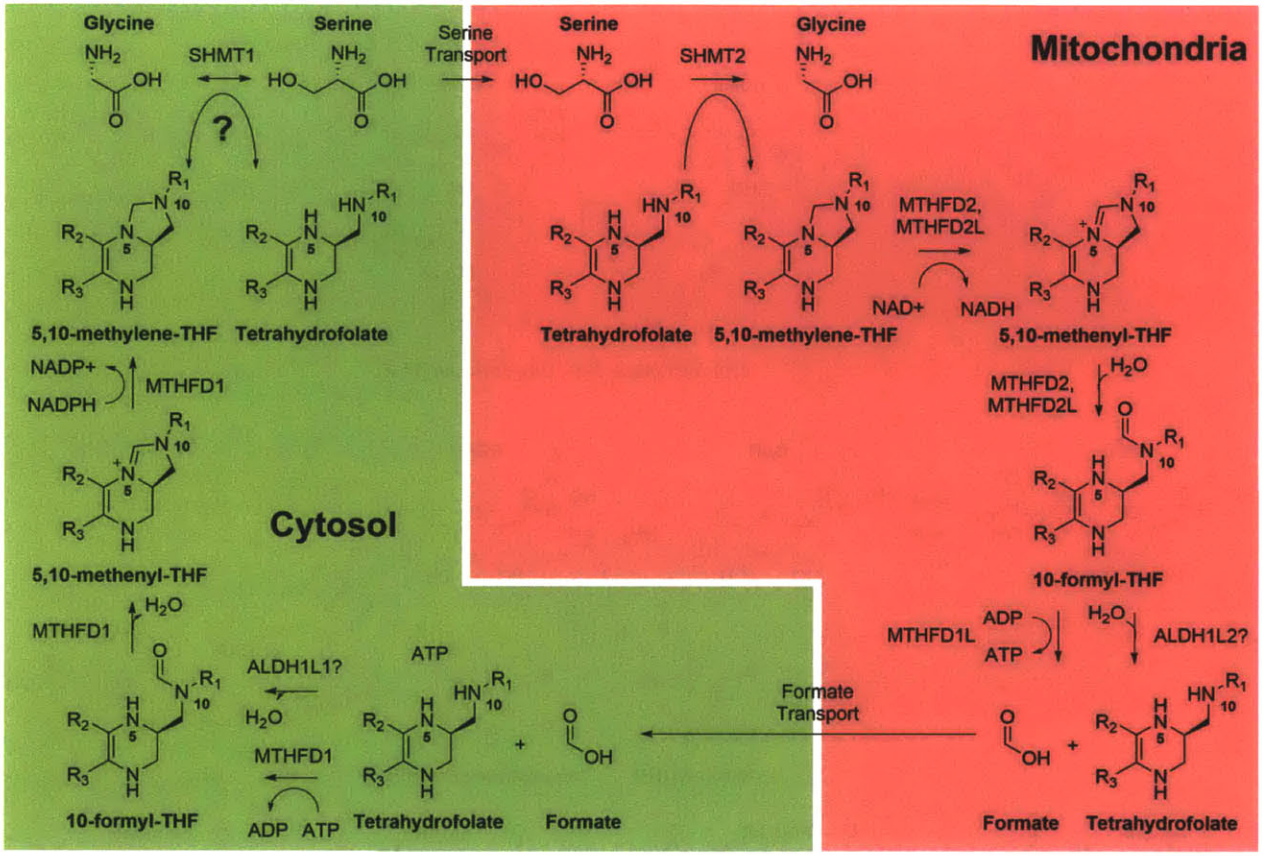

Figure 13 - Directionality of compartmentalized folate one-carbon metabolism. Note that directionality of SHMT1 may be specific to the experimental system or biological context within the same experimental system.

References

An S, Kumar R, Sheets ED, Benkovic SJ. (2008). Reversible compartmentalization of de novo purine biosynthetic complexes in living cells. Science 320, 103-6.

Anastasiou D, Poulogiannis G, Asara JM, Boxer MB, Jiang JK, Shen M, Bellinger G, Sasaki AT, Locasale JW, Auld DS, Thomas CJ, Vander Heiden MG, Cantley LC. (2011). Inhibition of pyruvate kinase M2 by reactive oxygen species contributes to cellular antioxidant responses. Science 334, 1278-83.

Anastasiou D, Yu Y, Israelsen WJ, Jiang JK, Boxer MB, Hong BS, Tempel W, Dimov S, Shen M, Jha A, Yang H, Mattaini KR, Metallo CM, Fiske BP, Courtney KD, Malstrom S, Khan TM, Kung C, Skoumbourdis AP, Veith H, Southall N, Walsh MJ, Brimacombe KR, Leister W, Lunt SY, Johnson ZR, Yen KE, Kunii K, Davidson SM, Christofk HR, Austin CP, Inglese J, Harris MH, Asara JM, Stephanopoulos G, Salituro FG, Jin S, Dang L, Auld DS, Park HW, Cantley LC, Thomas CJ, Vander Heiden MG. (2012). Pyruvate kinase M2 activators promote tetramer formation and suppress tumorigenesis. Nat Chem Biol 8, 839-47.

Anderson DD, Woeller CF, Chiang EP, Shane B, Stover PJ. (2012). Serine hydroxymethyltransferase anchors de novo thymidylate synthesis pathway to nuclear lamina for DNA synthesis. J Biol Chem 287, 7051-62.

Anonymous. (1839). Das enträthselte Geheimniss der geistigen Gährung. Ann Pharm 29, 100–104

Bailey RL, Mills JL, Yetley EA, Gahche JJ, Pfeiffer CM, Dwyer JT, Dodd KW, Sempos CT, Betz JM, Picciano MF. (2010). Unmetabolized serum folic acid and its relation to folic acid intake from diet and supplements in a nationally representative sample of adults aged > or =60 y in the United States. Am J Clin Nutr 92, 383-9.

Barnett JA. (2003). A history of research on yeasts 5: the fermentation pathway. Yeast 20, 509-43.

Barnett JA. (2005). Glucose Catabolism in Yeast and Muscle. In Florkin M, Stotz EH eds. Comprehensive Biochemistry v.44. Amsterdam, New York: Elsevier.

Ben-Haim S, Ell P. (2009). 18F-FDG PET and PET/CT in the evaluation of cancer treatment response. J Nucl Med 50, 88-99.

Betrán E, Wang W, Jin L, Long M. (2002). Evolution of the phosphoglycerate mutase processed gene in human and chimpanzee revealing the origin of a new primate gene. Mol Biol Evol 19, 654-663.

Blakley, RL. (1953). Folic acid as coenzyme for the interconversion of serine and glycine. Biochem J 56, xvii

Blakley, RL. (1954). The interconversion of serine and glycine: role of pteroylglutamic acid and other cofactors. Biochem J 58, 448-62.

Blakley, RL. (1955). The interconversion of serine and glycine: participation of pyridoxal phosphate. Biochem J 61, 315-23.

Blakley, RL. (1957a). The interconversion of serine and glycine; preparation and properties of catalytic derivatives of pteroylglutamic acid. Biochem J 65, 331-42.

Blakley, RL. (1957b). The interconversion of serine and glycine; some further properties of the enzyme system. Biochem J 65, 342-8.

Cairns RA, Mak TW. (2013). Oncogenic isocitrate dehydrogenase mutations: mechanisms, models, and clinical opportunities. Cancer Discov 3, 730-41.

Christofk HR, Vander Heiden MG, Wu N, Asara JM, Cantley LC. (2008a). Pyruvate kinase M2 is a phosphotyrosine-binding protein. Nature 452, 181-6.

Christofk HR, Vander Heiden MG, Harris MH, Ramanathan A, Gerszten RE, Wei R, Fleming MD, Schreiber SL, Cantley LC. (2008b). The M2 splice isoform of pyruvate kinase is important for cancer metabolism and tumour growth. Nature 452, 230-233.

Clower CV, Chatterjee D, Wang Z, Cantley LC, Vander Heiden MG, Krainer AR. (2010). The alternative splicing repressors hnRNP A1/A2 and PTB influence pyruvate kinase isoform expression and cell metabolism. PNAS 107, 1894-9.

Collet JF, Stroobant V, Van Schaftingen E. (1999). Mechanistic studies of phosphoserine phosphatase, an enzyme related to P-type ATPases. J Biol Chem 274, 33985-90.

Cortés-Cros M, Hemmerlin C, Ferretti S, Zhang J, Gounarides JS, Yin H, Muller A, Haberkorn A, Chene P, Sellers WR, Hofmann F. (2013). M2 isoform of pyruvate kinase is dispensable for tumor maintenance and growth. Proc Natl Acad Sci USA 110, 489-94.

Cowey CL, Rathmell WK. (2009). VHL gene mutations in renal cell carcinoma: role as a biomarker of disease outcome and drug efficacy. Curr Oncol Rep 11, 94-101.

Dang L, White DW, Gross S, Bennett BD, Bittinger MA, Driggers EM, Fantin VR, Jang HG, Jin S, Keenan MC, Marks KM, Prins RM, Ward PS, Yen KE, Liau LM, Rabinowitz JD, Cantley LC, Thompson CB, Vander Heiden MG, Su SM. (2009). Cancer-associated IDH1 mutations produce 2-hydroxyglutarate. Nature 462, 739-44.

David CJ, Chen M, Assanah M, Canoll P, Manley JL. (2010). HnRNP proteins controlled by c-Myc deregulate pyruvate kinase mRNA splicing in cancer. Nature 463, 364-8.

Deutscher J, Francke C, Postma PW. (2006). How phosphotransferase system-related protein phosphorylation regulates carbohydrate metabolism in bacteria. Microbiol Mol Biol Rev 70, 939-1031.

Dworkin MB, Dworkin-Rastl E. (1987). Metabolic regulation during early frog development. Identification of proteins labeled by 32P-glycolytic intermediates. J Biol Chem 262, 17038-45.

Eigenbrodt E, Leib S, Krămer W, Friis RR, Schoner W. (1983). Structural and kinetic differences between the M2 type pyruvate kinases from lung and various tumors. Biomed Biochim Acta 42, S278-82.

Fan J, Ye J, Kamphorst JJ, Shlomi T, Thompson CB, Rabinowitz JD. (2014). Quantitative flux analysis reveals folate-dependent NADPH production. Nature 510, 298-302.

Fang M, Shen Z, Huang S, Zhao L, Chen S, Mak TW, Wang X. (2010). The ER UDPase ENTPD5 promotes protein N-glycosylation, the Warburg effect, and proliferation in the PTEN pathway. Cell 143, 711-724.

Fell DA, Snell K. (1988). Control analysis of mammalian serine biosynthesis. Feedback inhibition on the final step. Biochem J 256, 97-101.

Fernandez CA, Des Rosiers C, Previs SF, David F, Brunengraber H. (1996). Correction of 13C mass isotopomer distributions for natural stable isotope abundance. J Mass Spectrom 31, 255-62.

Fiske BP, Vander Heiden MG. (2012). Seeing the Warburg effect in the developing retina. Nat Cell Biol 14, 790-1.

Florkin M, Stotz EH eds. (1972-83). A History of Biochemistry. Comprehensive Biochemistry v.30-35. Amsterdam, New York: Elsevier.

Gevers W, Krebs HA. (1966). The effects of adenine nucleotides on carbohydrate metabolism in pigeon-liver homogenates. Biochem J 98, 720-735.

Goldberg MS, Sharp PA. (2012). Pyruvate kinase M2-specific siRNA induces apoptosis and tumor regression. J Exp Med 209, 217-24.

Gui DY, Lewis CA, Vander Heiden MG. (2013). Allosteric regulation of PKM2 allows cellular adaptation to different physiological states. Sci Signal 6, pe7.

Herbig K, Chiang EP, Lee LR, Hills J, Shane B, Stover PJ. (2002). Cytoplasmic serine hydroxymethyltransferase mediates competition between folate-dependent deoxyribonucleotide and S-adenosylmethionine biosyntheses. J Biol Chem 277, 38381-9.

Hitosugi T, Kang S, Vander Heiden MG, Chung TW, Elf S, Lythgoe K, Dong S, Lonial S, Wang X, Chen GZ, Xie J, Gu TL, Polakiewicz RD, Roesel JL, Boggon TJ, Khuri FR, Gilliland DG, Cantley LC, Kaufman J, Chen J. (2009). Tyrosine phosphorylation inhibits PKM2 to promote the Warburg effect and tumor growth. Sci Signal 2, ra73.

Hoppe-Seyler F. (1877). Vorwort. Zeitschrift für Physiologische Chemie 1, I-III.

Hosios AM, Fiske BP, Gui DY, Vander Heiden MG. (2015). Lack of evidence for PKM2 protein kinase activity. In submission.

Israelsen WJ, Dayton TL, Davidson SM, Fiske BP, Hosios AM, Bellinger G, Li J, Yu Y, Sasaki M, Horner JW, Burga LN, Xie J, Jurczak MJ, DePinho RA, Clish CB, Jacks T, Kibbey RG, Wulf GM, Di Vizio D, Mills GB, Cantley LC, Vander Heiden MG. (2013). PKM2 isoform-specific deletion reveals a differential requirement for pyruvate kinase in tumor cells. Cell 155, 397-409.

Imamura K, Tanaka T. (1972). Multimolecular forms of pyruvate kinase from rat and other mammalian tissues. I. Electrophoretic studies. J Biochem 71, 1043-51.

Isaacs JS, Jung YJ, Mole DR, Lee S, Torres-Cabala C, Chung YL, Merino M, Trepel J, Zbar B, Toro J, Ratcliffe PJ, Linehan WM, Neckers L. (2005). HIF overexpression correlates with biallelic loss of fumarate hydratase in renal cancer: novel role of fumarate in regulation of HIF stability. Cancer Cell 8, 143-53.

Jain M, Nilsson R, Sharma S, Madhusudhan N, Kitami T, Souza AL, Kafri R, Kirschner MW, Clish CB, Mootha VK. (2012). Metabolite profiling identifies a key role for glycine in rapid cancer cell proliferation. Science 336, 1040-4.

Kalckar, HM. (1941). The Nature of Energetic Coupling in Biological Syntheses. Chem Rev 28, 71-178.

Keller KE, Tan IS, Lee YS. (2012). SAICAR stimulates pyruvate kinase isoform M2 and promotes cancer cell survival in glucose-limited conditions. Science 338, 1069-72.

Kim D, Fiske BP, Birsoy K, Freinkman E, Kami K, Possemato R, Chudnovsky Y, Pacold ME, Chen WW, Cantor JR, Shelton LM, Gui DY, Kwon M, Ramkissoon SH, Ligon KR, Kang SW, Snuderl M, Vander Heiden MG, Sabatini DM. (2015). SHMT2 drives glioma cell survival in the tumor microenvironment but imposes a dependence on glycine clearance. In submission.

Kim HK, Choi YH, Verpoorte R. (2011). NMR-based plant metabolomics: where do we stand, where do we go? Trends Biotechnol 29, 267-75.

Kolbe H. (1845). Beiträge zur Kenntnifs der gepaarten Verbindungen. Justus Liebigs Annalen der Chemie 54, 145-188.

Kung C, Hixon J, Choe S, Marks K, Gross S, Murphy E, DeLaBarre B, Cianchetta G, Sethumadhavan S, Wang X, Yan S, Gao Y, Fang C, Wei W, Jiang F, Wang S, Qian K, Saunders J, Driggers E, Woo HK, Kunii K, Murray S, Yang H, Yen K, Liu W, Cantley LC, Vander Heiden MG, Su SM, Jin S, Salituro FG, Dang L. (2012). Small molecule activation of PKM2 in cancer cells induces serine auxotrophy. Chem Biol 19, 1187-98.

Lehmann H. (1935). Über die enzymatische Synthese der Kreatinphosphorsäure durch Umesterung der Phosphobrenztraubensäure. Biochemische Zeitschrift 281, 271–291.

Lewis CA, Parker SJ, Fiske BP, McCloskey D, Gui DY, Green CR, Vokes NI, Feist AM, Vander Heiden MG, Metallo CM. (2014). Tracing compartmentalized NADPH metabolism in the cytosol and mitochondria of mammalian cells. Mol Cell 55, 253-63.

Linehan WM, Srinivasan R, Schmidt LS. (2010). The genetic basis of kidney cancer: a metabolic disease. Nat Rev Urol 7, 277-85.

Lipmann, F. (1941). Metabolic generation and utilization of phosphate bond energy. Adv Enzymol 1, 99-162.

Locasale JW, Grassian AR, Melman T, Lyssiotis CA, Mattaini KR, Bass AJ, Heffron G, Metallo CM, Muranen T, Sharfi H, Sasaki AT, Anastasiou D, Mullarky E, Vokes NI, Sasaki M, Beroukhim R, Stephanopoulos G, Ligon AH, Meyerson M, Richardson AL, Chin L, Wagner G, Asara JM, Brugge JS, Cantley LC, Vander Heiden MG. (2011). Phosphoglycerate dehydrogenase diverts glycolytic flux and contributes to oncogenesis. Nat Genet 43, 869-74.

Lohmann K, Meyerhof O. (1934). Über die enzymatische Umwandlung von Phosphoglycerinsaüre in Brenztraubeensaüre und Phosphorsaüre. Biochemische Zeitschrift 273, 60-72.

Losman JA, Looper RE, Koivunen P, Lee S, Schneider RK, McMahon C, Cowley GS, Root DE, Ebert BL, Kaelin WG Jr. (2013a). (R)-2-hydroxyglutarate is sufficient to promote leukemogenesis and its effects are reversible. Science 339, 1621-5.

Losman JA, Kaelin WG Jr. (2013b). What a difference a hydroxyl makes: mutant IDH, (R)-2-hydroxyglutarate, and cancer. Genes Dev 27, 836-52.

Lu C, Ward PS, Kapoor GS, Rohle D, Turcan S, Abdel-Wahab O, Edwards CR, Khanin R, Figueroa ME, Melnick A, Wellen KE, O'Rourke DM, Berger SL, Chan TA, Levine RL, Mellinghoff IK, Thompson CB. IDH mutation impairs histone demethylation and results in a block to cell differentiation. Nature 483, 474-8.

Lunt SY, Muralidhar V, Hosios AM, Israelsen WJ, Gui DY, Newhouse L, Ogrodzinski M, Hecht V, Xu K, Acevedo PNM, Hollern DP, Bellinger G, Dayton TL, Christen S, Elia I, Dinh AT, Stephanopoulos G, Manalis SR, Yaffe MB, Andrechek ER, Fendt SM, Vander Heiden MG. (2014). Pyruvate Kinase isoform expression alters nucleotide synthesis to impact cell proliferation. Mol Cell In press.

Lv L, Li D, Zhao D, Lin R, Chu Y, Zhang H, Zha Z, Liu Y, Li Z, Xu Y, Wang G, Huang Y, Xiong Y, Guan KL, Lei QY. (2011). Acetylation targets the M2 isoform of pyruvate kinase for degradation through chaperone-mediated autophagy and promotes tumor growth. Mol Cell 42, 719-30.

Macintyre AN, Rathmell JC. (2013). Activated lymphocytes as a metabolic model for carcinogenesis. Cancer Metab 1, 5.

Mardis ER, Ding L, Dooling DJ, Larson DE, McLellan MD, Chen K, Koboldt DC, Fulton RS, Delehaunty KD, McGrath SD, Fulton LA, Locke DP, Magrini VJ, Abbott RM, Vickery TL, Reed JS, Robinson JS, Wylie T, Smith SM, Carmichael L, Eldred JM, Harris CC, Walker J, Peck JB, Du F, Dukes AF, Sanderson GE, Brummett AM, Clark E, McMichael JF, Meyer RJ, Schindler JK, Pohl CS, Wallis JW, Shi X, Lin L, Schmidt H, Tang Y, Haipek C, Wiechert ME, Ivy JV, Kalicki J, Elliott G, Ries RE, Payton JE, Westervelt P, Tomasson MH, Watson MA, Baty J, Heath S, Shannon WD, Nagarajan R, Link DC, Walter MJ, Graubert TA, DiPersio JF, Wilson RK, Ley TJ. (2009). Recurring mutations found by sequencing an acute myeloid leukemia genome. NEJM 361, 1058-66.

Mazurek S. (2011). Pyruvate kinase type M2: a key regulator of the metabolic budget system in tumor cells. Int J Biochem Cell Biol 43, 969-80.

Mitchell, P. (1961). Coupling of phosphorylation to electron and hydrogen transfer by a chemi-osmotic type of mechanism. Nature 191, 144–8.

Narindrasorasak S, Bridger WA. (1977). Phosphoenolypyruvate synthetase of Escherichia coli: molecular weight, subunit composition, and identification of phosphohistidine in phosphoenzyme intermediate. J Biol Chem 252, 3121-3127.

National Academy of Sciences, Institute of Medicine, Food and Nutrition Board. *Dietary Reference Intakes for Thiamin, Riboflavin, Niacin, Vitamin B6, Folate, Vitamin B12, Pantothenic Acid, Biotin, and Choline*. Washington, DC: National Academy Press, 1998. Electronic, accessed 10 Oct 2014 at "http://www.nal.usda.gov/fnic/DRI//DRI_Thiamin/thiamin_full_report.pdf"

Negelein E, Brömel H. (1939). R-Diphosphoglycerin säure, ihre Isolierung und Eigenschaften. Biochemische Zeitschrift 303,132-44.

Neuhaus FC, Byrne WL. (1959a). Metabolism of phosphoserine. I. Exchange of L-serine with phosphoserine. J Biol Chem 234, 109-12.

Neuhaus FC, Byrne WL. (1959b). Metabolism of phosphoserine. II. Purification and properties of O-phosphoserine phosphatase. J Biol Chem 234, 113-21.

Neuhaus FC, Byrne WL. (1960). Metabolism of phosphoserine. III. Mechanism of O-phosphoserine phosphatase. J Biol Chem 235, 2019-24.

Parnas JK, Ostern P, Mann T. (1934). Über die Verkettung der chemischen Vorgänge im Muskel. Biochemische Zeitschrift 272, 64-70.

Parsons DW, Jones S, Zhang X, Lin JC, Leary RJ, Angenendt P, Mankoo P, Carter H, Siu IM, Gallia GL, Olivi A, McLendon R, Rasheed BA, Keir S, Nikolskaya T, Nikolsky Y, Busam DA, Tekleab H, Diaz LA Jr, Hartigan J, Smith DR, Strausberg RL, Marie SK, Shinjo SM, Yan H, Riggins GJ, Bigner DD, Karchin R, Papadopoulos N, Parmigiani G, Vogelstein B, Velculescu VE, Kinzler KW. (2008). An integrated genomic analysis of human glioblastoma multiforme. Science 321, 1807-12.

Pasteur L. (1857). Mémoire sur la fermentation appelée lactique. Comptes rendus des séances de l'Academie des Sciences 45, 913-916 and 1032-1036. Translated in Mol Med (1995) 1, 599-602.

Payen A, Persoz, JF. (1833). Mémoire sur la diastase, les principaux produits de ses réactions et leurs applications aux arts industriels. Annales de chimie et de physique 53, 73–92.

Planche LA. (1810). Note sur la sophistication de la resine de jalap et sur les moyens de la reconnaitre, etc. Bulletin de Pharmacie 2, 578-80.

Pollard PJ, Brière JJ, Alam NA, Barwell J, Barclay E, Wortham NC, Hunt T, Mitchell M, Olpin S, Moat SJ, Hargreaves IP, Heales SJ, Chung YL, Griffiths JR, Dalgleish A, McGrath JA, Gleeson MJ, Hodgson SV, Poulsom R, Rustin P, Tomlinson IP. (2005). Accumulation of Krebs cycle intermediates and over-expression of HIF1alpha in tumours which result from germline FH and SDH mutations. Hum Mol Genet 14, 2231-9.

Possemato R, Marks KM, Shaul YD, Pacold ME, Kim D, Birsoy K, Sethumadhavan S, Woo HK, Jang HG, Jha AK, Chen WW, Barrett FG, Stransky N, Tsun ZY, Cowley GS, Barretina J, Kalaany NY, Hsu PP, Ottina K, Chan AM, Yuan B, Garraway LA, Root DE, Mino-Kenudson M, Brachtel EF, Driggers EM, Sabatini DM. (2011). Functional genomics reveal that the serine synthesis pathway is essential in breast cancer. Nature 476, 346-50.

Ralser M, Wamelink MM, Struys EA, Joppich C, Krobitsch S, Jakobs C, Lehrach H. (2008). A catabolic block does not sufficiently explain how 2-deoxy-D-glucose inhibits cell growth. PNAS 105, 17807-11.

Rose ZB, Dube S. (1976). Rates of phosphorylation and dephosphorylation of phosphoglycerate mutase and bisphosphoglycerate synthase. J Biol Chem 251, 4817-4822.

Sakoda S, Shanske S, DiMauro S, Schon EA. (1988). Isolation of a cDNA encoding the B isozyme of human phosphoglycerate mutase (PGAM) and characterization of the PGAM gene family. J Biol Chem 263, 16899-16905.

Schirch L, Gross T. (1968). Serine transhydroxymethylase. Identification as the threonine and allothreonine aldolases. J Biol Chem 243, 5651-5.

Shane, Barry. "Folate Chemistry and Metabolism." *Folate in Health and Disease, Second Edition*. Ed. Lynn B Bailey. Boca Raton: Taylor and Francis Group, 2010. 1-24. Print.

Snell K, Fell DA. (1990). Metabolic control analysis of mammalian serine metabolism. Advances in Enzyme Regulation 30, 13-32.

Sørensen SPL, Høyrup H. (1917). On the composition and properties of egg-albumin separated in crystalline form by means of ammonium sulphate. Comptes rendus des travaux du laboratoire Carlsberg 12, 164-212.

Stein E, Tallman M, Pollyea DA, Flinn IW, Fathi AT, Stone RM, Levine RL, Agresta S, Schenkein D, Yang H, Fan B, Yen K, De Botton S. (2014). Clinical safety and activity in a phase I trial of AG-221, a first in class, potent inhibitor of the IDH2-mutant protein, in patients with IDH2 mutant positive advanced hematologic malignancies. In: Proceedings of the 105th Annual Meeting of the American Association for Cancer Research; 2014 Apr 5-9; San Diego, CA. Philadelphia (PA): AACR; 2014. #CT103.

Stover, Patrick J. "Folate Biochemical Pathways and Their Regulaiton." *Folate in Health and Disease, Second Edition*. Ed. Lynn B Bailey. Boca Raton: Taylor and Francis Group, 2010. 49-74. Print.

Sumner JB. (1926). The isolation and crystallization of the enzyme urease. J Biol Chem 69, 435–441.

Takeda K, Komuro Y, Hayakawa T, Oguchi H, Ishida Y, Murakami S, Noguchi T, Kinoshita H, Sekine Y, Iemura S, Natsume T, Ichijo H. (2009). Mitochondrial phosphoglycerate mutase 5 uses alternate catalytic activity as a protein serine/threonine phosphatase to activate ASK1. PNAS 106, 12301-12305.

Thompson, CB. (2009). Metabolic enzymes as oncogenes or tumor suppressors. N Engl J Med 360, 765-773.

Tibbetts AS, Appling DR. (2010). Compartmentalization of Mammalian folate-mediated one-carbon metabolism. Annu Rev Nutr 30, 57-81.

Tomlinson IP, Alam NA, Rowan AJ, Barclay E, Jaeger EE, Kelsell D, Leigh I, Gorman P, Lamlum H, Rahman S, Roylance RR, Olpin S, Bevan S, Barker K, Hearle N, Houlston RS, Kiuru M, Lehtonen R, Karhu A, Vilkki S, Laiho P, Eklund C, Vierimaa O, Aittomäki K, Hietala M, Sistonen P, Paetau A, Salovaara R, Herva R, Launonen V, Aaltonen LA; Multiple Leiomyoma Consortium. (2002). Germline mutations in FH predispose to dominantly inherited uterine fibroids, skin leiomyomata and papillary renal cell cancer. Nat Genet 30, 406-10.

Traube M. (1858). Zur Theorie der Gährungs - und Verwesungs erscheinungen, wie der Fermentwirkungen überhaupt. Annalen der Physik und Chemie 103, 331-34.

Vander Heiden MG, Locasale JW, Swanson KD, Sharfi H, Heffron GJ, Amador-Noguez D, Christofk HR, Wagner G, Rabinowitz JD, Asara JM, Cantley LC. (2010). Evidence for an alternative glycolytic pathway in rapidly proliferating cells. Science 329, 1492-1499.

Vander Heiden MG. (2011). Targeting cancer metabolism: a therapeutic window opens. Nat Rev Drug Discov 10, 671-84.

Wang HC, Ciskanik L, Dunaway-Mariano D, von der Saal W, Villafranca JJ. (1988). Investigations of the partial reactions catalyzed by pyruvate phosphate dikinase. Biochemistry 27, 625-633.

Warburg OH, Posener K, Negelein E. (1924). Über den Stoffwechsel der Carcinomzelle. Biochemische Zeitschrift 152, 309-344.

Warburg O, Christian W. (1939). Isolation and Crystallization of Proteins of the Oxidative Fermentation of Enzymes. Biochemische Zeitschrift 303, 40-68.

Ward PS, Lu C, Cross JR, Abdel-Wahab O, Levine RL, Schwartz GK, Thompson CB. (2013). The potential for isocitrate dehydrogenase mutations to produce 2-hydroxyglutarate depends on allele specificity and subcellular compartmentalization. J Biol Chem 288, 3804-15.

Wöhler F. (1828). Ueber künstliche Bildung des Harnstoffs. Annalen der Physik und Chemie 88, 253-56.

Yan H, Parsons DW, Jin G, McLendon R, Rasheed BA, Yuan W, Kos I, Batinic-Haberle I, Jones S, Riggins GJ, Friedman H, Friedman A, Reardon D, Herndon J, Kinzler KW, Velculescu VE, Vogelstein B, Bigner DD. (2009). IDH1 and IDH2 mutations in gliomas. N Engl J Med 360, 765-773.

Ye J, Mancuso A, Tong X, Ward PS, Fan J, Rabinowitz JD, Thompson CB. (2012). Pyruvate kinase M2 promotes de novo serine synthesis to sustain mTORC1 activity and cell proliferation. PNAS 109, 6904-9.

Yuan J, Bennett BD, Rabinowitz JD. (2008). Kinetic flux profiling for quantitation of cellular metabolic fluxes. Nat Protoc 3, 1328-40.

Zamboni N, Fendt SM, Rühl M, Sauer U. (2009). (13)C-based metabolic flux analysis. Nat Protoc 4, 878-92.

Zhao R, Goldman ID. (2003). Resistance to antifolates. Oncogene 22, 7431-57.

Zhao S, Lin Y, Xu W, Jiang W, Zha Z, Wang P, Yu W, Li Z, Gong L, Peng Y, Ding J, Lei Q, Guan KL, Xiong Y. (2009). Glioma-derived mutations in IDH1 dominantly inhibit IDH1 catalytic activity and induce HIF-1alpha. Science 324, 261-5.

Chapter 2 - An alternative glycolytic pathway in proliferating cells

Authorship Statement

Please note that some portion of the materials and methods section written in this chapter was paraphrased or copied verbatim from (Vander Heiden, 2010). Also note that the NMR spectroscopy as well as a portion of the NMR methods were the contribution of Jeff Simpson at the DCIF Chemistry NMR facility.

Introduction

As discussed in the introduction, an attempt to reconcile the dependence of proliferating cells on simultaneously decreased canonical PK activity and increased glycolysis led us to hypothesize that an enzyme that catalyzes an alternative reaction to PK may exist. This hypothesis motivated the search for a PEP-dependent kinase activity, the target of which was found to be PGAM1 using [^{32}P]PEP labeling (Vander Heiden MG, 2010). It was also suggested that this activity was associated with ADP-independent production of pyruvate from PEP (Chapter 1, Figure 7). While the PGAM1 target was cloned using traditional biochemical methods, the activity itself was only partially purified as the D0-500 fraction using weak anion exchange chromatography. We set out to determine the mechanism as well as the necessary and sufficient components for PGAM1 phosphoryltransfer from [^{32}P]PEP.

Results

We first decided to narrow down the location of the PGAM phosphoryltransfer activity that interacts with a weak anion exchange (D) column and elutes with 500 mM salt (termed D0-500) using an assay developed previously that tracks [^{32}P]PEP labeling of recombinant PGAM1 (rPGAM) (Vander Heiden MG, 2010). We initially found that finer fractionation of D0-500 using

stepwise elution in 50 mM NaCl increments resulted in loss of activity, which raised the possibility that we were separating more than one activity necessary for rPGAM phosphoryltransfer. By combining all D fractions pairwise, we found at least two such activities that eluted in separate fractions could together reconstitute the full activity seen in the input fraction, one primarily in D0-200, and the other in D200-500 (Figure 1a).

Next, we tested whether PEP was in fact the direct phosphoryl donor for PGAM phosphorylation, or rather if a product of PEP formed during the reaction was responsible for PGAM labeling. To answer this, we further characterized the D fractions by analyzing the same reactions used in our rPGAM phosphoryltransfer assay by thin-layer chromatography (TLC) to assess whether PEP was transformed into another metabolite during the course of the reaction. We found that an unknown intermediate (UI) accumulated over time upon addition of fractions from D0-200 (Figure 1b). We reasoned that if production of this intermediate was related to rPGAM phosphoryltransfer, then the D0-200 activity may contain an activity necessary for PGAM phosphoryltransfer that converts PEP to UI. The D200-500 did not contain this activity, so it seemed possible that this fraction might contain an activity that was either a UI-dependent PGAM kinase or a regulatory protein or cofactor required for PGAM autophoshoryltransfer. We next found that a methanol extract of the D200-500 fraction (D200-500ME) was active in combination with non-extracted D0-200 (Figure 1c), suggesting that the necessary and sufficient contribution of the D200-500 to PGAM phosphoryltransfer activity was methanol-extractable.

Because many polar metabolites but few proteins are methanol extractable, we focused on testing a number of candidate metabolites in an effort to guess the identity of the active metabolite in D200-500. One potential candidate was the previously characterized PGAM cofactor 2,3-DPG, which we found was able to substitute for D200-500 at concentrations as low as 50nM, and 2,3-DPG could further activate the combination of D0-200 and D200-500ME to

phosphorylate PGAM1 (Figure 2a). Given the known PGAM1 mechanism of catalytic phosphohistidine priming, we suspected that the 2,3-DPG inhibition seen at high concentrations might be due to 2-PG or 3-PG contamination, which can dephosphorylate [^{32}P]rPGAM and inhibit PGAM phosphoryltransfer completely at concentrations as low as 3uM (Figure S1).

In addition to purifying the PGAM phosphoryltransfer activity on the D anion exchange column, we also attempted purification on an S cation exchange column. Given the opposite affinities of the two columns, we were not surprised that activity was found only in the flow-through (SFT) fraction of the S column (Figure 2b, row 1). This activity also vanished upon desalting using size exclusion chromatography, which would be expected to remove any small metabolites. These findings supported the notion that the sufficient activity in D200-500 was one or more small metabolites (Figure 2b, row 3). However, we were puzzled that by TLC, additional UI producing activity could be found bound to the S column, yet these fractions had no PGAM phosphoryltransfer activity (Figure 2b). We were able to recover the correlation of UI production and PGAM phosphoryltransfer activity by adding 2,3-DPG to the reactions (Figure 2b, row 2). Recovery of activity upon adding back 2,3-DPG to the desalted fractions additionally confirmed that 2,3-DPG was sufficient for the metabolite component of the PGAM phosphoryltransfer activity (Figure 2b, row 4).

Having shown that 2,3-DPG was sufficient for the metabolite component of the PGAM phosphoryltransfer activity, we set out to determine whether UI itself was sufficient to explain the non-metabolite component, or whether additional factors were necessary. We reasoned that if UI production, which up to this point was only correlated with the non-metabolite component of the PGAM phosphoryltransfer activity, was sufficient to explain the requirement for D0-200, then substitution of methanol-extracted [^{32}P]UI for the D0-200 fraction would recover phosphorylation activity. We found that this was in fact the case (Figure 2c), and that even small amounts of UI

approaching the limits of detection by TLC were sufficient for PGAM phosphoryltransfer (Figure 2c, lane "D0-200@1min"). This stoichiometry was consistent with rPGAM1 being present in our reactions at ~1uM and total PEP (including cold carrier and [^{32}P]PEP) being present at ~10-15uM, making it plausible that <10% yield of UI from PEP could be sufficient for full labeling of rPGAM1. At this point, the possibility that enolase might be the activity contained in D0-200 fraction was raised, however, UI ran differently than 2-PG by TLC (Figure 2c). Nevertheless, consistent with the known mechanism of PGAM, [^{32}P]2-PG was sufficient for PGAM phosphoryltransfer activity in combination with 2,3-DPG (Figure 2c).

Having shown that [^{32}P]UI and 2,3-DPG were sufficient for PGAM phosphoryltransfer, we set out to identify UI. As a first step, we created a method to produce [^{32}P]UI using D0-200 and purify UI using HPLC (Figure 3a). Next, in order to obtain sufficient quantities of UI for NMR spectroscopy, we developed a method to extract more UI-producing enzyme from cells. In the process of testing various cellular extractions, we found that a large amount of UI-producing capacity could be found in the methanol portion of a buffered methanol/chloroform extraction performed directly on cells (MCE). We were able to confirm that [^{32}P]UI produced by MCE co-eluted within 15 seconds of [^{32}P]UI from D0-200. In addition, both pre- and post-HPLC fractions of UI from both D0-200 and MCE were sufficient for PGAM phosphoryltransfer in combination with 2,3-DPG (Figure 3b).

With methods for synthesis and purification of sufficient quantities of UI, we prepared a sample for NMR. The resulting ^{1}H and ^{1}H COSY spectra were consistent with a mixture of 4% PEP, 12% 2-PG, and 84% 3-PG. ^{1}H-^{13}C HSQC and HMBC further supported these identifications. The spectra were as follows: Phosphoenolpyruvic acid: ^{1}H NMR (500MHz, D_2O) δ 5.35 (s, 1 H), δ 5.17 (s, 1 H). 2-Phosphoglyceric acid: ^{1}H NMR (500MHz, D_2O) δ 4.46 (ddd, 1 H), δ 3.90-3.84 (m, 1 H), δ 3.79 (dd, 1 H); ^{13}C NMR (125MHz, D_2O) δ 76.5, 65.0. 3-Phosphoglyceric acid: ^{1}H

NMR (500MHz, D_2O) δ 4.17 (dd, *J* = 6.4, 2.8 Hz, 1 H), δ 4.01 (ddd, *J* = 11.0, 6.0, 2.7 Hz, 1 H), δ 3.87 (app dt, *J* = 11.0, 6.1 Hz, 1 H); ^{13}C NMR (125MHz, D_2O) δ 179.0, 73.0, 67.0.

These results suggested that the sufficient components for PGAM phosphoryltransfer contained in cell culture lysates were [^{32}P]2-PG or [^{32}P]3-PG and 2,3-DPG. Unfortunately, this result was consistent with the known mechanism of PGAM phosphorylation, where 2,3-DPG could act to phosphorylate endogenous or recombinant PGAM1 in the reaction, which then could be labeled by phosphoryltransfer from [^{32}P]2-PG or [^{32}P]3-PG (Figure 8, Introduction). How, then, could the D0-200 fraction without addition of rPGAM be producing 3-PG? If D0-200 contained both phosphorylated PGAM and Enolase, the existing reaction mechanisms of PGAM and Enolase already explain [^{32}P]3-PG production from [^{32}P]PEP (Figure 8, I and II, Introduction). Upon close examination, both D0-200 and an S fraction that were competent for UI synthesis in fact contained both PGAM and Enolase by Western blot (Figure 4), although consistent with previous studies, we found that a majority of Enolase does not bind to a D column. Nevertheless, because small amounts of both Enolase and phosphorylated PGAM can catalyze production of [^{32}P]3-PG from [^{32}P]PEP, and very small amounts of UI could account for PGAM phosphoryltransfer activity (Figure 2c), it appears that this mechanism can account for phosphorylation of rPGAM1.

Because this mechanism of PGAM phosphorylation involves a phosphoryl exchange on PGAM1 rather than a net phosphoryltransfer from PEP to produce pyruvate, it is not competent to produce pyruvate from PEP without addition of ADP. An ADP-independent pyruvate kinase activity was suggested to be on the order of 30 to 60uM/min in the D0-500 fraction using NMR detection (Vander Heiden MG, 2010), a rate that could potentially be tracked using an LDH-linked assay for pyruvate. Such an approach could be more convenient and sensitive to assay pyruvate production from PEP. We looked for consumption of NADH linked to the production of

pyruvate in order to determine whether a separate activity not involved with PGAM phosphoryltransfer could account for such an ADP-independent PK activity. However, no detectable ADP-independent PK activity was found in the D50-500 fraction, even upon addition of rPGAM and/or 2,3-DPG (Figure 5), suggesting that an alternative activity to convert PEP to pyruvate is not present in this fraction. It is possible that our NADH-linked assay failed to detect pyruvate or interfered with the activity, that the D0-50 fraction contains the ADP-independent PK activity, or that the activity was not present in the cell lines used for these experiments.

Discussion

We were unable to discover a novel activity in cell culture lysates that phosphorylates PGAM1. In addition, our current mechanism involves a phosphoryl-exchange reaction on PGAM1 rather than a net phosphoryltransfer, and is inconsistent with net production of pyruvate from PEP via this mechanism of PGAM1 phosphorylation. Consistent with these findings, an ADP-independent pyruvate kinase activity was also not observed in this fraction. While this mechanism uncovered for PGAM phosphoryltransfer from PEP is well described (Rose,1976), there is still no known net phosphoryl donor for PGAM in most cells. In fact, only red blood cells are capable of producing net 2,3-DPG via BPGM, the enzyme ascribed to net 2,3-DPG production in mammalian cells (Fujita,1998). It has been proposed that the unstable 1,3-DPG produced during normal glycolysis is capable of phosphorylating PGAM, but this has not been directly demonstrated (Bond, 2002). As for all other possible, and necessarily unfalsifiable, ADP-independent PK hypotheses, it is impossible to say for certain that ADP-independent PK activity does not exist. Subsequent work could look for such activities in other cell lines, tissues, and tumors, and should focus on assaying directly for ADP-independent pyruvate production using mass spectrometry. NADH-linked assays, while convenient, could be misleading. For instance, commercially available NADH is contaminated with adenine nucleotides, namely AMP,

and this alone could give the false appearance of ADP-independent activity. Use of cells with pyruvate kinase deleted using CRISPR technology or other genetic approaches would also greatly facilitate such a search by eliminating contaminating canonical pyruvate kinase activity that is otherwise very abundant in most cells.

Materials and Methods

Reagents

Enolase, rabbit muscle pyruvate kinase, and lactate dehydrogenase were all obtained from Sigma. [γ-^{32}P]ATP was obtained from Perkin Elmer. Goat anti-Enolase (C-19) was from Santa Cruz Biotech (sc-7455) and used at 1:500, goat anti-PGAM1 was from Novus (NB100-774) and used at 1:1000. Western blots were blocked with milk and developed using appropriate HRP-linked secondary antibodies and chemiluminescence. All other chemical reagents were obtained from Sigma.

Cell culture and lysate preparation

293F cells were obtained from Life Technologies and cultured in plastic erlenmeyer flasks using FreeStyle 293 Expression Medium (Life Technologies) at 37°C and 5% CO_2. Cells were split 1:4 when they reached $2x10^6$ cells/mL. Cells were lysed by hypotonic lysis by swelling on ice for 10min in two equivalents of 1xHypotonic Lysis Buffer (20mM HEPES pH 7.0, 5mM KCl, 1mM $MgCl_2$, 2mM DTT, 1tab/10mL Complete EDTA-free protease inhibitor (Roche)), then passing through a 26 gauge needle 3x, then spinning 10min at 4°C at 16,000xg. S100 was prepared by further spinning the resulting whole cell lysate supernatant for 1hr at 4°C at 100,000xg.

[^{32}P]PEP synthesis

[^{32}P]PEP was synthesized as in (Vander Heiden, 2010). Briefly, 600 μCi of 10 mCi/mL of [γ-^{32}P]ATP (~2.2 μM final concentration) was incubated with 800 mM pyruvate, 50 mM Tris (pH 7.5), 50 mM KCl, 5 mM MgCl2, 1 mM DTT, and 5 units of rabbit muscle pyruvate kinase (Sigma) at 37°C for 1 hour. [^{32}P]PEP was immediately separated from [γ-^{32}P]ATP using anion exchange chromatography according to a modification of previously published method (Mattoo, 1983) using a Vivapure Q column (Sartorius). Bound product was washed with reaction buffer, and the [^{32}P]PEP eluted stepwise using 0.3 mM and 0.6 mM triethylammonium bicarbonate (TEAB) (pH 8.5). No difference in [^{32}P]PEP activity was noted in either the 0.3 mM or 0.6 mM fraction and they were used interchangeably as a source of [^{32}P]PEP. Separation of [^{32}P]PEP from [γ-^{32}P]ATP and ^{32}Pi was also confirmed by thin layer chromatography using PEI cellulose and 0.25 M ammonium bicarbonate as the mobile phase as described previously (Mattoo, 1983)

rPGAM phosphoryltransfer activity assay

Recombinant PGAM was cloned and expressed as in (Vander Heiden, 2010). Unless otherwise noted, the rPGAM phosphoryltransfer assay was carried out in a total volume of 30uL in water, with 1uL fraction, 1uL 1mg/mL rPGAM, 1uL 30xBuffer A (450mM $MgCl_2$, 60mM $MnCl_2$), ~2uCi [^{32}P]PEP as described above, 1uL 300uM PEP, 1uL 30mM ATP, and 3uL 10xReaction Buffer (500mM Tris pH 7.5, 500mM KCl, 10mM DTT). Reactions were carried out at 30°C for 8 minutes unless otherwise noted and stopped by the addition of SDS loading dye or by loading and drying onto a TLC plate or by extraction with methanol. Reactions were analyzed using standard SDS-PAGE and autoradiography or TLC.

Thin layer chromatography

Thin layer chromatography was performed as previously described (Mattoo, 1983). Briefly, 0.5uL of each sample was spotted on PEI Cellulose plates (EMD Merck) and developed in a

glass TLC tank (Analtech) pre-equilibrated with 0.25M Ammonium Bicarbonate. Plates were pre-dried before spotting and dried after development with a hair dryer.

Cellular buffered extraction

4mL methanol, 950uL water, and 50uL 100XBuffer (2M HEPES pH 7.0, 500mM KCl, 100mM $MgCl_2$) were added to $5x10^8$ pelleted cells in a 15mL polypropylene conical. 10mL chloroform was then added and the sample was vortexed for 10min, then spun 10min at 4°C at 4000xg. Both methanol and chloroform layers were separated from the thick pellet at the solvent interface, mixed and re-spun together 10min at 4°C at 4000xg. The top layer (methanol/water) was aliquoted in 1mL portions and dried under dry nitrogen at room temperature. Aliquots were resuspended in 500uL 1xHypotonic Lysis Buffer (20mM HEPES pH 7.0, 5mM KCl, 1mM $MgCl_2$, 2mM DTT, 1tab/10mL Complete EDTA-free protease inhibitor (Roche)).

Methanol extraction

Methanol extraction was done at a final concentration of 80% ice-cold methanol. Samples were vortexed for 10min and spun down for 10min at 4°C at 16,000xg. Supernatant was transferred to another tube and dried under dry nitrogen gas at room temperature.

Ion-pairing reverse phase HPLC

Separation was achieved on an Agilent 1200 System HPLC equipped with a binary pump and a multiple wavelength detector. Analytical separations were achieved at 1mL/min flow rate on a 4.6x150mm, 5um ZORBAX SB-C18 column. Preparative separations were achieved at 4mL/min flow rate on a 9.4x150mm, 5um ZORBAX SB-C18 column. For separation of UI and PEP, 10-100uL of dried methanol-extracted UI synthesis reaction resuspended in water was injected once. Solvent A was 10mm tributylamine/15mM acetic acid in 100% water, Solvent B was 100% methanol . Gradient was as follows 0min:0%B, 5min:0%B, 7min:20%B,

17min:28%B, 25min:38%B, 31min:90%B, 35min:100%B, 45min:100%B, 55min:0%B. Before NMR, the sample was additionally injected into an isocratic flow of 10mM Ammonium Acetate/5mM Acetic Acid and recovered by scintillation counting to remove tributylamine.

NMR of UI

200uL of the cellular buffered extraction was incubated with 240uL water, 60uL 100mM PEP, 10uL 60mM ATP, 20uL 30x Buffer A (450mM $MgCl_2$, 60mM $MnCl_2$), 60uL 10xReaction Buffer (500mM Tris pH 7.5, 500mM KCl, 10mM DTT), and either 10uL freshly made [^{32}P]PEP or 0.3M Triethylammonium Bicarbonate Buffer (pH 8.0, Sigma). The reaction was incubated for 32min at 30°C and extracted with 800uL methanol and 1600uL chloroform. After vortexing for 10min, and spinning 10min at 4°C at 16,000xg, the upper layer (methanol/water) was aliquoted and dried under dry nitrogen at room temperature. The resulting pellet was resuspended in 110uL of water and 100uL was injected for HPLC. The radioactive sample was run first by HPLC after a blank run to determine the location of the UI-containing fraction, which was then collected on an adjacent run of the non-radioactive sample. These UI-containing fractions were dried directly under dry nitrogen at room temperature, then run on the isocratic gradient by HPLC and dried again to remove tributylamine; the radioactive sample was again used to guide fraction collection of the non-radioactive sample. The final dried fraction was dissolved in 35mM [U-^{2}H]Tris Base in 99.9% D_2O until it reached pH 7.5, then diluted with 99.9% D_2O and 35mM [U-^{2}H]Tris Base pH 7.5 in 99.9% D_2O (pHed with 35% w/v DCl in D_2O) until the final solution was 15mM [U-^{2}H]Tris-DCl pH7.5 in 700uL. NMR spectra were collected using a 500 MHz Varian Inova NMR spectrometer equipped with a 5mm pulse field gradient inverse probe.

The 1-D ^{1}H NMR spectrum was collected with a 90 degree pulse of 9.5us, a sweep width of 1546 Hz spanning a spectral window from 2.3 to 5.4 ppm. The FID acquisition time was 3 seconds and the relaxation delay was 2 seconds, giving a total of 5 seconds for each scan. A

total of eight scans were averaged to obtain the resulting spectrum. No apodization was applied to the time domain data because resonances showed sufficient natural line widths on the order of two Hz. Zero filling of the time domain data was done to generate a frequency spectrum with 256k points (128k complex).

The 2-D ^{1}H-^{1}H gCOSY NMR spectrum was collected with the same ^{1}H 90 degree pulse and spectral window as for the 1-D ^{1}H spectrum described above. A total of 32 transients were summed and 128 t1 time increments were used over the course of the data collection. The total size of the transformed data set was 512 x 512 (same resolution as 1024 x 1024 complex). The f2 data, with 256 data points, was collected for 166 ms. The f2 data was apodized with a squared sine bell function with a maximum at 83 ms. Linear prediction was used to double the size of the t1 data from 128 to 256 points. The t1 time domain data was also apodized with a squared sine bell function with a maximum at 83 ms.

The 2-D ^{1}H-^{13}C HSQC NMR spectrum was collected with the same ^{1}H 90 degree pulse and spectral window as above. A total of 2x48 transients were averaged for each t1 evolution time (real and imaginary), and with 128 t1 time increments the total number of FIDs acquired was therefore 256 (because the spectrum is phase sensitive). Acquisition of the t2 time domain data occurred for 100 ms in order to keep X-decoupling times short and sample heating to a minimum. With the narrowness of the ^{1}H spectral window, the short t2 acquisition time resulted in collecting just 310 points (155 x 2). The ^{13}C spectral window spanned from 0 to 220 ppm (27643.4 Hz), and the ^{13}C 90 degree pulse was 17.3 us. The t2 time domain data was apodized with a gaussian function with a 76 ms time constant. Linear prediction was used to extend the t1 time domain data from 128 to 512 (complex), and t1 time domain data was apodized with a gaussian function with a time constant of 9 ms. The final size of the 2-D data matrix was 256 complex points in f2 and 1024 complex points in f1.

The 2-D ^{1}H-^{13}C gHMBC NMR spectrum was collected with the same ^{1}H and ^{13}C parameters as the HSQC spectrum described above, with the following exceptions. A total of 96 transients were averaged for each t1 evolution time. The total number of t1 time increments was 396. The acquisition time of the t2 data was 165 ms and the total number of point collected was 256. The t2 time domain data was apodized with a sine bell function with a maximum at 83 ms. Linear prediction was used to extend the number of t1 data points from 396 to 512. The t1 time domain data was apodized with a sine bell with a maximum at 9 ms. The total size of the data matrix was 256 along the f2 frequency axis and 1024 along the f1 frequency axis.

Ion exchange fractionation

Unless otherwise noted, D and S ion exchange fractionation was achieved on Vivapure Mini H columns (Sartorius) as per Sartorius protocols in a fixed-rotor centrifuge at 4°C. 400uL of 9ug/uL S100 in 1xHypotonic Lysis Buffer (20mM HEPES pH 7.0, 5mM KCl, 1mM $MgCl_2$, 2mM DTT, 1tab/10mL Complete EDTA-free protease inhibitor (Roche)) was loaded after equilibration with 400uL 1xHypotonic Lysis Buffer. The column was then washed with 400uL of 1xHypotonic Lysis Buffer and fractionation proceeded in a gradient of NaCl in 1xHypotonic Lysis Buffer. Two 100uL elutions at each step of the gradient were collected and pooled.

Size exclusion desalting

G-25 Sephadex Fine (Sigma) was swelled overnight at 0°C in 20mL/g of 1xBuffer (20mM HEPES pH 7.0, 5mM KCl, 1mM $MgCl_2$, 2mM DTT). 4mL of resin was packed by gravity flow on a 5mL disposable column (Pierce) and 400uL of input was desalted by gravity flow. Bio-Rad bradford reagent was used to assay for protein and locate the high molecular weight desalted fractions.

LDH-linked PK Assay

2ug (or fraction equivalent) of lysate was assayed with 500uM final PEP or water, 600uM final ATP or water, 180uM final NADH, and 0.16mg/mL LDH in 1xReaction Buffer (50mM Tris pH 7.5, 50mM KCl, 1mM DTT) in 100uL total at 37°C. Decrease in NADH fluorescence was followed in a Tecan plate reader and a regression on the slope of the decrease was taken as the activity. Activity was converted to uM of NADH by running a standard curve.

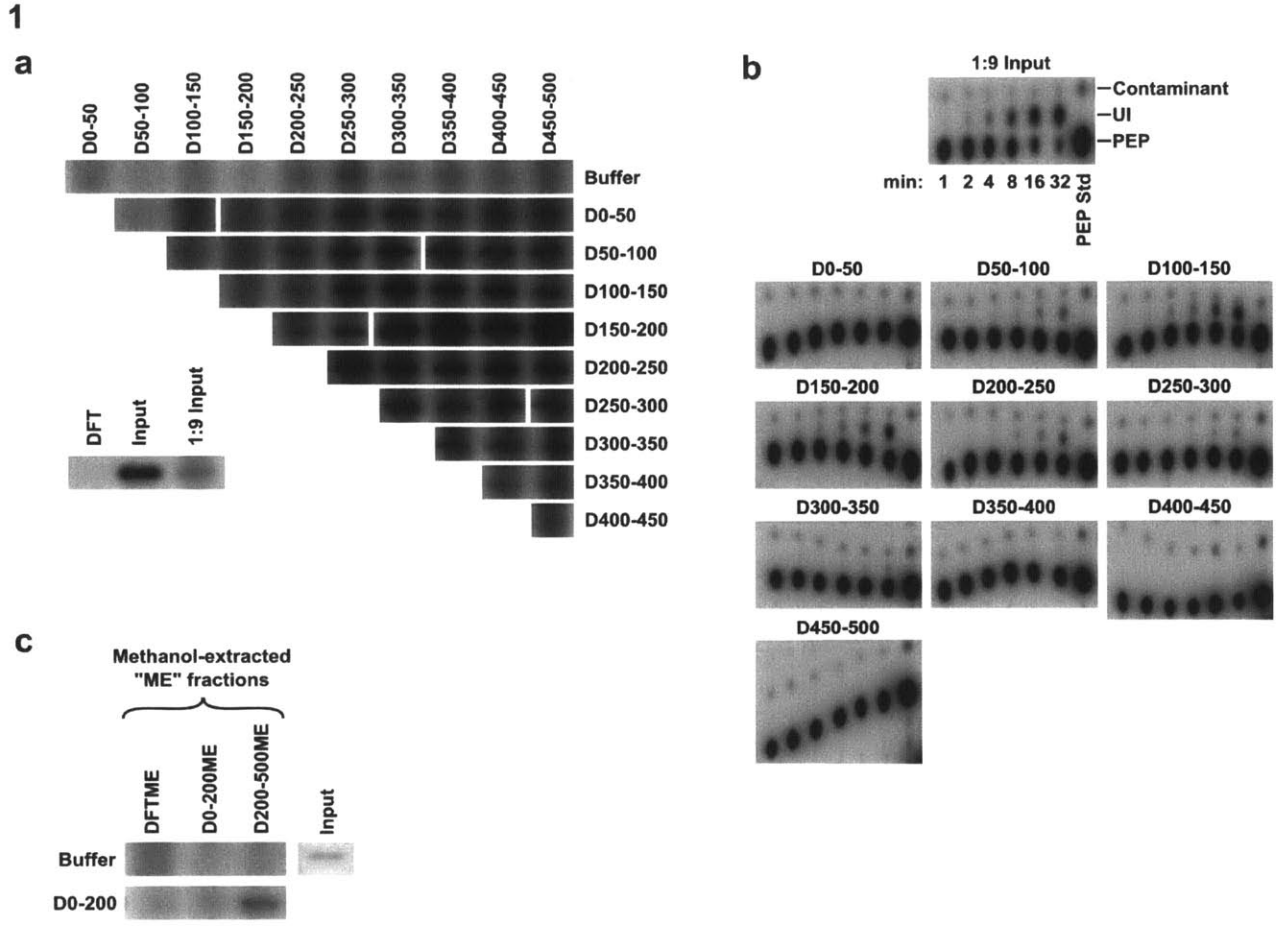

Figure 1 - The PGAM phosphoryltransfer activity has at least two necessary components, one associated with an enzymatic activity and the other a metabolite. a) 293F cells were lysed, and S100 from these cells was fractionated on a D column stepwise with sodium chloride from 0 to 500mM. The flow-through (FT) was also collected. Fractions were combined pairwise and assayed for rPGAM phosphoryltransfer activity from [^{32}P]PEP after an 8 minute incubation. b) The same reactions were assayed separately by TLC at the indicated times. This showed accumulation of an unknown intermediate (UI) and consumption of PEP. The location of PEP by TLC was identified by running a standard (PEP Std). c) D column fractions were extracted with 80% methanol, dried under nitrogen gas, and combined with buffer control or a fresh non-extracted D0-200 fraction as indicated. Input rPGAM phosphoryltransfer activity from [^{32}P]PEP prior to fractionation is also shown.

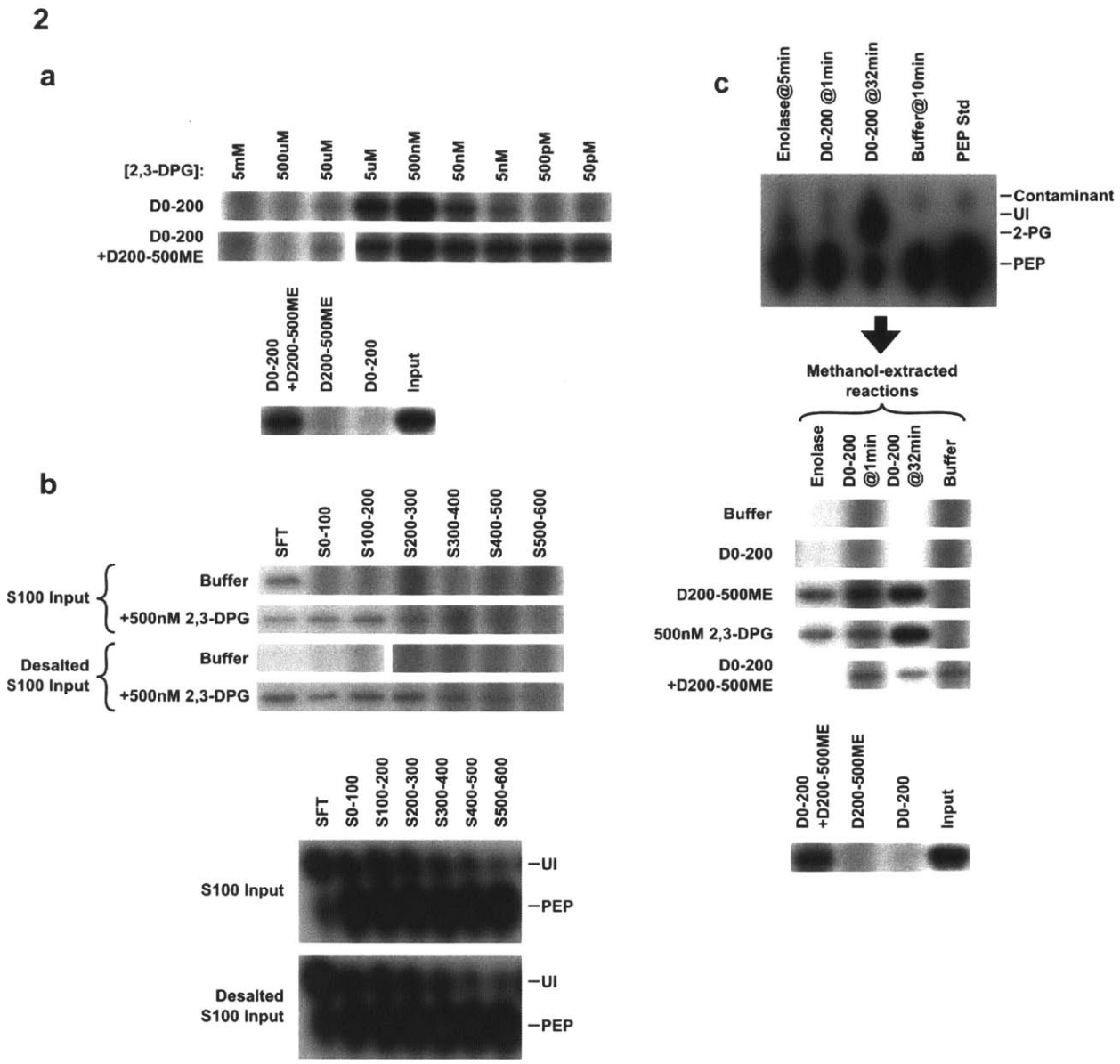

Figure 2 - 2,3-DPG is sufficient for the metabolite portion of the activity, and the unknown intermediate (UI) is sufficient for the enzyme-associated portion of the activity. a) 293F cells were lysed and S100 from these cells was fractionated on a D column stepwise with sodium chloride from 0mM to 500mM. Some fractions were additionally methanol extracted (ME). Fractions were assayed separately and in combination with various amounts of added 2,3-DPG for rPGAM phosphoryltransfer activity from [^{32}P]PEP. Input rPGAM phosphoryltransfer activity from [^{32}P]PEP prior to fractionation is also shown. b) 293F S100 was desalted or used as input directly on an S column, which was eluted stepwise with sodium chloride from 0mM to 600mM. Fractions were assayed in combination with 2,3-DPG for rPGAM phosphoryltransfer activity from [^{32}P]PEP, or by TLC without rPGAM for production of UI from [^{32}P]PEP. c) 293F S100 was fractionated as in (a) and the resulting D fractions and rabbit muscle enolase were reacted with [^{32}P]PEP but without rPGAM for the indicated times. The reactions were assayed

by TLC for production of 2-PG and UI, then extracted with 80% methanol and dried. These extracts were then combined with fresh and methanol extracted D fractions from 293F S100 without [^{32}P]PEP but with rPGAM and assayed for rPGAM phosphoryltransfer activity.

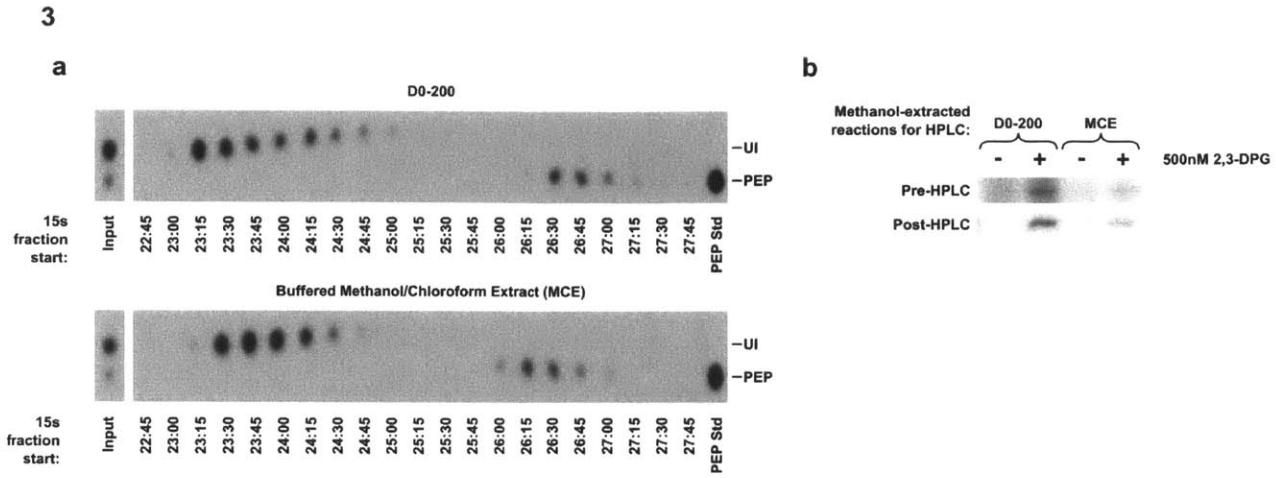

Figure 3 - The unknown intermediate (UI) can be purified in an active form via HPLC. a) 293F cells were extracted directly in a HEPES-buffered biphasic Methanol/Water/Chloroform solvent system and the methanol/water fraction was dried under nitrogen (MCE). Separately, 293F S100 was fractionated on a D column stepwise with sodium chloride from 0mM to 200mM. Fractions were incubated with [^{32}P]PEP without rPGAM with either 10uM (D0-200) or 1mM (MCE) cold carrier PEP to form UI and then reactions were extracted in 80% methanol and dried. Ion-pairing reverse phase HPLC was performed and 15s fractions were collected and run on TLC plates to confirm separation of UI and PEP, as well as co-elution of UI from MCE and UI from D0-200. b) Methanol-extracted reactions as in (a), except performed with 10uM carrier PEP for both MCE and D0-200, were fractionated on HPLC as in (a) and the UI-containing fractions were collected and dried down. The resulting fractions were added to 2,3-DPG and assayed for rPGAM phosphoryltransfer activity pre- and post-HPLC fractionation for UI.

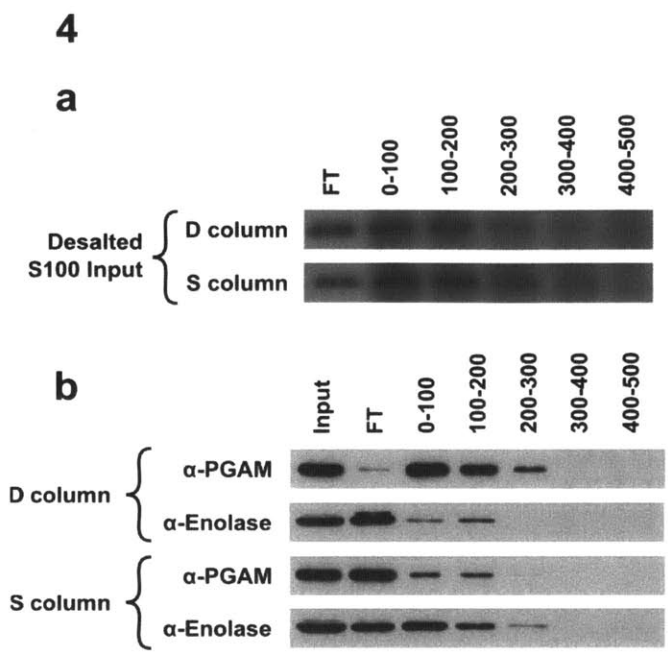

Figure 4 - Enolase and PGAM are both present in the UI-producing fractions. a) Desalted 293F S100 was used as input to a D and S column fractionation using sodium chloride from 0mM to 500mM. Fractions were combined with 500nM 2,3-DPG and assayed for rPGAM phosphoryltransfer activity. b) Western blots for enolase and PGAM on fractions used in (a)

5

LDH-linked Pyruvate Kinase assay (uM/min)

Fraction	[PEP]	[ADP]	+Buffer	+rPGAM	+rPGAM +DPG
S100 1ug/uL	0uM	0uM	0.60	0.00	0.00
	500uM	0uM	0.83	0.00	0.14
	500uM	600uM	28.45	41.30	34.85
S50-400	0uM	0uM	0.00	0.00	0.00
	500uM	0uM	0.00	0.00	0.00
	500uM	600uM	0.61	0.48	0.53
D50-500	0uM	0uM	0.00	0.00	0.00
	500uM	0uM	0.00	0.01	0.00
	500uM	600uM	0.00	0.00	0.00

Figure 5 - There is no significant ADP-independent pyruvate kinase activity associated with the PGAM phosphoryltransfer activity bound to the D column. 9ug/uL 293F S100 was used as input to a D and S column fractionation using sodium chloride at the indicated concentrations. Each fraction was assayed in a 100uL total LDH-linked PK assay with the indicated concentrations of ADP and PEP at 37°C. Activities were converted to uM/min using an NADH standard curve and normalized to 2ug of input lysate.

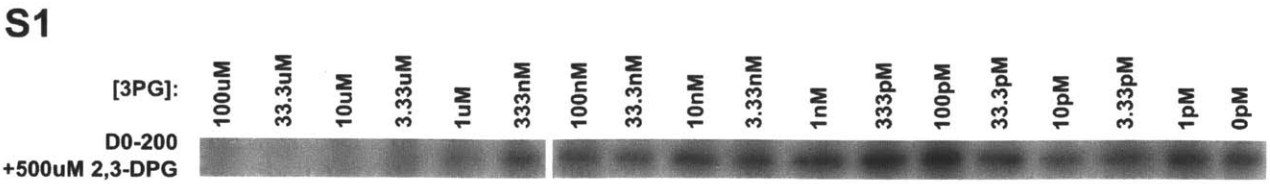

Figure S1 - Cold 3-PG can inhibit the PGAM phosphoryltransfer assay. 293F S100 was fractionated on a D column using sodium chloride from 0mM to 200mM. The resulting D0-200 was assayed with 500nM 2,3-DPG and varying concentrations of 3-PG for rPGAM phosphoryltransfer activity.

References

Bond CS, White MF, Hunter WN. (2002). Mechanistic implications for Escherichia coli cofactor-dependent phosphoglycerate mutase based on the high-resolution crystal structure of a vanadate complex. J Mol Biol 316, 1071-81.

Fujita T, Suzuki K, Tada T, Yoshihara Y, Hamaoka R, Uchida K, Matuo Y, Sasaki T, Hanafusa T, Taniguchi N. (1998). Human erythrocyte bisphosphoglycerate mutase: inactivation by glycation in vivo and in vitro. J Biochem 124, 1237-44.

Mattoo RL, Waygood EB. (1983). An enzymatic method for [32P]phosphoenolpyruvate synthesis. Anal Biochem 128, 245-9.

Rose ZB, Dube S. (1976). Rates of phosphorylation and dephosphorylation of phosphoglycerate mutase and bisphosphoglycerate synthase. J Biol Chem 251, 4817-4822.

Vander Heiden MG, Locasale JW, Swanson KD, Sharfi H, Heffron GJ, Amador-Noguez D, Christofk HR, Wagner G, Rabinowitz JD, Asara JM, Cantley LC. (2010). Evidence for an alternative glycolytic pathway in rapidly proliferating cells. Science 329, 1492-1499.

Chapter 3 - Glycolytic serine biosynthesis modulates flux of folate one-carbon units[2]

Authorship Statement

Portions of the materials and methods are modified from or copied verbatim from (Lewis, 2014, Lunt, 2014 and Mattaini, 2015)
Figure 1f is in submission in (Mattaini, 2015)
Figures 1d and 1e are courtesy of Katie Mattaini
Figure 2b is courtesy of Aaron Hosios and Caroline Lewis
Figure 4, 5a, and 5b are modified from (Lewis, 2014)

Introduction

Given what was known about the connection between PK activity and glycolytic serine biosynthesis, we examined whether modulation of serine synthesis could explain the requirement for regulated pyruvate kinase activity in proliferating cells. Increased expression of PHGDH to increase serine synthesis is observed in some cancers, however serine itself fails to rescue reduced viability upon PHGDH knockdown in these cells (Locasale, 2011 and Possemato, 2011) arguing that increased serine synthesis from glycolytic intermediates provides another advantage for cells beyond serving as a source of serine. We evaluated four mutually exclusive hypotheses consistent with non-serine rescue of decreased glycolytic serine biosynthesis and discovered a mechanism that could explain for the first time how PK inhibition supports biomass accumulation. We found that a unique product of the serine biosynthesis pathway, phosphoserine, can limit the use of glycine to synthesize serine in the cytosol and "waste" one-carbon units in the folate pool that are required for nucleotide synthesis. These data suggest a way for metabolism to directly sense the availability of glucose, transaminatable nitrogen, and one-carbon equivalents to control de novo nucleotide synthesis and proliferation.

[2] This chapter represents core elements of a manuscript I am collaborating with others to publish in the next year.

Results

To understand the contribution of de novo serine biosynthesis to cancer cell serine availability, we characterized the glycolytic serine biosynthesis pathway across several cell lines. As PHGDH is an important component that catalyzes the first step in this pathway, and is genomically amplified to increase expression in human cancer (Beroukhim, 2010), we surveyed several lines for PHGDH expression (Figure 1a), intracellular phosphoserine levels (Figure 1b), and contribution from [U-^{13}C]glucose to m+3 serine (Figure 1c). Lack of PHGDH expression in MDA-MB-231 and MCF7 cells was correlated with decreased phosphoserine, and decreased flux from glucose to serine, while expression of PHGDH supported varying levels of phosphoserine and use of glucose to generate serine, possibly due to variable activity of PSAT and PSPH across cells. We also confirmed that re-expression of wild-type PHGDH, but not a mutant lacking catalytic activity (R236E) (Mattaini, 2015) rescues both phosphoserine levels as well as pathway flux in MDA-MB-231 cells (Figures 1a-c). Many of the cell lines examined, including MDA-MB-468 and TT cells, are known to be dependent on PHGDH expression (Locasale, 2011, Possemato, 2011, and Mattaini, 2015) and we are able to show that a 10x increase of media serine does not rescue proliferation arrest caused by shRNA knockdown of PHGDH expression (Figure 1d). These findings are consistent with observations in other cell lines showing serine supplementation could not rescue loss of serine synthesis pathway activity (Locasale, 2011 and Possemato, 2011). We additionally confirmed that the increased serine was accompanied by increased serine uptake in these cells, excluding the possibility that lack of rescue was due to a defect in serine transport (Figure 1e). Lastly, proliferation arrest caused by shRNA knockdown of PHGDH was rescued by PHGDH expression but not expression of catalytically dead PHGDH (Figure 1f). This supports that the effects of PHGDH shRNA are on-target and that enzymatic activity is necessary for proliferation in PHGDH-dependent lines.

Creating stable cell lines with PHGDH knockdown in PHGDH-dependent but not PHGDH-independent cell lines was difficult, so we used a PHGDH inhibitor developed in the Sabatini lab to characterize the requirements for PHGDH activity in cells. As an added benefit, this reagent also allowed us to inhibit PHGDH with more rapid kinetics than an shRNA, which is dependent on the rate of protein turnover. The inhibitor has been fully characterized and is thought to bind at least partially in the 3-PG binding pocket, and counter-screens against a variety of other dehydrogenases suggest it is relatively specific for PHGDH (Pacold, in preparation). We confirmed in our own hands that the inhibitor abrogated flux from [U-^{13}C]glucose to m+3 serine in TT and MDA-MB-468 cells (Figure 2a). PHGDH-dependent cell lines treated with inhibitor exhibited proliferation arrest followed by cell death within 48-96h. To determine whether the cells were arresting at a specific phase of the cell cycle prior to death, we examined DNA content in cells treated with PHGDH inhibitor or vehicle control. Interestingly, we found an accumulation of S-phase cells 24-48h after exposure to PHGDH inhibitor, suggesting that PHGDH inhibition causes a block in S-phase progression (Figure 2b).

Having initially characterized genetic and chemical inhibition of PHGDH in dependent cell lines, we next examined several hypotheses for why PHGDH expression and/or glycolytic serine synthesis could be important for proliferation. First, we considered whether PHGDH had a non-enzymatic function; however, the failure of catalytically dead PHGDH to rescue PHGDH loss argued strongly against this possibility (Figure 1f). Second, we considered whether glycolytic serine biosynthesis is required for glutamine metabolism to supply alpha-ketoglutarate for TCA cycle anaplerosis in dependent lines, a previously suggested hypothesis consistent with serine non-rescue of PHGDH inhibition (Possemato, 2011). To examine this possibility, we measured the fraction of glutamine transamination net flux accounted for by net serine production in dependent cell lines using an [alpha-^{15}N]glutamine tracer and quantitated absolute levels of m+1 amino acids in media using GC-MS. To be ensure that m+1 species evaluated represent net

transamination flux rather than isotope exchange flux, we focused on amino acids whose transamination is protected from net exchange by an irreversible step (for example PSPH-catalyzed dephosphorylation to produce serine), or amino acids which are not supplied in the media and thus must be synthesized de novo. Even considering both serine and glycine together, and comparing with new alanine synthesis, it was clear that glycolytic serine production accounts for <20% of total net transamination in cells (Figure 2c). These data suggest alanine transamination is orders of magnitude higher than serine/glycine transamination, and argue against transamination to generate serine as a major source of alpha-KG. They also suggest that replenishment of TCA cycle carbon may not be the sole driver of PHGDH dependence, at least in cell culture.

Thirdly, we explored whether glycolytic serine and exogenous serine were channeled to different fates in cells. Given our data suggesting that serine synthesis might be required for S-phase progression (Figure 2b), we considered whether glycolytic serine was preferentially channeled to nucleotide production in comparison to exogenous serine. The carbons at positions 1 and 6 of glucose become the carbons on position 3 of serine, which is also the serine carbon donated to the folate one-carbon pool for nucleotide synthesis when serine is metabolized to glycine. Because the 1 position carbon is scrambled by the pentose phosphate pathway for incorporation into serine and other downstream metabolites, we compared labeling with [6-^{13}C]glucose versus [3-^{13}C]serine, with the caveat that [6-^{13}C]glucose should label at most half of the glucose-derived serine. To measure folate one-carbon contributions to nucleotide metabolism, we used labeled cells for 10 days and measured ^{13}C incorporation into the pyrimidines dTMP and dCMP in DNA. Folate one-carbon units do not contribute to dCMP synthesis, whereas the 5'-methyl group of dTMP is derived from 5,10-methylene-THF, a direct product of serine to glycine conversion. Thus, any m+1 shift of the mass isotopomer distribution from dCMP to dTMP is due to labeling from the folate one-carbon pool, and would be derived

from the 3 carbon of serine. As a control, we examined ^{13}C incorporation in serine present in whole cell protein. [6-^{13}C]glucose and [3-^{13}C]serine labeling led to similar amounts of m+1 shift from dCMP to dTMP as their contribution to serine in protein, 5-10% and 70-80%, respectively (Figure 2d). These data suggest that either glucose-derived serine is not channeled to folate one-carbon pools for dTMP biosynthesis or that the 3-position of serine is in rapid equilibrium such that channeling cannot be measured using this approach. We found evidence for the latter, as serine was observed to isotopically equilibrate with phosphoserine, despite the net irreversibility of the PSPH step (Figure 2e). After 24h of labeling with [U-^{13}C]serine, the mass isotopomer distribution of serine was identical to that of phosphoserine. These findings are consistent with the known mechanism of the PSPH phosphatase, which occurs via a phosphoenzyme intermediate rather than directly cleaving the phosphoserine phosphoryl group with water (Collet, 1999 and Neuhaus, 1959a, 1959b, 1960, also see Figure 9 in introduction). Therefore, distinguishing phosphoserine derived from de novo synthesis and free serine is not possible, and this argues that if channeling were occurring in cells, it would not be detectable using ^{13}C-labeling experiments. Regardless, the rapid equilibration of free serine and phosphoserine implies that the exogenous and newly synthesized serine pools are well mixed and argues against substrate channeling as the explanation for cell dependence on new serine production.

Lastly, we considered the general set of possibilities that one or more intermediates in the serine biosynthesis pathway is important for proliferative metabolism in PHGDH-dependent cells. Specifically, given our result that serine and phosphoserine isotopically equilibrate, we wondered whether phosphoserine could be a substrate for serine-dependent folate one-carbon reactions, as this would not be detected by traditional ^{13}C labeling experiments in cells. If true, this could explain how PHGDH activity allows progression through S phase by replenishing the folate one-carbon pool for nucleotide biosynthesis. In support of this hypothesis, while serine

levels are insensitive to PHGDH inhibition in dependent cell lines, phosphoserine is almost completely eliminated (Figure 3a). To determine whether SHMT1, the cytosolic enzyme that catalyzes serine breakdown to folate one-carbon units, could distinguish between serine and phosphoserine as a substrates, we examined the ability of the enzyme to use either substrate in vitro. Preliminarily, we find that neither cytosolic SHMT1 nor mitochondrial SHMT2 use phosphoserine as a substrate. Instead, phosphoserine inhibits the serine-dependent SHMT1 reaction. This result is currently being replicated to produce publication-quality data. This provides a mechanism by which levels of phosphoserine can have a biological effect on cells to influence one-carbon metabolism in cells.

We reasoned that SHMT1 inhibition by phosphoserine could increase availability of one-carbon units if SHMT1 catalyzes serine production from glycine and removes folate one-carbon units from the cytosol. To test this possibility, we examined the directionality of folate one-carbon metabolism, which is compartmentalized between the cytosol and mitochondria (see Figures 10 and 13 in the Introduction). Folate one-carbon metabolism is proposed to result in serine breakdown to formate in the mitochondria and ligation/reduction to 10-formyl-THF and 5,10-methylene-THF for A,G, and T synthesis in the cytosol (Tibbetts, 2010), although others have suggested cytosolic folate species can be derived from serine in the cytosol directly though SHMT1 (Fan, 2014). To further confirm that this is the case and provide the first direct evidence for directionality of the folate one-carbon cycle (see Figure 13 in introduction), we utilized a previously published system that allowed us to measure compartmentalized NAD(P)(H) flux (Lewis, 2014). Our system relies on expression of mutant IDH isoforms in the cytosol (mtIDH1-C) or mitochondria (mtIDH2-M), which produce 2-HG from compartmentalized pools of aKG and NAD(P)H. Because 2-HG accumulates and is not appreciably broken down in the cell, measuring labeling on 2-HG in cell lines expressing compartmentalized mutant IDH allows us to infer labeling from the reducing hydride of compartmentalized NAD(P)H. We had previously

confirmed that labeling on 2-HG in mtIDH1-C and mtIDH2-M cells from glucose deuterated on specific positions was consistent with known compartmentalization of metabolism (Figures 4a and 4b). [3-^{2}H]glucose labels cytosolic NADPH through the pentose phosphate pathway (Figure 4a), whereas [4-^{2}H]glucose labels cytosolic NADH, which can isotopically equilibrate with mitochondrial NADH via the malate-aspartate shuttle (Figure 4b). We had previously used this system to test the directionality of the MTHFD reaction downstream of serine-glycine interconversion in the cytosol and mitochondria with labeling from [2,3,3-^{2}H]serine and [3,3-^{2}H]serine (Figure 5a). We found that in A549 cells, mitochondrial MTHFD oxidizes 5,10-methylene-THF, whereas cytosolic MTHFD does not have oxidative flux (Figure 5b). We are working to extend this result to other cell lines in support of folate one-carbon units being primarily derived from mitochondrial formate, although the consumption of folate species to produce serine from glycine has been proposed to limit proliferation in other systems (Labuschagne, 2014).

Another established method to ascertain the directionality of the folate one-carbon cycle is to trace [3,3-^{2}H]serine into thymidine (Herbig, 2002). One-carbon units derived via mitochondrial formate retain only m+1 label, whereas one-carbon units derived via SHMT1 without equilibration across the cytosolic MTHFD step retain m+2 label (Figure 5a). Assuming that cytosolic MTFHD isotopic equilibration is constant, the m+2/m+1 ratio in thymidine from DNA obtained from [3,3-^{2}H]serine reflects the relative net flux from serine to glycine across SHMT1 normalized to flux from serine through mitochondrial formate to cytosolic 5,10-methylene-THF. In MDA-MB-468 cells after 10d of labeling with [3,3-^{2}H]serine, we found that there was no detectable m+2 thymidine in DNA, consistent with SHMT1 inhibition by phosphoserine in these PHGDH-dependent cells. However, in our MDA-MB-231 cells with minimal PHGDH expression and undetectable phosphoserine, we find m+2 thymidine in DNA consistent with SHMT1-derived folates contributing to thymidine in these cells. When wild-type, but not catalytically

dead (R236E) PHGDH, is expressed, lower m+2/m+1 labeling is observed, consistent with increased serine pathway flux limiting SHMT1 flux in these cells (Figure 5c). These data suggest that phosphoserine can limit SHMT1 activity in cells.

Having demonstrated inhibition of SHMT1 in cells when PHGDH activity is increased, we sought to determine the importance of this inhibition in PHGDH-dependent cells. We reasoned that PHGDH-dependent cells should "waste" folates through SHMT1 at baseline, and set out to measure this using [^{13}C]formate contribution to serine across a panel of PHGDH-dependent and non-dependent cell lines. Only the PHGDH-dependent lines MDA-MB-468 and TT exhibited appreciable wasting of folates from formate as measured by formate incorporation into serine (Figure 5d, corrected natural abundance is ~5%), suggesting that SHMT1 inhibition by phosphoserine could be important for conservation of folate one-carbon pools in these dependent cell lines. We continue to test the hypothesis that phosphoserine inhibition of SHMT1 is a cause of PHGDH-dependence in some contexts.

Discussion

Central carbon and amino acid metabolism are two of the most ancient and conserved biologic processes. Therefore, it is often a concern that elements of these pathways are no longer relevant in mammalian, let alone cancer biology, and are merely relics that evolved to meet the needs of a much simpler organism. After all, mammalian cells have myriad other seemingly more sophisticated ways of processing information about cell state and effecting regulation, from transcription factors, to posttranslational modifications, to microRNAs. In fact, gene regulation itself was first understood in the context of metabolism with studies of the *lac* operon. It is therefore interesting to consider why mammalian cells use phosphoserine to inhibit SHMT1 and control proliferation in the context of PHGDH-dependent cells. Indeed, even assuming that

serine prototrophy is a desirable trait in mammals, there are at least three other ways to make serine: from glycine, from hydroxypyruvate (a pathway mammals lack), and from cysteine.

The model where phosphoserine control of SHMT1 is involved in control of proliferative metabolism is supported by two additional pathway features apart from SHMT1 inhibition. First, the phosphatase PSPH works via an unusual phosphoenzyme intermediate which preserves phosphoserine under high serine conditions. Second, the entire pathway is unusual in that it is not product inhibited at the first step (PHGDH) as in some bacterial species (Fell, 1988), which allows for accumulation of phosphoserine when serine is abundant. We would propose that a primary reason to use this unusual glycolytic pathway is to integrate the simultaneous availability of glucose, serine, and transaminatable nitrogen. These three components together form a necessary and sufficient set of ingredients for purine and pyrimidine biosynthesis even if exogenous serine is the primary source of serine in most cells. In addition, our preliminary data that SHMT2 is not inhibited by phosphoserine suggests that phosphoserine inhibition of SHMTs is not simply due to chemical similarity between serine and phosphoserine. Both the peculiar regulation of glycolytic serine synthesis and lack of phosphoserine-dependent SHMT2 inhibition support a model where glycolytic control of SHMT is important specifically in the cytosolic compartment.

But why not turn off SHMT1 using a metabolite-sensing transcription factor, or modulate epigenetic markers and transcription factors as in the commonly accepted mechanisms for isocitrate dehydrogenase and fumarate hydratase (Losman, 2013 and Pollard, 2005)? There are two possibilities. Metabolic control of nucleotide production provides a direct as well as rapid way to coordinate information about precursor species in the cell that may vary on timescales faster than can be modulated by gene expression. Another more intriguing possibility is that phosphoserine regulation of SHMT1 is a mechanism for cells to also

coordinate new serine synthesis from glycine and glucose. Decreased serine will both activate the glycolytic serine pathway as well as decrease phosphoserine, which then de-inhibits SHMT1 and activates serine synthesis from glycine, providing a second route of serine synthesis. Beyond simple allostery, phosphoserine inhibition of SHMT1 and the properties of the glycolytic serine pathway that support it form an example of how multiple metabolic inputs can be processed and modulate proliferative metabolism.

In addition to its role as a fast and efficient integrator of precursors for nucleotide synthesis and coordinator of serine synthesis from glucose and glycine, phosphoserine inhibition of SHMT1 may also explain the importance of elevated rates of glycolysis and the requirement for regulating PKM2 to decrease activity in proliferative metabolism. In fact, many aspects of our work have been inspired by the recent discoveries that chemical activation of PKM2 downregulates glycolytic serine synthesis (Kung, 2012), and PKM1-induced proliferation arrest in MEF is rescuable by thymidine (Lunt, 2015). Maintenance of elevated levels of phosphoserine in cells may be one way decreased PKM2 activity supports proliferative metabolism.

Materials and Methods

Reagents

anti-PHGDH was rabbit polyclonal from Sigma (HPA021241) and used at 0.2ug/ml, anti-HSP90 was from CellSignaling (4877S) at 1ug/ml. All cells were cultured in DMEM -pyruvate from Cellgro (10-017-CV) with 10% Fetal Bovine Serum from Sigma (F2442). Metabolomics experiments were performed in media with 10% dialyzed fetal bovine serum from Sigma (F0392). [^{13}C]Formate (CLM-583), [U-^{13}C]glucose (CLM-1396), [6-^{13}C]glucose (CLM-1396), [4-^{2}H]glucose (DLM-9294), [3-^{2}H]Glucose (DLM-3557), [U-^{13}C]serine (CLM-1574-H), [3-^{13}C]serine

(CLM-1572), [3,3-^{2}H]serine (DLM-161), and [alpha-^{15}N]glutamine (NLM-1016) were from Cambridge Isotope Labs. [U-^{14}C]serine was from Perkin Elmer (NEC-286E). DNA stain FxCycle Violet from Life Technologies (F-10347) was used for flow cytometry. MOX reagent was from Thermo (TS-45950), TBDMS was from Sigma-Aldrich (375934). All other solvents and chemicals were from Sigma-Aldrich.

Cell Lines, Tissue Culture, and Media

All lines used were grown as adherent cell lines in DMEM supplemented with 100U/mL penicillin/streptomycin and 4mM L-glutamine with 10% fetal bovine serum or 10% dialyzed fetal bovine serum for tracer experiments.The pSLIK-cell lines were maintained as above, but FBS was substituted for Tet-free FBS (Clonetech). Cell number was determined using an automated cell counter (Nexcelom) or by hemocytometer.

Generation of cell lines stably expressing inducible forms of flag-tagged mutant IDH

To generate the doxycycline-inducible IDH mutant cell lines, full-length cDNA for IDH1-R132H and IDH2-R172K (kindly provided by Patrick Ward, U. Penn) was amplified by PCR and cloned into the p3xFLAG-CMV14 vector (Sigma) to generate C-terminal Flag-tagged constructs. cDNA for IDH1-R132H-FLAG and IDH2-R172K-FLAG was then amplified by PCR and cloned into the pEN_TTmcs entry vector (Addgene; (Shin, 2006)) for recombination into the pSLIK-hygro lentiviral vector (Addgene; (Shin, 2006)). Lentiviruses were produced by transfecting HEK-293T cells with the pSLIK-hygro-IDH1-R132H or pSLIK-hygro-IDH2-R172K plasmids along with the lentiviral packaging plasmids pMDLg/pRRE and pRSV-Rev and the envelope plasmid pMD2.G (all from Addgene). Supernatants containing lentiviral particles were collected 48 hours after transfection and used to infect sub-confluent H1299 and A549 cells. Infected cells were allowed to recover for 24 hours before being placed under selection with 350 ug/mL hygromycin

(Invitrogen) for ten days. Protein expression was induced using 0.1 ug/mL doxycycline hyclate (Sigma) for 24 hours.

Site-directed mutagenesis

The PHGDH R236E mutant was generated using the QuickChange II XL Site-Directed Mutagenesis Kit from Agilent with the following primers: 5'-tgtggtgaactgtgccgagggagggatcgtggacg-3' and 5'- cgtccacgatccctccctcggcacagttcaccaca-3'. To generate shRNA-resistant PHGDH we used the same kit and the following primers: 5'-cccaaagggaccatccaagttatcacacagggaacatccc-3' and 5'-gggatgttccctgtgtgataacttggatggtccctttggg-3'.

PHGDH shRNA and cDNA expression

We stably introduced shRNA-resistant PHGDH cDNAs into cells using the retroviral vector pLHCX and selected with 150 ug/ml hygromycin. To decrease PHGDH expression, shRNA constructs TRCN0000028548 with target sequence 5'-AGGTGATAACACAGGGAACAT-3' and TRCN0000028545 with target sequence 5'-CTTAGCAAAGAGGAGCTGATA-3' were used. Cells were infected with lentivirus to express shRNAs, selected for 3 days in 1 ug/ml puromycin and proliferation assessed on subsequent days.

Metabolite extraction and LC-MS analysis

For all metabolite profiling, cells were usually left plated for 24-48 h after a media change before extraction in order to allow for media conditioning. Polar metabolites were extracted from cells growing in a 6-well dish using 400 µL of ice cold 80% methanol with 20 ng/mL valine-d8 (LC-MS) or 10ug/mL norvaline (GC-MS) as an internal extraction standard. After scraping the cells, 400 µL of chloroform was added before vortexing for 10 min at 4°C, centrifugation for 10 min at 4°C at 16,000xg, and drying 150 µL of the upper methanol/water phase under nitrogen gas.

Media was extracted by adding 80uL of 100% methanol with 10ug/mL norvaline to 20uL media, centrifugation for 10 min at 4°C at 16,000xg, and drying 80 µL of the supernatant under nitrogen gas. Total protein hydrolysate was obtained by hydrolyzing 10^6 cells washed in isotonic saline in 400uL 6M HCl for 24h at 105°C, then drying 100uL aliquots of the resulting liquid at room temperature under nitrogen gas on a teflon-coated dryer. Total DNA/RNA was hydrolyzed to dNMPs/NMPs by extracting 10^7 cells washed in isotonic saline and resuspended in 400uL MilliQ water with 400uL phenol/chloroform/isoamyl alcohol (25:24:1 pH 8.0) twice, and then with chloroform twice. Total nucleic acid was precipitated with 0.1 volumes 3M sodium acetate pH 5.2 and 3 volumes of 100% ethanol at -20°C overnight. Dried and washed pellets were resuspended in 45uL MilliQ, and 20uL of this was digested with .1uL 0.02U/uL Bovine Spleen Phosphodiesterase II (Sigma P9041) and .1uL 2000GelUnits/uL Micrococcal Nuclease (NEB 0247) with 6uL 100mM Succinic Acid-NaOH 50mM CaCl2 pH5.9 buffer. Samples were then extracted with 90uL 2:1 chloroform:methanol similar as above and the methanol/water layer was dried under nitrogen gas. All dried samples were stored at -80°C. Metabolite samples for LC-MS were then resuspended in 40 µL 50% acetonitrile/50% water immediately before analysis. dNMPs/NMPs from DNA/RNA hydrolysis were resuspended in 50% acetonitrile/50% water as if making a 100ng/uL sample of the original DNA/RNA hydrolysis reaction. Samples for GC-MS were derivatized in 16uL of MOX reagent at 37°C for 90minutes, then 20uL TBDMS was added and samples were further incubated for 60min at 60°C.

For GC-MS, derivatized samples were analyzed by GCMS using a DB-35MS column (30m x 0.25mm i.d. x 0.25 µm, Agilent J&W Scientific) installed in an Agilent 7890A gas chromatograph (GC) interfaced with an Agilent 5975C mass spectrometer (MS). Mass isotopomer distributions were determined by integrating metabolite ion fragments and corrected for natural abundance using in-house algorithms adapted from (Fernandez, 1996). GC-MS data is shown in 1c, 2c, the protein data in 2d, 4a, 4b, and 5b.

LC-MS metabolite profiling was performed on a Dionex UltiMate 3000 ultra-high performance liquid chromatography system coupled to a Q Exactive benchtop Orbitrap mass spectrometer, which was equipped with an Ion Max source and a HESI II probe (Thermo Fisher Scientific). External mass calibration was performed every 7 days. Chromatographic separation was achieved by injecting 10 µL of sample on a SeQuant ZIC-pHILIC Polymeric column (2.1x150 mm 5 uM, EMD Millipore). Flow rate was set to 100 µL/min, column compartment was set to 25°C, and autosampler sample tray was set to 4°C. Mobile Phase A consisted of 20 mM ammonium carbonate, 0.1% ammonium hydroxide. Mobile Phase B was 100% acetonitrile. The mobile phase gradient (%B) was as follows: 0 min 80%, 5 min 80%, 30 min 20%, 31 min 80%, 42 min 80%. All mobile phase was introduced into the ionization source set with the following parameters: sheath gas = 40, auxiliary gas = 15, sweep gas = 1, spray voltage = -3.1kV or +3.0kV, capillary temperature = 275°C, S-lens RF level = 40, probe temperature = 350°C. In experiments to measure steady-state levels of metabolites other than phosphoserine, metabolites were monitored using a polarity-switching full-scan method. In experiments utilizing tracers or measuring phosphoserine, metabolites were monitored using a targeted selected ion monitoring (tSIM) method in negative mode with the quadrupole centered on the M-H ion m+1.5, m+2.5, or m+3.5 mass with a 8 amu isolation window, depending on the number of carbons in the target metabolite. Resolution was set to 70,000, full-scan AGC target was set to 10^6 ions, and tSIM AGC target was set to 10^5 ions. For tracing experiments, samples were collected at various time points as indicated. Data were acquired and analyzed using Xcalibur v2.2 software (Thermo Fisher Scientific). Data for LC-MS tracer experiments currently shown in 2d, 2e, 5c, and 5d are not corrected for natural abundance or quadrupole bias.

Absolute quantitation of media metabolites was done by running a standard curve of media components, and appropriately adjusting for the volume of media extracted. Absolute

quantitation of cellular metabolites was done by running a standard curve of quantitated metabolites, and adjusting for total cell volume extracted using coulter counter data.

Serine uptake assay

Serine uptake was measured by washing near-confluent 6 wells of TT cells 2x with PBS, then incubating cells in PBS at 37°C for 15min. The PBS was replaced with 1mL of 400nM [U-^{14}C]serine in DMEM with no or 3.6mM extra serine (for final of 10x) added. Cells were incubated in tracer media for 30min at 37°C, then washed 3x with PBS and lysed in 550uL of 0.03% SDS for 10min at 37°C. 500uL of this solution was then counted in 5mL of scintillation fluid in a scintillation counter, along with labeled media as a calibration standard.

Flow cytometry

Cells were dual stained for DNA content and new DNA synthesis with the Click-iT EdU Alexa Fluor 488 Kit and FxCycle Violet Stain (Life Technologies F-10347), respectively. Briefly, cells were incubated with 10 μM 5-ethynyl-2'-deoxyuridine (EdU) for 2 hours and then fixed and stained according to the manufacturer's instruction. Cells were analyzed on the BD FACSCanto II using FACS Diva software.

Coulter counting for determination of cell volume

Three wells of a 6-well dish were seeded identically alongside wells to be extracted for metabolite profiling. Wells were trypsinized in 1mL and 500uL of trypsinized cells were added to 10mL isotone. Total cell volume was as integrated for particles >10um diameter.

Expression and in vitro assay of SHMT

pET28a His-SHMT1, His-deltaMTS-SHMT2, and His-MTHFD were transformed into BL21 E. coli. SHMT1 and SHMT2 were from human cDNA, and were N-terminally His-tagged, the

deltaMTS-SHMT2 construct lacking the mitochondrial localization sequence, whereas MTHFD was cloned from BL21 E. coli. and C-terminally tagged. Single colonies from these plates were inoculated into LB plus kanamycin and grown at 37°C and 225 rpm overnight. The next day, cultures were diluted 1:100 and grown to OD_{600} = 0.4, then 0.5 mM IPTG was added before incubating at room temperature (SHMT1 and deltaMTS-SHMT2) or 37°C (MTHFD) and 225 rpm for 4 hours. The bacteria were pelleted at 6000xg for 15 min, and the pellet was flash frozen and stored at -80°C. All protein purification steps were performed at 4°C, except for His-column purification at room temperature. To purify protein, bacterial pellets were resuspended in 30 ml lysis buffer (20mM Tris pH 7.5, 500mM KCl, 5mM imidazole, 10uM pyridoxal phosphate, 5mM glycine), sonicated, and the lysate centrifuged at 20,000xg for 45 min. Care was taken throughout as pyridoxal phosphate is light sensitive. The lysate was mixed with 2 ml of Ni-NTA agarose (Qiagen) beads in lysis buffer. This mixture was shaken gently for 2 hours, Ni-NTA beads pelleted and washed four times with wash buffer (20mM Tris pH 7.5, 500mM KCl, 30mM imidazole, 10uM pyridoxal phosphate, 5mM glycine). The beads and lysate were transferred to an empty column and protein recovered in elution buffer (20mM Tris pH 7.5, 500mM KCl, 250mM imidazole, 10uM pyridoxal phosphate, 5mM glycine) with 1 ml fractions collected. Those fractions with high protein content were determined by Bradford assay. Fractions containing appreciable protein were pooled and immediately desalted into hypotonic lysis buffer (20 mM HEPES pH 7.0, 5 mM KCl, 1 mM $MgCl_2$, 1mM DTT, 10uM pyridoxal phosphate, 5mM glycine) on a HiTrap 5mL desalting column. The resulting proteins were immediately assayed on the same day.

SHMTs were assayed using the following protocol. First, tetrahydrofolate in a single-use vial was dissolved at 10mM in THF storage buffer (100mM ascorbic acid, 20mM MES, pH 5.5 with KOH) and aliquoted before snap freezing on liquid nitrogen and single-use storage at -80°C. THF storage buffer itself is oxidation-sensitive and so was stored at 10x at -80°C in single-use

aliquots. Care was taken throughout as THF is light-sensitive. SHMT and MTHFD were assayed together at room temperature, MTHFD in excess at ~.1ug/mL final, and each SHMT titrated so that the reaction reached completion in approximately 5min. The assay mix also included the following at their final concentrations: 1mM NADP+, 50mM HEPES-KOH pH7.5, 20mM KCl, 2mM $MgCl_2$, 1:1000 beta-mercaptoethanol, 1mM THF in THF storage buffer. Serine and phosphoserine were also added when required by the experiment. Increase in NADPH fluorescence was followed in a Tecan plate reader and a regression on the slope of the increase was taken as the activity.

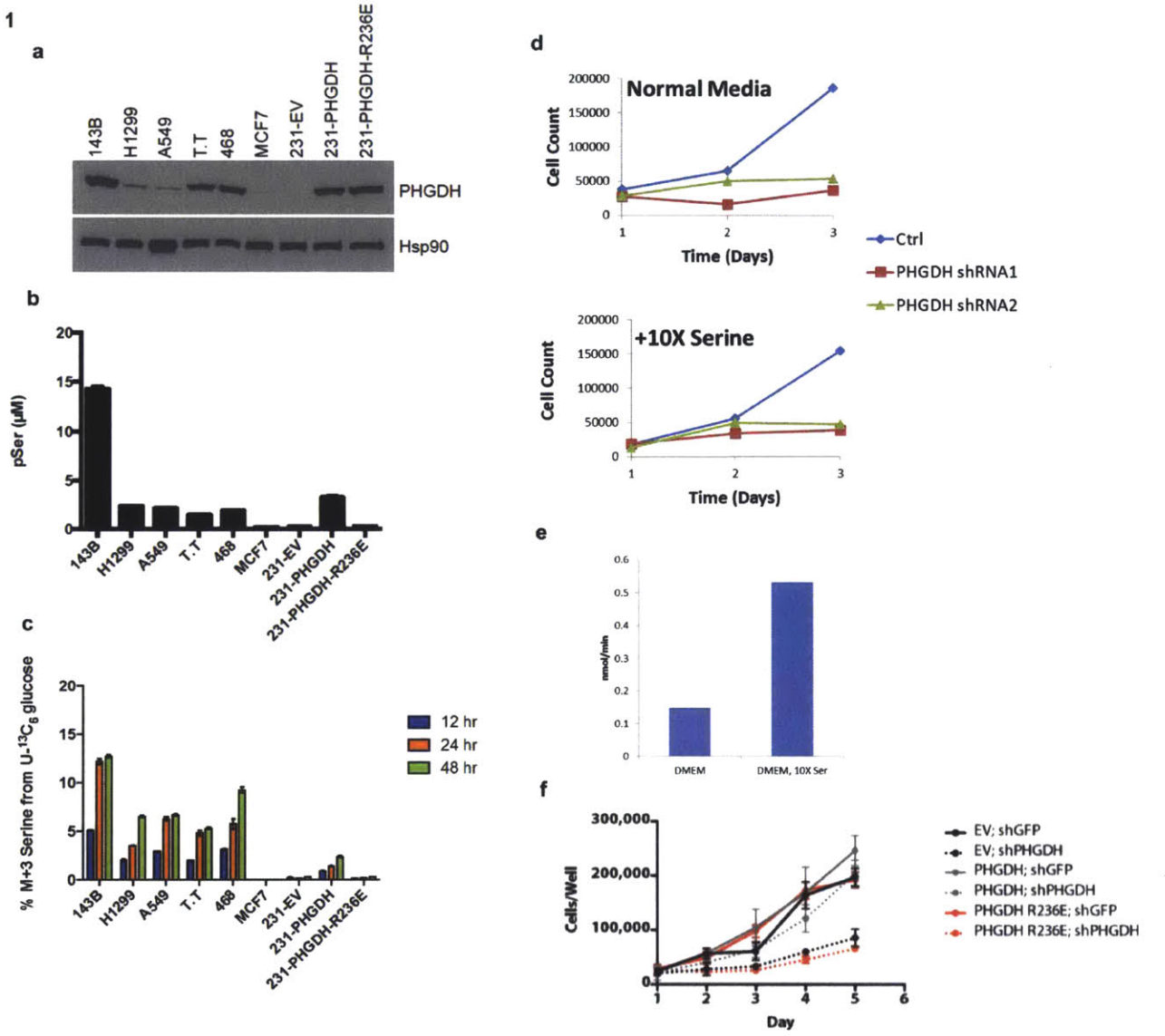

Figure 1 - PHGDH enzymatic activity is essential for glycolytic serine biosynthesis and viability of PHGDH-dependent cells, but is not rescuable by serine. a) Western blot of PHGDH across several cell lines, including MDA-MB-231 cell lines expressing exogenous PHGDH and a PHGDH enzymatically dead mutant (R236E). b) Intracellular levels of phosphoserine across the same cell lines by LC-MS. c) %m-3 serine in media from [U-^{13}C]glucose labeled cells after 24, 48, and 72h. d) Growth curve of TT cells expressing control or PHGDH shRNA in normal or 10x serine DMEM by GC-MS. e) Serine uptake as measured by [U-^{14}C]serine entry into TT cells in normal and 10x serine media. f) Growth curve of TT cells expressing shGFP or shPHGDH and rescue EV, PHGDH, and PHGDH-R236E (catalytically dead) constructs. n=3 for b,c, and f, n=1 for all others, error bars are SEM.

2

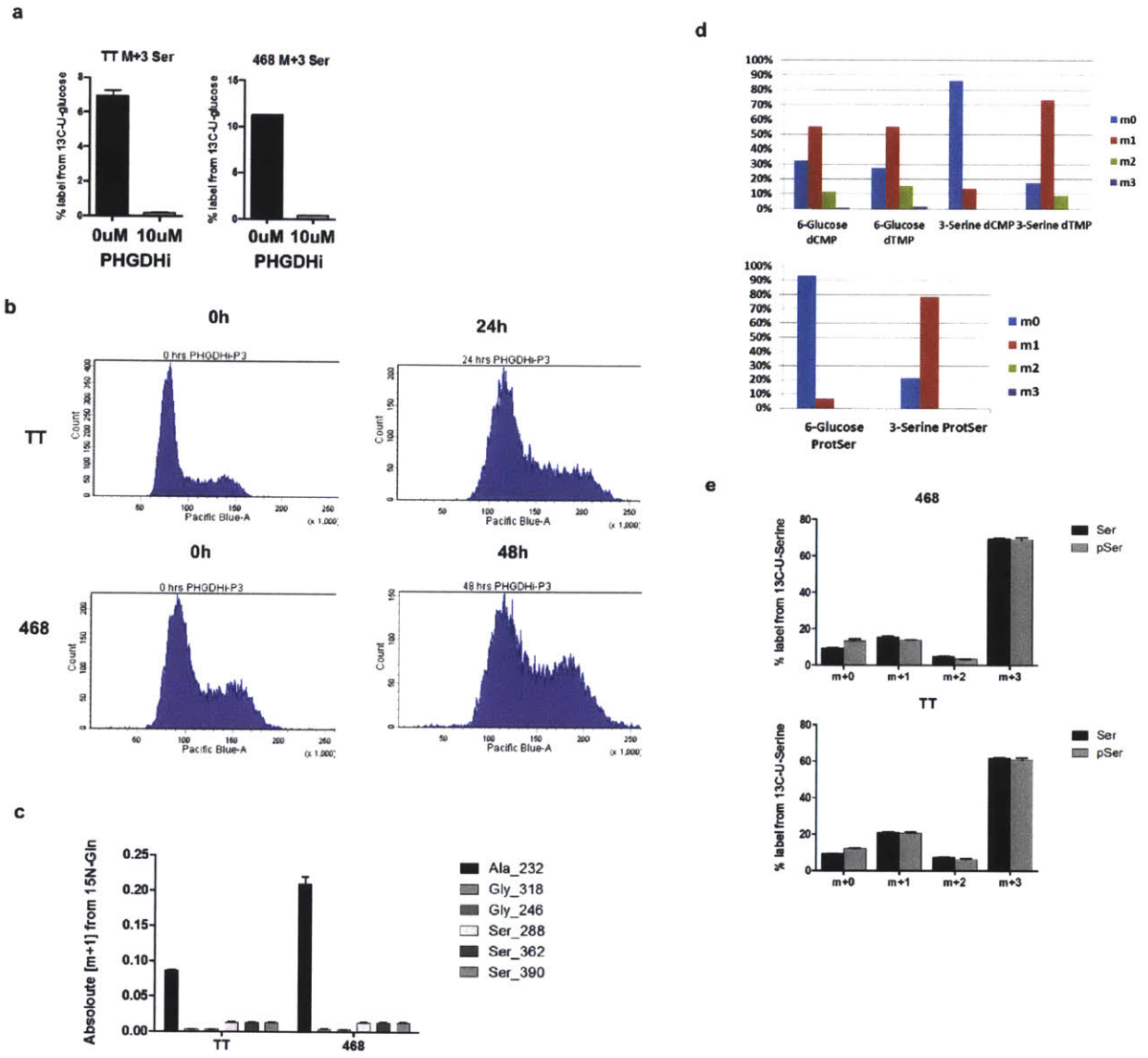

Figure 2 - PHGDH inhibitors cause S-phase arrest in dependent cell lines and the mechanism is not well explained by decreased glutamine anaplerosis or channeling. a) %m+3 cellular serine in [U-^{13}C]glucose labeled TT and MDA-MB-468 cells exposed for 24h to either 10uM PHGDH inhibitor or vehicle control by LC-MS. b) DNA content analysis by flow cytometry of TT and MDA-MB-468 cells exposed to either 10uM PHGDH inhibitor or vehicle control. c) Absolute media levels in mM of amino acid m+1 species by GC-MS after 72h labeling with [alpha-^{15}N]glutamine. d) Mass isotopomer distributions of dCMP and dTMP in DNA by LC-MS and serine in protein by GC-MS after 10d labeling of MDA-MB-468 cells with [6-^{13}C]glucose or [3-^{13}C]serine. e) Mass isotopomer distributions of intracellular serine and phosphoserine in MDA-MB-468 and TT cells labeled for 24h with [U-^{13}C]serine. n=3 for a, c, and e, n=1 for all others, error bars are SEM.

3

a

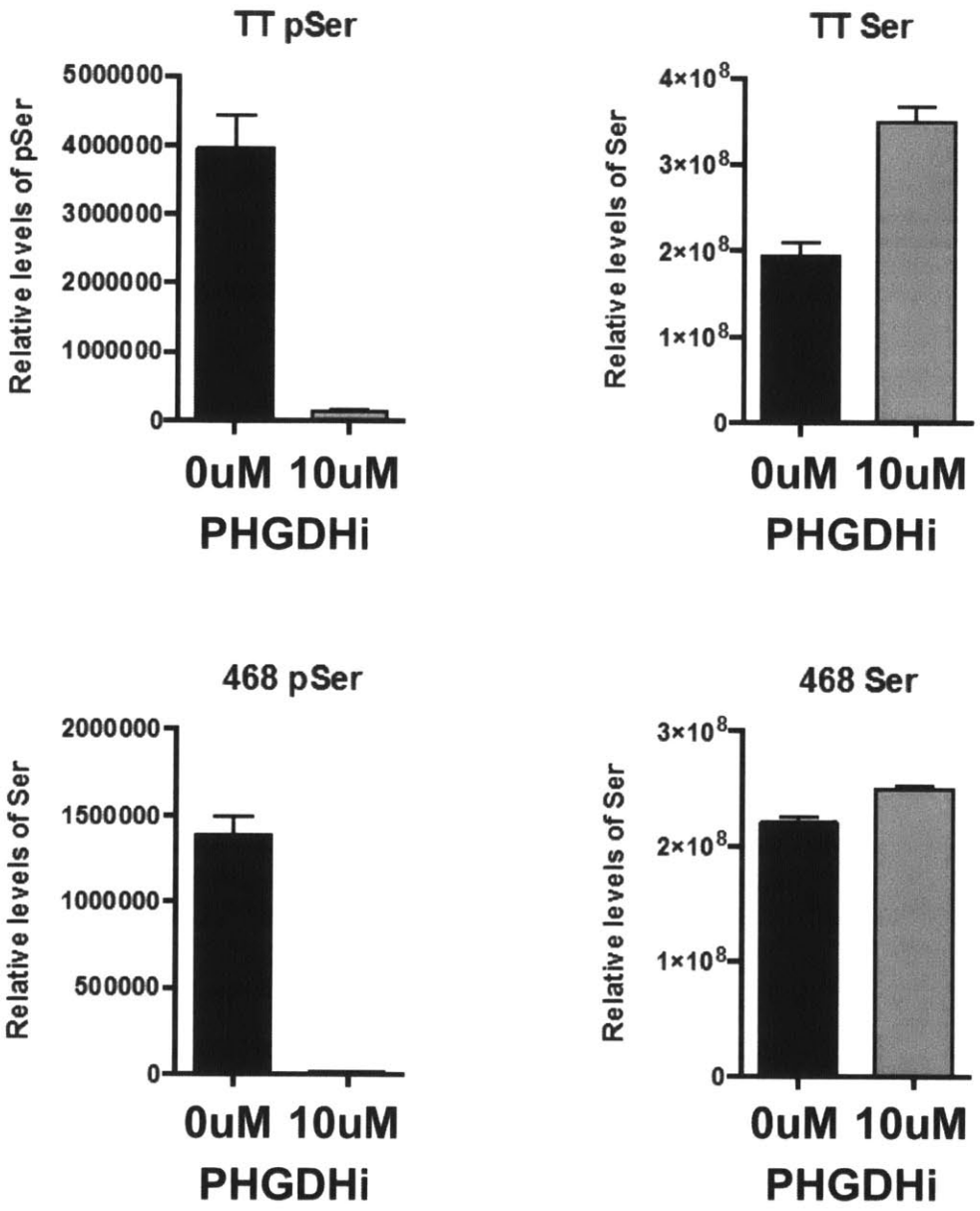

Figure 3 - Phosphoserine inhibits SHMT1 but not SHMT2. a) Levels of intracellular phosphoserine and serine in MDA-MB-468 and TT cells exposed to either 10uM PHGDH inhibitor or vehicle control by LC-MS.

4

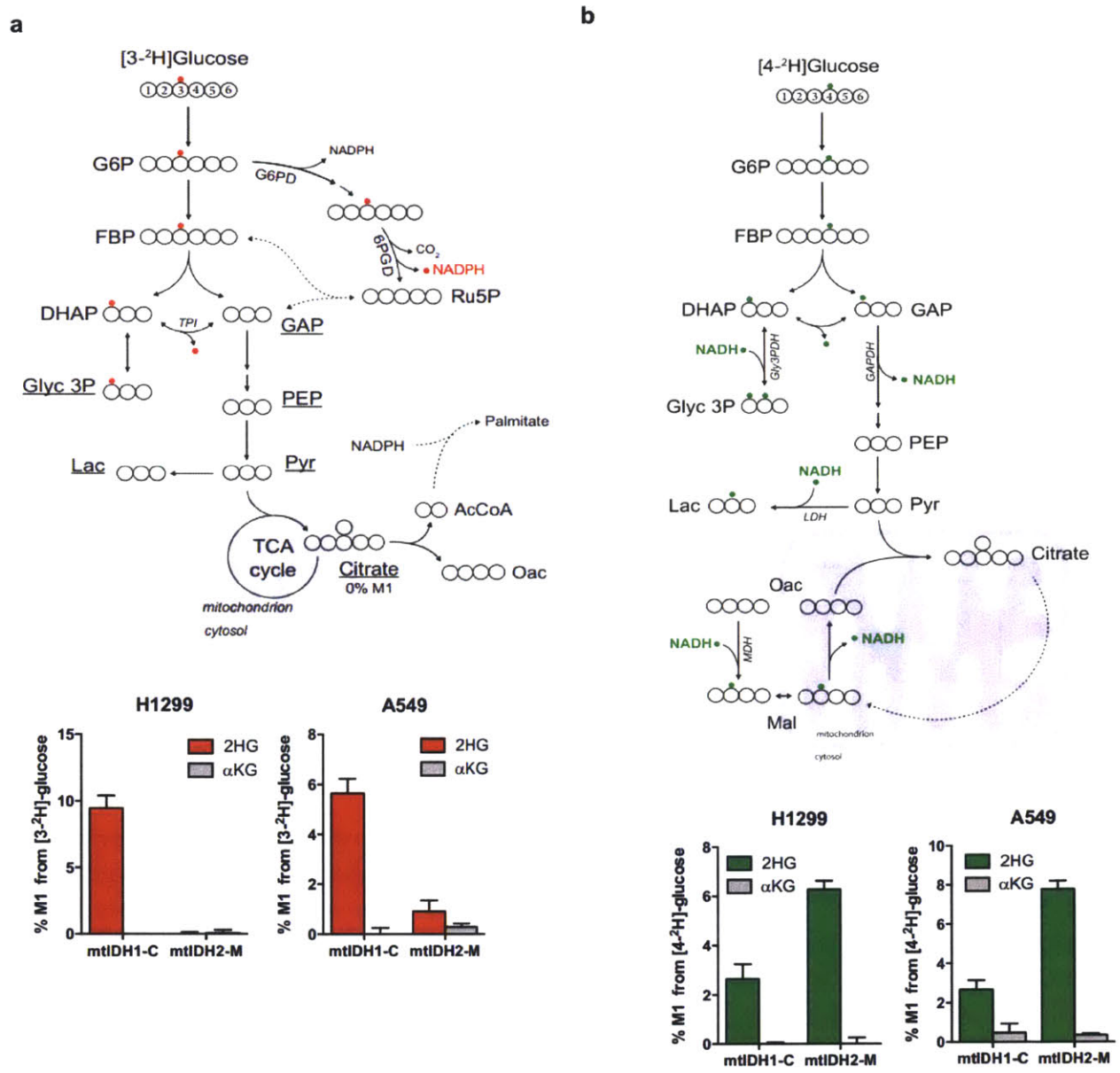

Figure 4 - Expression of 2-HG producing mutant IDH in the cytosol or mitochondria allows compartmentalized redox tracing. a) Diagram of [3-^{2}H]glucose tracing through glycolysis and ^{2}H label onto cytosolic NADPH as well as graph showing selective detection of ^{2}H m+1 label on 2-HG in cytosolic mtIDH1-C but not mitochondrial mtIDH2-M-expressing A549 and H1299 cells. b) Diagram of [4-^{2}H]glucose tracing through glycolysis and ^{2}H label onto cytosolic and mitochondrial NADH as well as graph showing detection of ^{2}H m+1 label on 2-HG in cytosolic mtIDH1-C and mitochondrial mtIDH2-M-expressing A549 and H1299 cells. n=3 for all figures, error bars are SEM.

5

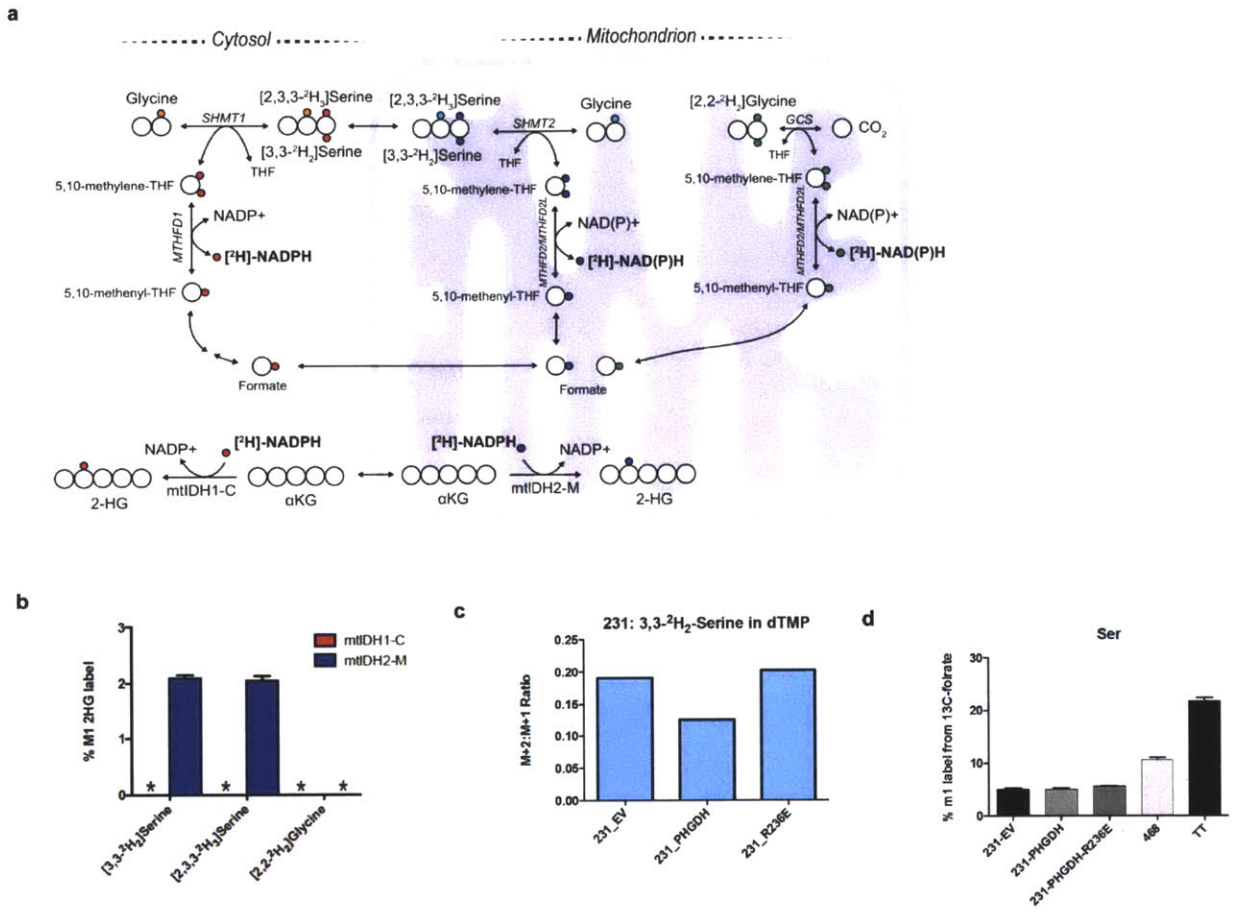

Figure 5 - Folate one-carbon flux directionality and consequences for phosphoserine-mediated SHMT1 inhibition in cells. a) Schematic of folate one-carbon metabolism labeling from [3,3-^{2}H]serine and [2,3,3-^{2}H]serine. b) Measurement of serine-derived folate one-carbon unit oxidation by MTHFDs in the cytosol and mitochondria using [3,3-^{2}H]serine and [2,3,3-^{2}H]serine in A549 cells using the 2-HG system as measured by GCMS. c) m+2/m+1 ratio in dTMP from DNA by LC-MS after 10d labeling with [3,3-^{2}H]serine in MDA-MB-231 cell lines expressing EV, PHGDH, or PHGDH-R236E cDNAs. d) %m+1 serine in media after 24h labeling with 2mM [^{13}C]formate across several cell lines by LC-MS. n=3 for b, d, n=1 for all others, error bars are SEM.

References

Beroukhim R, Mermel CH, Porter D, Wei G, Raychaudhuri S, Donovan J, Barretina J, Boehm JS, Dobson J, Urashima M, Mc Henry KT, Pinchback RM, Ligon AH, Cho YJ, Haery L, Greulich H, Reich M, Winckler W, Lawrence MS, Weir BA, Tanaka KE, Chiang DY, Bass AJ, Loo A, Hoffman C, Prensner J, Liefeld T, Gao Q, Yecies D, Signoretti S, Maher E, Kaye FJ, Sasaki H, Tepper JE, Fletcher JA, Tabernero J, Baselga J, Tsao MS, Demichelis F, Rubin MA, Janne PA, Daly MJ, Nucera C, Levine RL, Ebert BL, Gabriel S, Rustgi AK, Antonescu CR, Ladanyi M, Letai A, Garraway LA, Loda M, Beer DG, True LD, Okamoto A, Pomeroy SL, Singer S, Golub TR, Lander ES, Getz G, Sellers WR, Meyerson M. (2010). The landscape of somatic copy-number alteration across human cancers. Nature 463, 899-905.

Collet JF, Stroobant V, Van Schaftingen E. (1999). Mechanistic studies of phosphoserine phosphatase, an enzyme related to P-type ATPases. J Biol Chem 274, 33985-90.

Fan J, Ye J, Kamphorst JJ, Shlomi T, Thompson CB, Rabinowitz JD. (2014). Quantitative flux analysis reveals folate-dependent NADPH production. Nature 510, 298-302.

Fell DA, Snell K. (1988). Control analysis of mammalian serine biosynthesis. Feedback inhibition on the final step. Biochem J 256, 97-101.

Fernandez CA, Des Rosiers C, Previs SF, David F, Brunengraber H. (1996). Correction of 13C mass isotopomer distributions for natural stable isotope abundance. J Mass Spectrom 31, 255-62.

Herbig K, Chiang EP, Lee LR, Hills J, Shane B, Stover PJ. (2002). Cytoplasmic serine hydroxymethyltransferase mediates competition between folate-dependent deoxyribonucleotide and S-adenosylmethionine biosyntheses. J Biol Chem 277, 38381-9.

Kung C, Hixon J, Choe S, Marks K, Gross S, Murphy E, DeLaBarre B, Cianchetta G, Sethumadhavan S, Wang X, Yan S, Gao Y, Fang C, Wei W, Jiang F, Wang S, Qian K, Saunders J, Driggers E, Woo HK, Kunii K, Murray S, Yang H, Yen K, Liu W, Cantley LC, Vander Heiden MG, Su SM, Jin S, Salituro FG, Dang L. (2012). Small molecule activation of PKM2 in cancer cells induces serine auxotrophy. Chem Biol 19, 1187-98.

Labuschagne CF, van den Broek NJ, Mackay GM, Vousden KH, Maddocks OD. (2014). Serine, but not glycine, supports one-carbon metabolism and proliferation of cancer cells. Cell Rep 7, 1248-58.

Lewis CA, Parker SJ, Fiske BP, McCloskey D, Gui DY, Green CR, Vokes NI, Feist AM, Vander Heiden MG, Metallo CM. (2014). Tracing compartmentalized NADPH metabolism in the cytosol and mitochondria of mammalian cells. Mol Cell 55, 253-63.

Locasale JW, Grassian AR, Melman T, Lyssiotis CA, Mattaini KR, Bass AJ, Heffron G, Metallo CM, Muranen T, Sharfi H, Sasaki AT, Anastasiou D, Mullarky E, Vokes NI, Sasaki M, Beroukhim R, Stephanopoulos G, Ligon AH, Meyerson M, Richardson AL, Chin L, Wagner G, Asara JM, Brugge JS, Cantley LC, Vander Heiden MG. (2011). Phosphoglycerate dehydrogenase diverts glycolytic flux and contributes to oncogenesis. Nat Genet 43, 869-74.

Losman JA, Kaelin WG Jr. (2013). What a difference a hydroxyl makes: mutant IDH, (R)-2-hydroxyglutarate, and cancer. Genes Dev 27, 836-52.

Lunt SY, Muralidhar V, Hosios AM, Israelsen WJ, Gui DY, Newhouse L, Ogrodzinski M, Hecht V, Xu K, Acevedo PNM, Hollern DP, Bellinger G, Dayton TL, Christen S, Elia I, Dinh AT, Stephanopoulos G, Manalis SR, Yaffe MB, Andrechek ER, Fendt SM, Vander Heiden MG. (2014). Pyruvate Kinase isoform expression alters nucleotide synthesis to impact cell proliferation. Mol Cell In press.

Mattaini KR, Brignole EJ, Kini M, Fiske BP, Drennan CL, Vander Heiden MG. (2015). An epitope tag alters phosphoglycerate dehydrogenase structure and impairs ability to support cell proliferation. In submission.

Neuhaus FC, Byrne WL. (1959a). Metabolism of phosphoserine. I. Exchange of L-serine with phosphoserine. J Biol Chem 234, 109-12.

Neuhaus FC, Byrne WL. (1959b). Metabolism of phosphoserine. II. Purification and properties of O-phosphoserine phosphatase. J Biol Chem 234, 113-21.

Neuhaus FC, Byrne WL. (1960). Metabolism of phosphoserine. III. Mechanism of O-phosphoserine phosphatase. J Biol Chem 235, 2019-24.

Pollard PJ, Brière JJ, Alam NA, Barwell J, Barclay E, Wortham NC, Hunt T, Mitchell M, Olpin S, Moat SJ, Hargreaves IP, Heales SJ, Chung YL, Griffiths JR, Dalgleish A, McGrath JA, Gleeson MJ, Hodgson SV, Poulsom R, Rustin P, Tomlinson IP. (2005). Accumulation of Krebs cycle intermediates and over-expression of HIF1alpha in tumours which result from germline FH and SDH mutations. Hum Mol Genet 14, 2231-9.

Possemato R, Marks KM, Shaul YD, Pacold ME, Kim D, Birsoy K, Sethumadhavan S, Woo HK, Jang HG, Jha AK, Chen WW, Barrett FG, Stransky N, Tsun ZY, Cowley GS, Barretina J, Kalaany NY, Hsu PP, Ottina K, Chan AM, Yuan B, Garraway LA, Root DE, Mino-Kenudson M, Brachtel EF, Driggers EM, Sabatini DM. (2011). Functional genomics reveal that the serine synthesis pathway is essential in breast cancer. Nature 476, 346-50.

Shin KJ, Wall EA, Zavzavadjian JR, Santat LA, Liu J, Hwang JI, Rebres R, Roach T, Seaman W, Simon MI, Fraser ID. (2006). A single lentiviral vector platform for microRNA-based conditional RNA interference and coordinated transgene expression. Proc Natl Acad Sci U S A 103, 13759-64.

Tibbetts AS, Appling DR. (2010). Compartmentalization of Mammalian folate-mediated one-carbon metabolism. Annu Rev Nutr 30, 57-81.

Chapter 4 - Folate one-carbon metabolism modulates glycolytic flux and the fate of pyruvate

Authorship Statement

Please note that the majority of this chapter is modified or copied verbatim from (Kim D, 2014). Although much of the work excerpted for this thesis is my personal contribution to that paper, there are portions I was not personally involved in (Figures 1,2,3,4b,4g,4h,5c,5d), which are presented here solely for context.

Introduction

After demonstrating that glycolytic flux through the serine biosynthesis pathway branching from glycolysis can regulate folate one-carbon unit metabolism, we hypothesized as to whether there was reciprocal regulation of glycolysis by folate one-carbon pools. It was therefore of great interest when the purine biosynthetic intermediate SAICAR (Figure 12) was found to be an activator of PKM2 (Keller, 2012). SAICAR is one step upstream of AICAR formyltransferase, which adds the second 10-formyl-THF unit in de novo purine biosynthesis. We find that some cells are dependent on SHMT2 to keep cellular formate levels high and reduce levels of SAICAR such that PKM2 activity remains low (Kim, 2015). Given the importance of glycolysis and folate one-carbon metabolism for proliferation, it is not surprising that these two pathways are coordinately regulated.

Results

Dohoon Kim in the Sabatini laboratory uncovered a connection between SHMT2 and GLDC-expression in glioma, leading to collaboration that intersected with my work on connections between one carbon metabolism and PKM2 regulation. He found that GLDC, a mitochondrial enzyme that is part of the glycine cleavage system, was necessary for avoidance of glycine

toxicity generated by SHMT2 in glioma cells. It became clear that in contrast to the toxic effects of glycine cleavage system knockdown, loss of SHMT2 did not affect the proliferation or survival of multiple cell lines under standard culture conditions (Figure 1). As it seemed unlikely that cancer cells would exhibit high SHMT2 expression if it did not provide a benefit to the cells under some condition, we considered that SHMT2 might have a context-dependent role and examined SHMT2 and GLDC expression in sections of human GBM tumors. In normal brains SHMT2 and GLDC expression were not detected in most cells and were seen at low levels in astrocytes and vessels (Fig. 2a, 3a,d,e). In GBM tumors, however, both SHMT2 and GLDC were expressed at high levels (Fig. 2a, 3a,d,e) such that individual cancer cells migrating into the brain parenchyma were observed (Fig. 2a, 3b,c). Importantly, the highest levels of SHMT2 and GLDC expression appeared as distinct bands surrounding necrotic and acellular regions, highlighting cells of what is referred to as the pseudopalisading necrosis (Fig. 2a-c, 3a,f,g). This feature, which is unique to glioblastomas, consists of a dense layer of "pseudopalisading" viable cells that outline an ischemic tumor region that is thought to form upon the collapse or occlusion of an intratumoral vessel (Rong, 2006).

The expression of SHMT2 in ischemic tumor zones suggested that it might have a key role in cells in environments with limited oxygen or nutrient levels. Indeed, under hypoxic conditions (0.5% oxygen), SHMT2 suppression impaired and SHMT2 overexpression enhanced LN229 cell proliferation (Fig. 2d, 3h). To begin to understand why this might be, we surveyed the metabolic consequences of SHMT2 suppression in LN229 cells. To further characterize the metabolic changes that occur as a consequence of SHMT2 knockdown, we carried out untargeted metabolite profiling, which identified AICAR, SAICAR, and fructose bisphosphate (FBP) as amongst the most highly elevated metabolites (Fig. 4a). Furthermore, upon SHMT2 suppression cells increased oxygen consumption almost twofold (Fig. 4b), which may reflect increased TCA cycle activity. The increase in the sequential intermediates SAICAR and AICAR

can be explained because 10-formyl-THF, a downstream product of SHMT2 and SHMT1 activity, is required for the conversion of AICAR to FAICAR during de novo purine biosynthesis (Fig. 5b). While a link between SHMT2 and FBP is less clear, we nonetheless noted that the suppression of SHMT2 significantly increases levels of all three known activators of pyruvate kinase isoform M2 (PKM2) –serine, FBP, and SAICAR (Ibsen, 1976, Gui, 2013, and Keller, 2012) – raising the possibility that SHMT2 antagonizes PKM2 activity by decreasing the levels of its activators.

Consistent with the increase in metabolites known to activate PKM2 (Fig. 4a), PKM2 activity was significantly increased in cells with suppressed SHMT2, despite no change in PKM2 protein levels (Fig. 4c). To determine whether SHMT2 silencing induces changes in central carbon metabolism that are consistent with increased pyruvate kinase activity, we measured kinetic flux through glycolysis in live cells using ^{13}C-stable isotope labeled glucose ([U-^{13}C]glucose) (Fig. 4d-f). The ^{13}C labeling rate of pyruvate, the product of PKM2, was elevated in cells with suppressed SHMT2, indicating increased PKM2 activity, which was also confirmed in cells overexpressing PKM2 (Fig. 4d). By calculating the sum ^{13}C labeling of lactate, citrate, and alanine, the major downstream fates of pyruvate (Lunt, 2011), we estimate that the total pyruvate kinase flux is increased by ~70% following SHMT2 knockdown (Fig. 4e). Furthermore, these changes as well as changes in metabolite levels and oxygen consumption were suppressed by overexpression of an RNAi-resistant SHMT2 cDNA (Fig. 4b-e, 5a), arguing against off-target RNAi effects. These results support a model in which SHMT2 suppression leads to increased pyruvate kinase activity and carbon flux into the TCA cycle, while cells that express high levels of SHMT2 limit PKM2 activity and flux into the TCA cycle (Fig. 4f). This may confer a survival benefit in ischemic tumor contexts, as it has been shown that limiting pyruvate entry into TCA cycle, and thus limiting oxygen consumption, provides a survival advantage under hypoxia (Papandreou, 2006).

If the effects of SHMT2 on oxygen consumption and survival within an ischemic microenvironment occur via suppression of PKM2 activity, then forced activation of PKM2 should antagonize these effects. Indeed, either overexpression of PKM2 or the addition of the PKM2 product pyruvate to the media increased the oxygen consumption rate in LN229 cells to the equivalent levels observed following SHMT2 knockdown (Fig. 4g,h). These findings argue that pyruvate kinase activity is a determinant of oxygen consumption in these cells. Furthermore, overexpression of PKM2, or the pharmacological activation of PKM2 using TEPP-46 or DASA-58 (Anastasiou, 2012) reduced LN229 survival in 0.5% hypoxia to a similar extent as SHMT2 suppression (Fig. 5d). These findings support a model in which SHMT2 expression rewires metabolism to suppress PKM2 activity and promote survival in the ischemic tumor environment (Fig. 5e).

Discussion

SHMT2 is elevated in a subset of cancer cells and promotes changes in metabolism that allow cells to survive in an ischemic tumor microenvironment via inhibition of PKM2. It is already appreciated that hypoxia/ischemia selects for cancer cells with increased tumorigenicity and therapy-resistance, and manifestations of tumor ischemia, such as pseudopalisading necrosis, are associated with poor prognoses (Brown, 2004, Hockel, 1996). More broadly, these findings suggest that glycolysis and central carbon metabolism are regulated by folate one-carbon pathway status. Given our findings in Chapter 3 about glycolysis and its branchpoints regulating folate one-carbon pathways, folate one-carbon regulation of SAICAR levels and PKM2 activity may serve to complete a feedback loop between folates and glycolysis in proliferating cells.

Materials and Methods

Reagents

The following antibodies were used: antibodies to GLDC (HPA002318), SHMT2 (HPA020549) from Sigma; antibodies to actin (sc-1616), SHMT1 (sc-100849), and GCAT(sc-86466) from Santa Cruz; anti-GCSH (H00002653-A01)from Abnova; anti-SOX-2 (MAB2018) from R & D systems; anti-GFAP (IF03L) from Calbiochem; anti-cleaved-PARP (19F4) and anti-PKM2 (D78A4) from Cell Signaling Technologies; anti-GCAT (ab85202) from Abcam; HRP-conjugated anti-mouse, anti-rabbit, and anti-goat secondary antibodies from Santa-Cruz Biotechnology.

The following cell culture reagents were used: Neurobasal medium, N-2 and B-27 supplements from Invitrogen; Recombinant Human FGF basic (4114-TC) and EGF (236-EG) from R & D systems; DMEM and RPMI-1640 media, doxycycline (D9891) from Sigma; Leucine ethyl ester hydrochloride (61850), Arginine ethyl ester hydrochloride (A2883), Alanine ethyl ester hydrochloride (855669), Valine ethyl ester hydrochloride (220698), Lysine ethyl ester dihydrochloride (62880), Ethylamine (395064) from Sigma; Glycine ethyl ester hydrochloride (sc-295020) and Polybrene (sc-134220) from Santa Cruz.

Additional materials used: formalin from VWR; Borg Decloaker RTU solution and pressurized Decloaking Chamber from Biocare Medical; Prolong Gold Antifade reagent from Invitrogen; CellTiter-Glo Luminescent Assay from Promega; [U-^{14}C]serine from MP Biomedicals; Matrigel (356230) from BD Biosciences.

Cell lines, tissue culture, and media

Cell lines (LN229, ACHN, A2058, U251, T47D, MCF7, HMC-1-8, U87, DoTc2-4510, and PC3) were cultured as adherent cell lines in DMEM unless otherwise noted. For experiments

measuring oxygen consumption and for untargeted metabolite profiling experiments, RPMI was used, which does not contain the PKM2 product pyruvate.

shRNA expressing lentivirus generation and sequences

For each gene of interest (GLDC, SHMT2, GCAT, GCSH), 5 lentiviral shRNA constructs were obtained from The RNAi Consortium (TRC) and recombinant lentivirus containing supernatant was produced using a transient transfection protocol. Each lentivirus was separately transduced into LN229 by overnight incubation of virus in trypsin dissociated cells (20,000 cells per ml, 2 ml into each well of a 6-well plate) in the presence of polybrene. Lentiviral expression of shGFP and shLacZ served as negative controls for gene knockdown, and noninfected cells served as negative controls for transduction. Cells were selected with puromycin for 3 days to ensure transduction, and for each gene, the two (or three) most effective shRNAs, in terms of knockdown of protein expression by western blot, were chosen for use in our experiments.

The following shRNA sequences were used:

shGFP: TRCN0000072186, target sequence: TGCCCGACAACCACTACCTGA

shLacZ: TRCN0000072235, target sequence: CCGTCATAGCGATAACGAGTT

shGLDC_1: TRCN0000036599, target sequence: CGAGCCTACTTAAACCAGAAA

shGLDC_2: TRCN0000036603, target sequence: GAAGTTTATGAGTCTCCATTT

shGLDC^{dox}: target sequence same as shGLDC_2, cloned into dox-inducible vector (pLKO_GC11)

shSHMT2_1: TRCN0000238795, target sequence: CGGAGAGTTGTGGACTTTATA

shSHMT2_2: TRCN0000034804, target sequence: CCGGAGAGTTGTGGACTTTAT

shSHMT2_3: TRCN0000234657, target sequence: GTCTGACGTCAAGCGGATATC

shGCSH_1: TRCN0000083395, target sequence: GTGAACTCTATTCTCCTTTAT

shGCSH_2: TRCN0000428788, target sequence: TGAGGAACACCACTATCTTAA

shGCAT_1: TRCN0000034579, target sequence: CCTTAACTTCTGTGCCAACAA

shGCAT_2: TRCN0000034580, target sequence: CCAGAGGTTCCGTAGTAAGAT

Cell viability assays with shRNA transduction

For cell viability experiments involving transduction of a single shRNA (e.g. shGLDCs), cell lines (LN229, ACHN, A2058, U251, T47D, MCF7, HMC-1-8, U87, DoTc2-4510, and PC3) were seeded in 96-wells at 3,500 to 5,000 cells per well. The next day, cell lines were infected via overnight incubation of virus and polybrene prior to a media change. Puromycin selection was started 24h after infection. Cells were incubated for 4-6 additional days as indicated, and overall cell viability was quantified using the Cell Titer Glo (CTG) reagent (Promega) and measuring luminescence. As doubling times and luminescence values per viable cell differ between different cell lines, values are normalized to the same cells transduced in parallel with innocuous shGFP hairpins as indicated.

When comparing sensitivity to GLDC (or GCSH, SHMT2) knockdown across different cell lines, two identical sets of experiments, one which receives puromycin selection and one which does not, were carried out in parallel. Comparing the two ensures that the toxicity observed in the 'sensitive' cell lines is due to GLDC knockdown and not due to selection of nontransduced cells, because identical toxicity is also seen in the nonselected plate. Conversely, we can ensure that low toxicity observed in the 'insensitive' cell lines is not an artifact of poor transduction because if they had been poorly transduced, then toxicity would be observed in the puromycin selected plate. In this manner, we verified full transduction of cells that we have examined for GLDC effects on viability.

For some experiments, cells are transduced with more than one shRNA and this was carried out in a sequential manner. Cells were infected with the first lentivirus expressing an shRNA

(shGFP, shSHMT2_1, or shSHMT2_2, shGCAT_1, shGCAT_2) as described, then selected in puromycin for 3 days, and expanded for 2-5 more days. Equal numbers of each stable cell line were infected with the second lentivirus (shGFP, shGLDC_1, or shGLDC_2), seeded in 96-well plates, and at 5 days following infection, cell viability was measured. Because in some cases (e.g. shGCAT hairpins) the primary transduction itself moderately impairs cell proliferation, viability values for the cells secondarily transduced with shGLDCs are always expressed as relative to the same primary transduced cells, processed in parallel, which are secondarily infected with a control hairpin (shGFP). Because the secondary transduction cannot be selected for (since the cells are already puromycin resistant from the first round of transduction), effective knockdown of the second gene was verified by Western blot.

For cell proliferation experiments, cell counts were determined using a Coulter Counter (Beckman).

Histology and immunohistochemistry

Immunohistochemical analyses were performed on discarded archival biopsy (7) and autopsy (7) specimens of glioblastoma, World Health Organization Grade IV, seen at the Departments of Pathology, Massachusetts General Hospital and NYU Langone Medical Center, from 2010 to 2013. Approval from respective Institutional Review Board was obtained, and because we used discarded tissue only, a waiver of informed consent was received. Formalin-fixed, paraffin-embedded brain biopsy tissues were stained with routine hematoxylin and eosin stain (H&E), and cases were reviewed by a neuropathologist (M.S.) to select the most representative block/s for immunohistochemical analysis. Paraffin sections of GBM tumors and normal brains, fixed in 10% formalin, were subjected to deparaffinization and antigen retrieval with Borg Decloaker RTU solution pressurized Decloaking Chamber (Biocare Medical). Antibodies were diluted in in 4% horse serum and 0.1% tween in PBS, which was also used for blocking. Vectastain ABC

immunoperoxidase detection kit (Vector Labs) and DAB+ substrate kit (Dako) was used for chromogenic labeling. It was noted that antigen presentation for SHMT2 was much weaker in autopsy sections compared to tumor biopsy sections, likely a result of postmortem interval, and thus a more concentrated primary antibody incubation and longer chromogenic development was required for these sections to get comparable signal to the biopsy sections.

Images were acquired using an Olympus BX41microscope and CellSens^{R} software. For immunofluorescence staining of GBM tumors and normal brains, as well as rapid tumor xenografts, fixed in 10% formalin, the same deparaffinization, antigen retrieval, and blocking/antibody incubation steps were used as above. Immunoreactivity was detected using Alexa-fluor 488 and 568 antibodies and nuclei labeled with Hoechst 33352 (Life Technologies), and Prolong^{R} Gold antifade reagent (Life Technologies) was used as mounting medium. Images were acquired using a Zeiss Axiovert 200M inverted fluorescent microscope and AxioVision Software. For all image-based data, acquisition and processing steps were carried out using the same parameters across the entire set, aside from the increased antibody concentration and longer chromogenic development for the set of autopsy sections for SHMT2 immunostaining as described.

Metabolite extraction and LC-MS analysis

Untargeted metabolite profiling, flux experiments, and amino acetone measurements were performed on a Dionex UltiMate 3000 ultra-high performance liquid chromatography system coupled to a Q Exactive benchtop Orbitrap mass spectrometer, which was equipped with an Ion Max source and a HESI II probe (Thermo Fisher Scientific). External mass calibration was performed every 7 days.

For untargeted metabolite profiling and flux experiments, polar metabolites were extracted from cells growing in a 6-well dish using 400 µL of ice cold 80% methanol with 20 ng/mL valine-d8 as an internal extraction standard. After scraping the cells, 400 µL of chloroform was added before vortexing for 10 min at 4°C, centrifugation for 10 min at 4°C at 16,000xg, and drying 150 µL of the upper methanol/water phase under nitrogen gas. Dried samples were stored at -80°C then resuspended in 40 µL 50% acetonitrile/50% water immediately before analysis. Cells were usually left plated for 24-48 h after a media change before extraction in order to allow for media conditioning. Accordingly, [U-^{13}C]glucose labelling of cells was achieved by adding a concentrated stock to a final concentration of 11.1 mM after 24 h of media conditioning. Chromatographic separation was achieved by injecting 10 µL of sample on a SeQuant ZIC-pHILIC Polymeric column (2.1x150 mm 5 uM, EMD Millipore). Flow rate was set to 100 µL/min, column compartment was set to 25°C, and autosampler sample tray was set to 4°C. Mobile Phase A consisted of 20 mM ammonium carbonate, 0.1% ammonium hydroxide. Mobile Phase B was 100% acetonitrile. The mobile phase gradient (%B) was as follows: 0 min 80%, 5 min 80%, 30 min 20%, 31 min 80%, 42 min 80%. All mobile phase was introduced into the ionization source set with the following parameters: sheath gas = 40, auxiliary gas = 15, sweep gas = 1, spray voltage = -3.1kV or +3.0kV, capillary temperature = 275°C, S-lens RF level = 40, probe temperature = 350°C. In experiments to measure steady-state levels, metabolites were monitored using a polarity-switching full-scan method. In experiments utilizing [U-^{13}C]glucose tracing, metabolites were monitored using a targeted selected ion monitoring (tSIM) method in negative mode with the quadrupole centered on the M-H ion m+1.5, m+2.5, or m+3.5 mass with a 8 amu isolation window, depending on the number of carbons in the target metabolite. Resolution was set to 70,000, full-scan AGC target was set to 10^6 ions, and tSIM AGC target was set to 10^5 ions. For tracing experiments, samples were collected at various time points as indicated. Labeling rate was calculated from counts at 6 minutes, and detailed methods for determining the labeling rate and overall flux are provided in the first three worksheets of

Supplemental Table 8. Data were acquired and analyzed using Xcalibur v2.2 software (Thermo Fisher Scientific). Full-scan untargeted data was analyzed using Progenesis CoMet v2.0 software (Nonlinear Dynamics) to identify differential peaks (Supplemental Table 4 and 5) and the identified metabolites with greatest predicted change were further analyzed with Xcalibur. Retention times for selected metabolites appearing in the untargeted analyses (AICAR and SAICAR) were confirmed by running a standard. All standards were obtained commercially, except for SAICAR, which was synthesized enzymatically from AICAR and purified by ion-exchange chromatography as described (Keller, 2012).

Oxygen consumption measurements

Oxygen consumption of LN229 cells was measured using an XF24 Extracellular Flux Analyzer (Seahorse Bioscience). 60,000 cells were plated per well the night before the experiments, and RPMI 8226 media (US Biological #9011) containing 2 mM glutamine and 10 mM glucose without serum was used as the assay media. Oxygen consumption measurements were normalized based on protein concentration obtained from the same plate used for the assay.

Lactate dehydrogenase (LDH)-linked pyruvate kinase activity assay

Concentrated (5-10 mg/mL) hypotonic lysate was prepared from cells by swelling on ice for 10min in one equivalent of 1xHypotonic Lysis Buffer (20 mM HEPES pH 7.0, 5 mM KCl, 1 mM $MgCl_2$, 2 mM DTT, 1 tablet/10mL Complete EDTA-free protease inhibitor (Roche)), then passing through a 26 gauge needle 3x, then spinning 10min at 4°C at 16,000xg. Concentrated lysate was diluted 1:100 in 1xHypotonic Lysis Buffer and immediately assayed with 500 µM final PEP, 600 µM final ATP, 180 µM final NADH, and 0.16mg/mL LDH in 1xReaction Buffer (50 mM Tris pH 7.5, 50 mM KCl, 1 mM DTT) in 100 µL total. Decrease in NADH fluorescence was followed in a Tecan plate reader and a regression on the slope of the decrease was taken as the activity.

Bradford assay was performed on the concentrated lysate and activities were normalized to total protein.

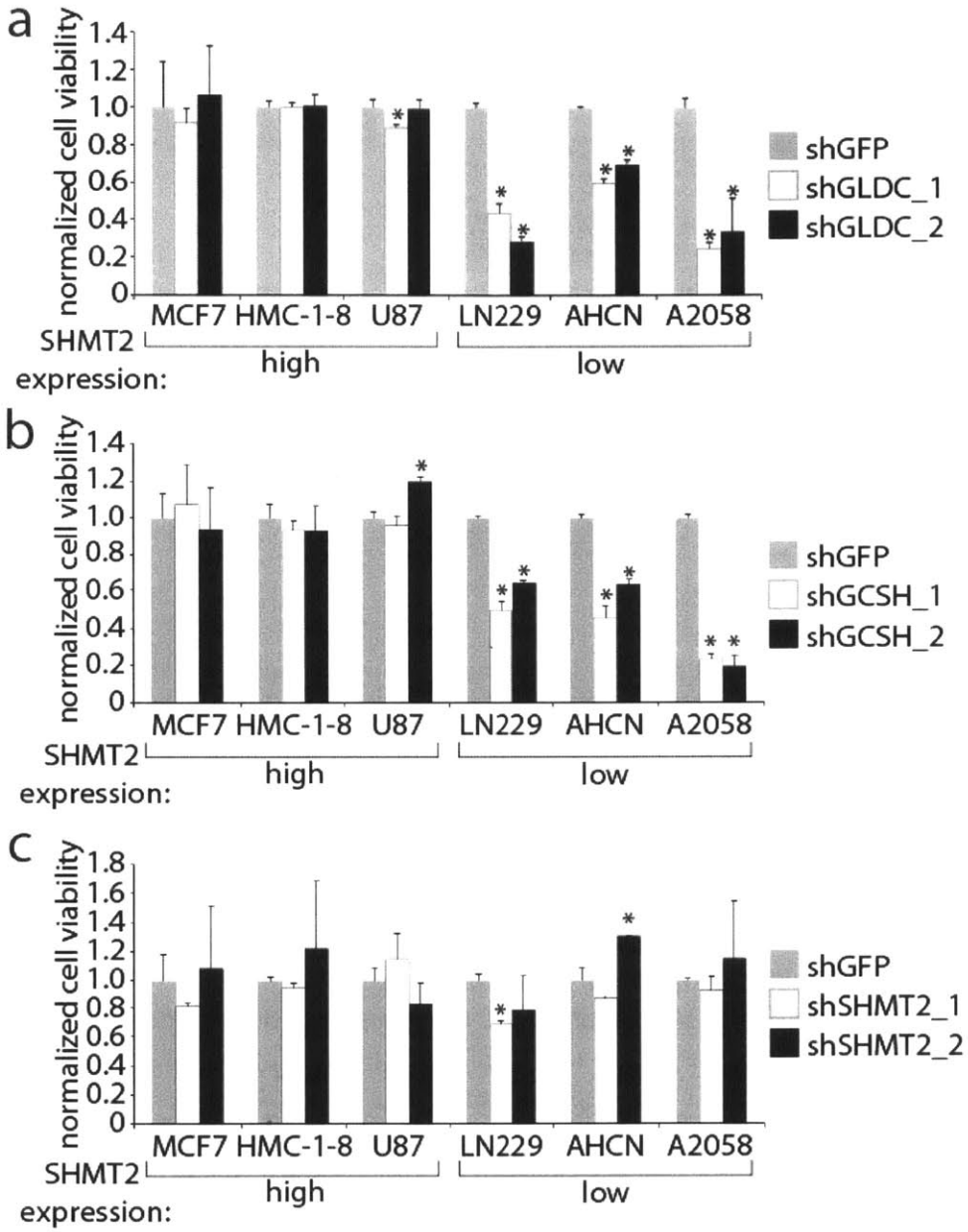

Figure 1 - Effects of glycine cleavage system inhibition on cells with high or low SHMT2 expression levels. Viability of various cell lines transduced with shRNAs targeting (a) GLDC, (b) GCSH (glycine cleavage system protein H, another integral component of the glycine cleavage system), or (c) SHMT2. Values are relative to those of the cells expressing shGFP, which were grown in parallel. For all panels, error bars are SD (n=3). *P<0.05 (student's t test).

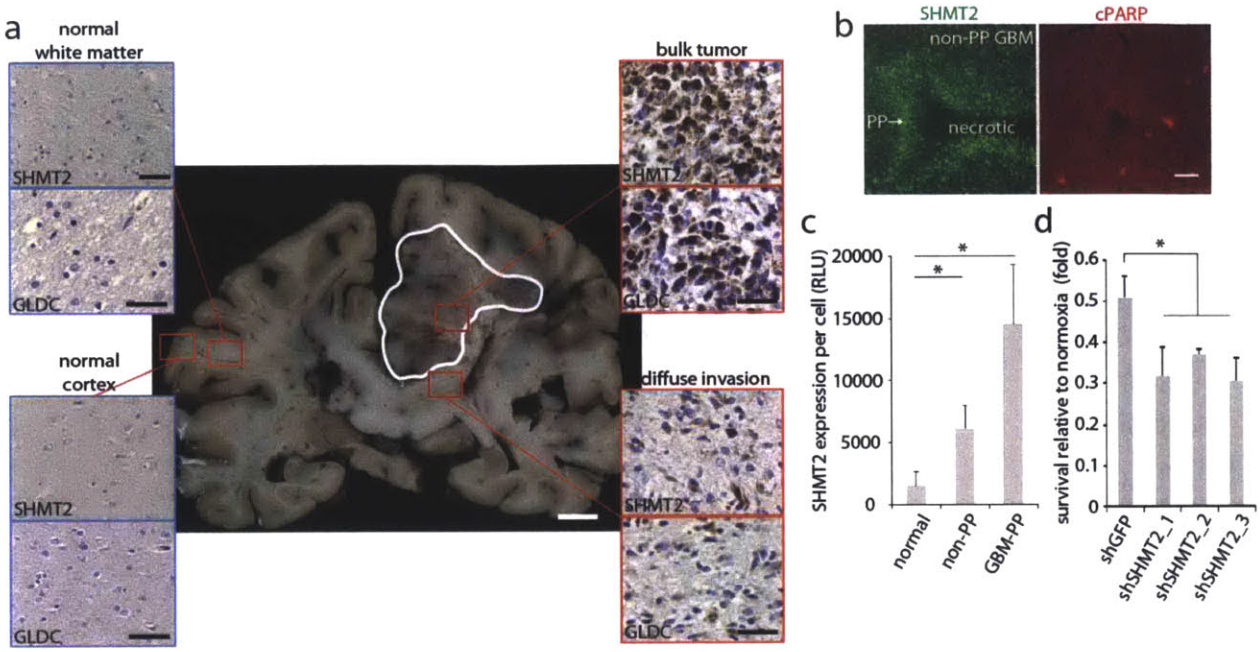

Figure 2 - SHMT2 expression provides a survival advantage in the ischemic tumor microenvironment a) SHMT2 and GLDC expression across GBM and normal brain regions as examined in autopsy sections. A whole coronal section is shown, with the GBM bulk tumor outlined in white. Insets indicate magnified micrographs from the regions, indicated by the small red squares, from the same brain. For the bulk tumor insets, cells around the pseudopalisading necroses are shown. Additional GBM and normal brain are shown in Figure 3. Scale bar for whole coronal section = 1 cm, and for insets = 100 μm. b) SHMT2 immunofluorescence in the cells in the pseudopalisades and in the non-pseudopalisade GBM regions. Glial fibrillary acidic protein (GFAP), a general GBM cell marker, does not show increased signal in pseudopalisades. c) Quantification of SHMT2 expression, measured as fluorescence intensity per cell, in normal brain regions, non-pseudopalisade GBM regions, and pseudopalisade regions (n=5 per group). Error bars are SD. d) Cell number counts from LN229 cells expressing shRNAs against GFP or SHMT2 and cultured in 0.5% hypoxia for 8 days. Values are relative to the counts of the same cells cultured in parallel in normoxia. Error bars are SD (n=3).

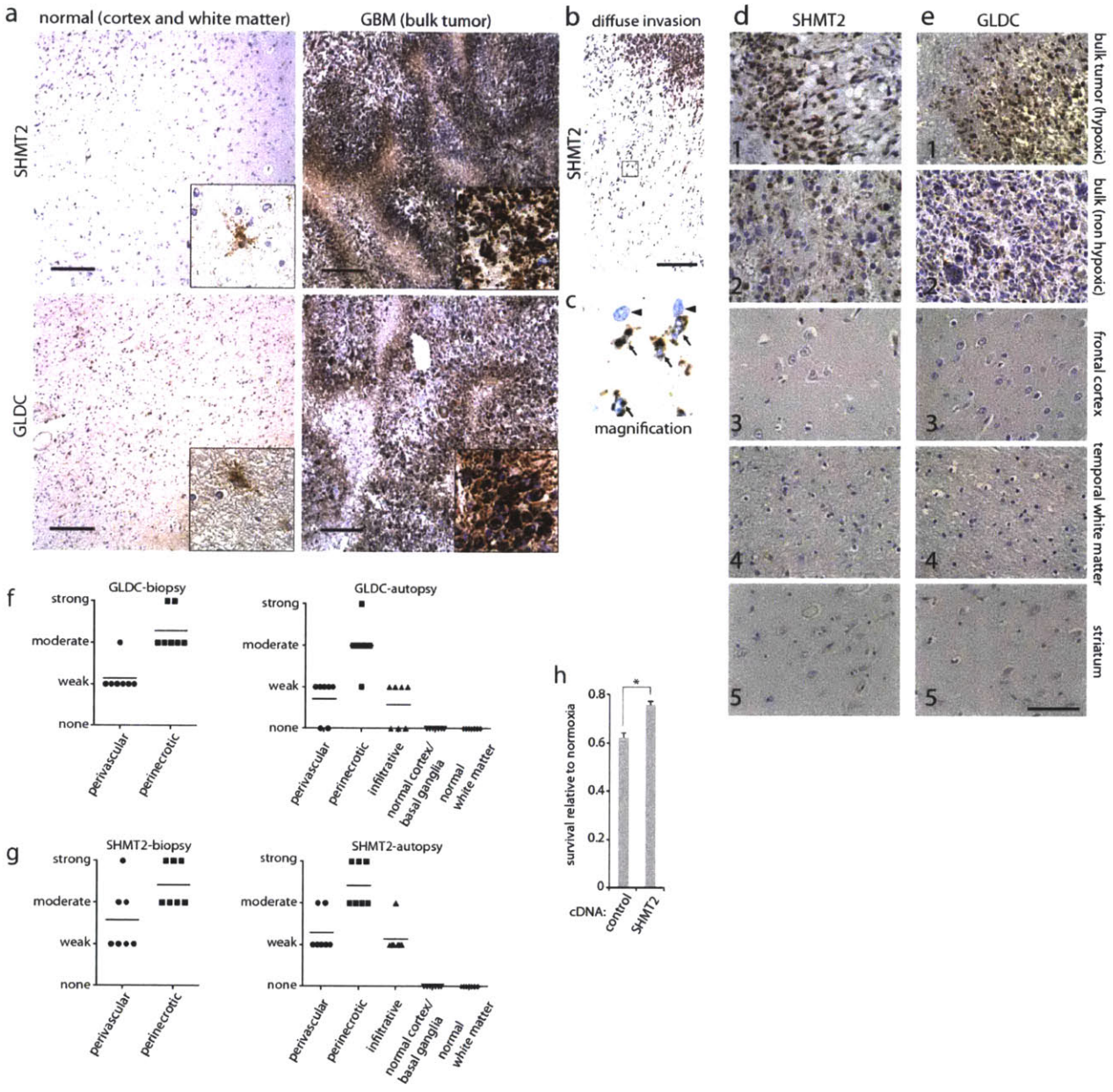

Figure 3 - GLDC and SHMT2 expression in GBM tumors a) SHMT2 and GLDC expression in normal human brain and GBM tumors. Insets are 5X fold magnifications of the indicated fields. Representative images are shown. Scale bar = 200 μm. b) SHMT2 expression at the GBM-normal brain interface, showing SHMT2-immunoreactivity in migrating cells. Scale bar = 100 mm. c) Magnified image of the boxed region in b. d and e) High magnification micrographs of SHMT2 and GLDC expression, respectively, in 1) perinecrotic GBM tumor, 2) non-ischemic bulk tumor, 3) frontal cortex, 4) temporal white matter, and 5) striatum from autopsy cases. Scale bar = 100 mm. f) Semi-quantitative scoring of GLDC staining intensity by neuropathologist (M.S.) on 7 tumor biopsy cases (left) and 7 autopsy cases (right). g) Semi-quantitative scoring of SHMT2 staining intensity by neuropathologist (M.S.) on 7 tumor biopsy cases (left) and 7

autopsy cases (right). h) Cell number counts from LN229 cells expressing an empty vector control or SHMT2 cDNA and cultured in 0.5% hypoxia for 8 days. Values are relative to the counts of the same cells cultured in parallel in normoxia. Bars indicate the mean, error bars are SD (n=3). *P<0.05 (student's t test).

a

cDNA:	empty	SHMT2^{res}
metabolite	fold Δ shSHMT2 /shGFP	fold Δ shSHMT2 /shGFP
glycineamideribotide (GAR)	+12.4	+1.4
AICAR*	+8.7	+1.6
SAICAR*	+4.6	+1.1
acetylcarnitine	+3.6	+1.6
fructose bisphosphate	+2.8	+1.5
phosphoethanolamine	-2.8	-1.4
CDP-ethanolamine	-3.3	-1.5
serine	+1.5	+1.2
glycine	-1.2	+1.2
citrate	+1.5	-1.1

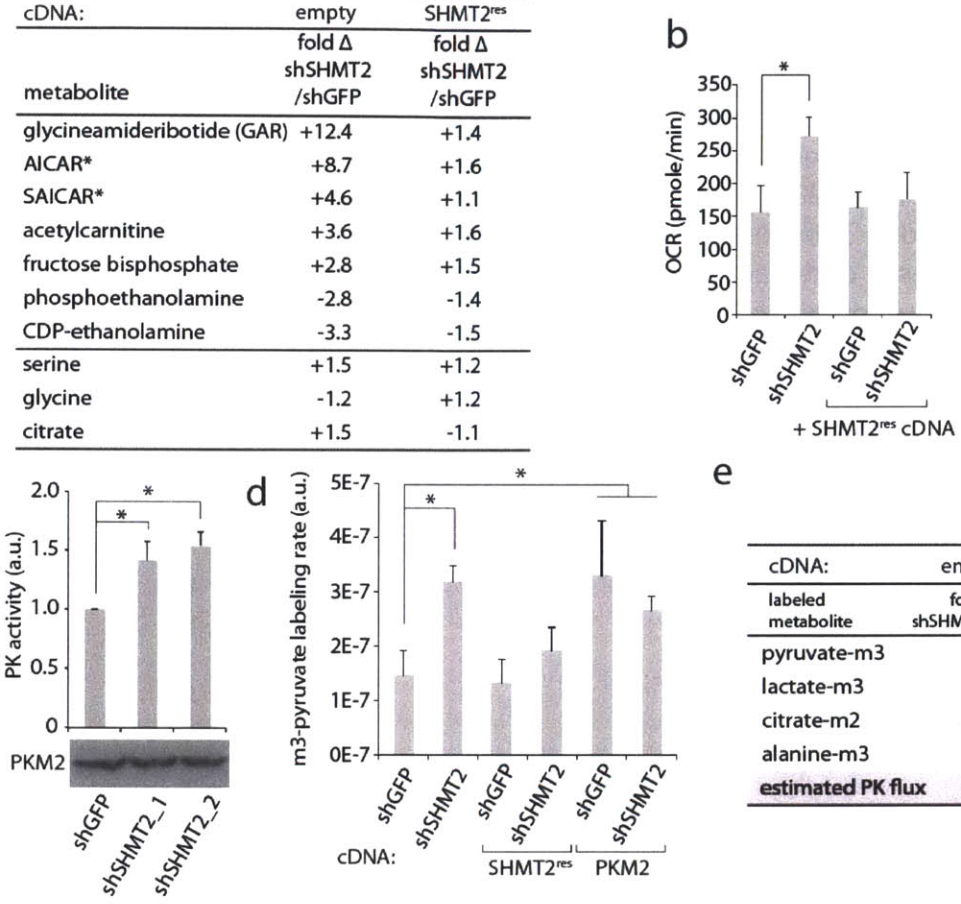

e

cDNA:	empty	SHMT2^{res}
labeled metabolite	fold Δ shSHMT2/shGFP	fold Δ shSHMT2/shGFP
pyruvate-m3	2.2	1.4
lactate-m3	1.7	1.2
citrate-m2	2.0	1.6
alanine-m3	1.3	1.1
estimated PK flux	**1.7**	**1.2**

Figure 4 - SHMT2 elicits a PKM2-dependent metabolic rewiring that is advantageous to cancer cells in an ischemic environment a) LC-MS based, untargeted discovery of metabolites that change in abundance following SHMT2 knockdown in LN229 cells. Differential peaks were identified and quantified as described in the Methods, and the identified metabolites

with largest change are listed, as well as serine, glycine, and citric acid. Metabolite levels are relative and are expressed as fold change in cells transduced with shSHMT2_1 versus cells transduced with shGFP, with or without the RNAi-resistant SHMT2 cDNA. All differences between LN229 cells expressing shSHMT2_1 and shGFP were significant (n=3, $P<0.05$) with the exception of glycine. b) Oxygen consumption in LN229 cells (in RPMI media) transduced with indicated shRNAs and cDNAs. Error bars are SD (n=4). c) Pyruvate kinase activity assay from lysates of LN229 cells transduced with indicated shRNAs. Error bars are SD (n=3). d) m3-pyruvate labeling rates in LN229 cells transduced with shRNAs and cDNAs as indicated, and fed [U-^{13}C]-glucose media. Error bars are SE (n=3). e) ^{13}C labeling rates of pyruvate and its downstream metabolites in cells from d. Labeling rates are relative and expressed as fold changes in cells transduced with shSHMT2_1 versus cells transduced with shGFP, with or without RNAi-resistant SHMT2 cDNA. Estimated PK flux is the calculated total flux to the four product species in moles of ^{13}C per unit time. f) Summary diagram of labeling rate changes seen in e as a result of SHMT2 silencing. Colored arrows indicate increased flux according to the heat map, while gray arrows indicate non-determined labeling rates. g) Oxygen consumption in LN229 cells expressing shGFP or shSHMT2_1 in RPMI media with or without 1 mM pyruvate. Error bars are SD (n=4). h) Oxygen consumption in LN229 cells (in RPMI) expressing shGFP or shSHMT2_1 with or without PKM2 cDNA. Error bars are SD (n=5). For all panels, *$P<0.05$ (student's t test).

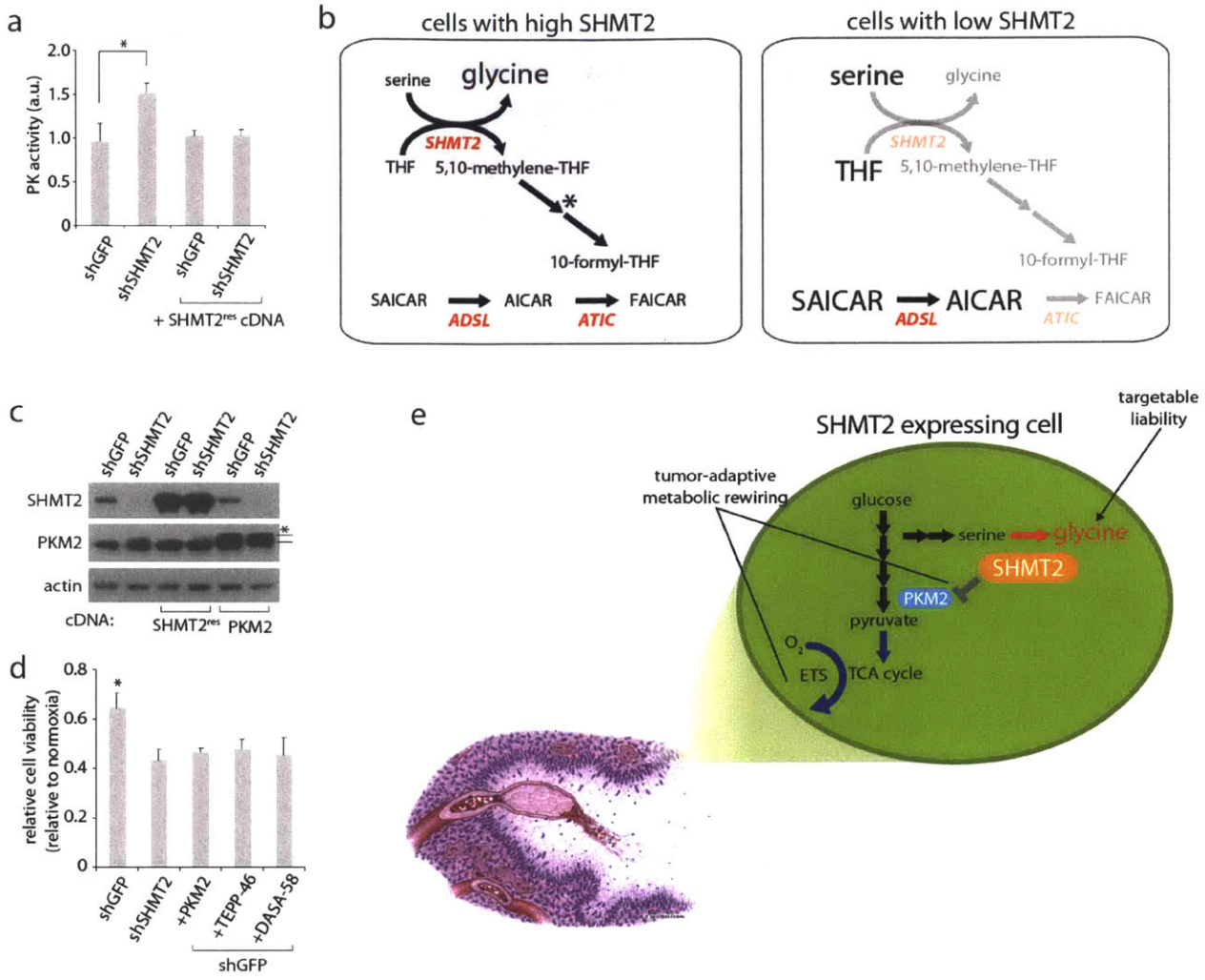

Figure 5 - Effects of SHMT2 expression on PKM2 activity and cell metabolism a) Pyruvate kinase activity assay from lysates of U251 cells transduced with indicated shRNAs or cDNAs. Error bars are SD (n=3). b) Proposed mechanism by which SHMT2 inhibition could lead to an increase in AICAR and SAICAR. In cells with high SHMT2 expression, 10-formyl-THF, which is a downstream product of SHMT2 activity, serves as a cofactor for cytosolic 5-aminoimidazole-4-carboxamide ribonucleotide formyltransferase (ATIC) in the conversion of AICAR to FAICAR during purine biosynthesis. In the absence of SHMT2, a lack 10-formyl-THF production could lead to accumulation of AICAR and SAICAR. As indicated by the asterisk, the contribution of SHMT2 to cytosolic 10-formyl-THF formation may be direct, occur via export of formate from the mitochondria, or occur indirectly by changing serine/glycine levels and thereby altering SHMT1 activity. c) SHMT2 and PKM2 expression in LN229 cells transduced with shRNAs and cDNAs as indicated. Asterisk indicates the overexpressed PKM2, which shows higher migration due to Flag tag. d) Viability of LN229 cells transduced with shRNAs or cDNAs as indicated, and also treated with vehicle or 50 uM of TEPP-46 or DASA-58 as indicated, then subjected to hypoxia for 6 days. Values are relative to the same cells grown in parallel in normoxia. e) Overview of

effects of SHMT2 expression on cell metabolism, tumor cell survival, and liability to toxic glycine accumulation. Red arrow indicates upregulation, and blue arrow indicates downregulation. Gray bar indicates the inhibitory effect of SHMT2 activity on PKM2 activity. Depiction of pseudopalisading necrosis is adapted from a previous review (Brat and Meir, Laboratory Investigation 84(4):397-405). Illustration by Mica Duran.

References

Anastasiou D, Yu Y, Israelsen WJ, Jiang JK, Boxer MB, Hong BS, Tempel W, Dimov S, Shen M, Jha A, Yang H, Mattaini KR, Metallo CM, Fiske BP, Courtney KD, Malstrom S, Khan TM, Kung C, Skoumbourdis AP, Veith H, Southall N, Walsh MJ, Brimacombe KR, Leister W, Lunt SY, Johnson ZR, Yen KE, Kunii K, Davidson SM, Christofk HR, Austin CP, Inglese J, Harris MH, Asara JM, Stephanopoulos G, Salituro FG, Jin S, Dang L, Auld DS, Park HW, Cantley LC, Thomas CJ, Vander Heiden MG. (2012). Pyruvate kinase M2 activators promote tetramer formation and suppress tumorigenesis. Nat Chem Biol 8, 839-47.

Brown JM, Wilson WR. (2004). Exploiting tumour hypoxia in cancer treatment. Nat Rev Cancer 4, 437-47.

Gui DY, Lewis CA, Vander Heiden MG. (2013). Allosteric regulation of PKM2 allows cellular adaptation to different physiological states. Sci Signal 6, pe7.

Hockel M, Schlenger K, Aral B, Mitze M, Schaffer U, Vaupel P. (1996). Association between tumor hypoxia and malignant progression in advanced cancer of the uterine cervix. Cancer Res 56, 4509-15.

Ibsen KH, Marles SW. (1976). Inhibition of chicken pyruvate kinases by amino acids. Biochemistry 15, 1073-9.

Keller KE, Tan IS, Lee YS. (2012). SAICAR stimulates pyruvate kinase isoform M2 and promotes cancer cell survival in glucose-limited conditions. Science 338, 1069-72.

Kim D, Fiske BP, Birsoy K, Freinkman E, Kami K, Possemato R, Chudnovsky Y, Pacold ME, Chen WW, Cantor JR, Shelton LM, Gui DY, Kwon M, Ramkissoon SH, Ligon KR, Kang SW, Snuderl M, Vander Heiden MG, Sabatini DM. (2015). SHMT2 drives glioma cell survival in the tumor microenvironment but imposes a dependence on glycine clearance. In submission.

Lunt SY, Vander Heiden MG. (2011). Aerobic glycolysis: meeting the metabolic requirements of cell proliferation. Annu Rev Cell Dev Biol 27, 441-64.

Papandreou I, Cairns RA, Fontana L, Lim AL, Denko NC. (2006). HIF-1 mediates adaptation to hypoxia by actively downregulating mitochondrial oxygen consumption. Cell Metab 3, 187-97.

Rong Y, Durden DL, Van Meir EG, Brat DJ. (2006). 'Pseudopalisading' necrosis in glioblastoma: a familiar morphologic feature that links vascular pathology, hypoxia, and angiogenesis. J Neuropathol Exp Neurol 65, 529-39.

Appendix - Lack of evidence for PKM2 protein kinase activity

Authorship Statement

The entirety of this appendix is copied verbatim with only minor edits from the following manuscript in submission: Hosios AM, Fiske BP, Gui DY, Vander Heiden MG. (2015). Lack of evidence for PKM2 protein kinase activity. In submission.

Introduction

The M2 isoform of pyruvate kinase (PKM2) is expressed in cancer cells and many normal cells with proliferative capacity and/or anabolic functions. Several lines of evidence argue that PKM2 is important for cancer cell proliferation in some contexts. PKM2 is expressed in cancers and cell lines, and regulation of PKM2 enzymatic activity can influence cell proliferation (Anastasiou et al., 2012; Chaneton et al., 2012; Israelsen et al., 2013; Lunt et al., 2015; Parnell et al., 2013). Two models, which are not mutually exclusive, seek to explain the importance of PKM2 expression in cancer (McKnight, 2014). One proposes that PKM2 exerts its effects through its canonical activity, which is regulated to control cell metabolism and synthesis of macromolecules. The other proposes that PKM2 is a protein kinase, regulating gene expression downstream of growth signaling.

Pyruvate kinase catalyzes the final step in glycolysis, transferring a phosphoryl group from phosphoenolpyruvate (PEP) to ADP to produce pyruvate and ATP. There are four mammalian isoforms, and alternative splicing of the *PKM* gene produces the isoforms PKM1 and PKM2. The exon unique to PKM2 is reported to confer protein kinase activity as well as regulatory properties that are lacking in PKM1. For example, PKM2 requires its allosteric activator fructose-1,6-bisphosphate (FBP) to be fully active, while PKM1 activity is constitutively high

(Dombrauckas et al., 2005; Morgan et al., 2013). In support of a metabolic role for pyruvate kinase in proliferation the glycolytic enzyme activity of PKM2, but not PKM1, can be inhibited by growth signaling in rapidly proliferating cells, and the resulting low levels of pyruvate kinase activity facilitate tumor growth (Christofk et al., 2008; Hitosugi et al., 2009). PKM2 is also allosterically activated by the metabolites serine and SAICAR (a purine precursor), enabling regulation of this enzyme by nutrient conditions and coordination of its activity with metabolic pathways outside of glycolysis (Chaneton et al., 2012; Keller et al., 2012; Kung et al., 2012). Synthetic activators of PKM2 impair tumor growth by raising PKM2 activity to PKM1 levels (Anastasiou et al., 2012), and high pyruvate kinase activity impairs proliferation of mouse embryonic fibroblasts (MEFs) by limiting precursors for DNA replication (Lunt et al., 2015). Deletion of PKM2 does not prevent tumor growth, and results in compensatory PKM1 expression in non-proliferating cells in the tumor, arguing that the ability of PKM2 to be active or inactive allows this isoform to support different metabolic cell states in tissues (Israelsen et al., 2013).

The protein kinase activity reported for PKM2 is distinct from a role in glycolysis. Transfer of a phosphoryl group from PEP to proteins, which also generates pyruvate, has been reported to occur as a result of a kinase activity that is unique to PKM2 among pyruvate kinase isoforms. PEP-dependent phosphorylation is uncommon in cells, but has been observed in both bacterial and mammalian systems (Deutscher et al., 2006; Vander Heiden et al., 2010). In both cases, a phosphoryl group is transferred from PEP to a histidine residue on a protein, and the bacterial PEP-dependent histidine kinases have no homology to PKM2 or other enzymes in glycolysis. PKM2 has been reported to function as a dual-specificity kinase, transferring phosphoryl groups to serine/threonine and tyrosine residues on different proteins (Gao et al., 2012; Yang et al., 2012a). When studied, PKM2 protein kinase activity is catalyzed by dimeric PKM2, a state with much lower canonical glycolytic enzyme activity when compared with fully active tetrameric

PKM2. In particular, dimeric PKM2 localizes to the nucleus where it acts as a Stat3 kinase (Gao et al., 2012). An R399E mutant was reported to be an obligate dimer with elevated protein kinase activity. Subsequent work suggested that it also phosphorylates histone H3. EGFR signaling to ERK1/2 can result in nuclear translocation of PKM2, where PKM2 protein kinase activity leads to c-Myc and cyclin D1 expression to drive cell cycle progression beyond the G1/S checkpoint (Yang et al., 2012a; Yang et al., 2012b). PKM2 is also reported to be a kinase of spindle assembly checkpoint protein Bub3, playing an important role in ensuring faithful chromosome segregation (Jiang et al., 2014). Finally, SAICAR, the allosteric activator of canonical PKM2 activity, was reported to synergize with ERK2 to stimulate protein kinase activity of PKM2, enabling it to phosphorylate a large number of proteins (Keller et al., 2012). This observation is in contrast to other reports that FBP, another activator of canonical PKM2 activity, inhibits protein kinase activity (Gao et al., 2012).

Although tumors express PKM2, this enzyme is not essential for growth of all tumors. PKM2 deletion does not prevent tumorigenesis in a mouse model of breast cancer and loss of PKM2 can promote tumor progression (Israelsen et al., 2013). PKM2 is also not required for hematopoietic stem cell or leukemia cell proliferation, but PKM2 expression enhances transplantation of hematopoietic stem cells (Wang et al., 2014). Finally, knockdown of PKM2 using RNA interference does not alter formation or maintenance of xenograft tumors, although it partially obstructs proliferation *in vitro* (Cortes-Cros et al., 2013). These data argue against any model where PKM2 is essential for regulating cell cycle mediators or other events that are important for eukaryotic cell proliferation.

To date, studies examining PKM2 functions in cancer have not resolved differential roles for PKM2 in signaling and regulation of metabolism. We investigated the protein kinase activity of PKM2; however, we were unable to demonstrate PKM2-dependent phosphorylation of any

proteins *in vitro* using either PEP or ATP as a phosphate donor. Instead, all PKM2-dependent phosphoryltransfer events observed involved regeneration of ATP from ADP and PEP, the known function of PKM2 in glycolysis. This study also establishes methods to track PEP-dependent protein phosphorylation in cells.

Results

PEP-dependent phosphorylation events are well described as part of two-component signaling in bacteria (Deutscher et al., 2006). Transfer of the phosphoryl group from [^{32}P]-PEP to phosphoglycerate mutase (PGAM) has been shown in eukaryotic cell lysates, but this activity is not dependent on PKM2 (Vander Heiden et al., 2010). To identify other PEP-dependent phosphorylation events in mammalian cells, including those that might be dependent on PKM2, we tracked [^{32}P]-phosphoryltransfer to proteins as a sensitive measure of protein phosphorylation. The phosphorylation reaction was performed in the presence of orthovanadate to inhibit phosphatase activity, and also to minimize PGAM1 labeling as orthovandate promotes PGAM1-His11 dephosphorylation (Carreras et al., 1982). Labeling of PGAM1 from PEP is the dominant species generated in this reaction (Vander Heiden et al., 2010), and we sought to minimize this to avoid masking phosphorylation events involving less abundant proteins. Of note, pervanadate was included as a phosphatase inhibitor in past studies of PKM2 protein kinase activity and thus is not expected to inhibit this enzyme activity of PKM2 (Gao et al., 2012; Yang et al., 2012a). [^{32}P]-PEP was added to hypotonic cell lysates prepared to minimize disruption of endogenous protein complexes and protein phosphorylation was visualized by SDS-PAGE and autoradiography (Figure 1). PGAM1 labeling was observed when phosphatase inhibitors were not included (Figure S1). To determine whether the phosphoryltransfer events were dependent on ATP or PEP as a phosphoryl donor, 1 mM unlabeled PEP or ATP was added as a competitor for the reaction, a control lacking from

published demonstrations of PKM2 protein kinase activity that rely heavily on antibodies to detect phosphorylation events and thus fail to distinguish whether the phosphoryl group is derived directly from PEP. Most protein labeling events observed are competed by non-radioactive ATP and not non-radioactive PEP. This finding is consistent with ATP serving as the direct phosphoryl donor for most phosphorylation events and is consistent with previous reports (Vander Heiden et al., 2010). Interestingly, diffuse bands of variable intensity that migrated on SDS-PAGE with the 15-20 kDa and 100-120 kDa molecular weight markers were labeled from [^{32}P]-PEP that were sensitive to competition by non-radioactive PEP but not non-radioactive ATP. To determine if these were dependent on transfer to protein in cell lysates, [^{32}P]-PEP or [γ-^{32}P]-ATP were added to loading buffer in the absence of added protein (Figure S2). The same bands were observed when [^{32}P]-PEP, but not [γ-^{32}P]-ATP, was subjected to SDS-PAGE, and were sensitive to the addition of non-radioactive PEP to the loading dye. The same bands are observed when [^{32}P]-PEP is loaded with glycerol alone, arguing that these events reflect an artifact and are not protein phosphorylation events.

Consistent with PEP-dependent phosphorylation being uncommon, most other phosphorylation events from [^{32}P]-PEP were competed by 1 mM ATP and not 1 mM PEP; however phosphorylation of a species migrating at ~45 kDa that was not blocked by excess ATP was observed in both H1299 (human non-small cell lung carcinoma) (Figure 1A) and mouse embryonic fibroblast (MEF) (Figure 1B) hypotonic cell lysates. No reported substrates of PKM2-dependent protein phosphorylation are consistent with this molecular weight, suggesting that this event is a previously uncharacterized target of PEP-dependent phosphorylation.

To determine whether addition of PKM2 would result in additional phosphorylation events, we included recombinant PKM2 (rPKM2) in the reaction. rPKM2 has been used previously to show PKM2-dependent phosphorylation (Gao et al., 2012; Keller et al., 2014; Yang et al., 2012a);

however, we did not observe any PEP-dependent phosphorylation events upon addition of either wild type (WT) rPKM2 or a mutant PKM2 (R399E) that is reported to have higher protein kinase activity (Gao et al., 2012) (Figure 1A). Both WT- and R399E-rPKM2 enzymes exhibit pyruvate kinase activity as a glycolytic enzyme as both can support synthesis of [γ-^{32}P]-ATP from [^{32}P]-PEP and cold ADP; although consistent with reports that the R399E mutant favors the inactive dimeric form of the enzyme, this protein is less efficient than WT PKM2 in transferring the [^{32}P]-phosphoryl group from PEP to ADP (Figure S3). Because most substrates of PKM2-dependent phosphorylation are nuclear, we also tested the ability of PKM2 to phosphorylate proteins in a nuclear extract and again failed to observe any PEP-dependent phosphorylation events with or without rPKM2 included in the reaction.

Because PKM2 is an abundant protein (Beck et al., 2011), we considered the possibility that endogenous PKM2 present in the H1299 hypotonic and nuclear lysates (Figure S4) could be sufficient to catalyze PKM2-dependent phosphorylation, and that this might explain why addition of rPKM2 did not produce any additional phosphorylated species. To definitively assess a requirement for PKM2 in any PEP-dependent phosphoryltransfer events, we utilized PKM2-deleted MEFs (Lunt et al., 2015) and confirmed that PKM2-specific exon 10 was deleted from the genome and that PKM2 protein is absent from these cells (Figure S5). Phosphoryltransfer from PEP was similar to that in H1299 cells, and we did not observe phosphorylation dependent on the addition of rPKM2 to *PKM2*$^{-/-}$ lysates (Figure 1B). PKM2 protein kinase activity is reported to be important specifically for glioblastoma development downstream of EGFR activation (Gao et al., 2012; Keller et al., 2014; Yang et al., 2012a; Yang et al., 2012b), however, we also failed to observe PEP-dependent protein kinase activity in hypotonic and nuclear lysates of U87 glioblastoma multiforme cells and U87 cells expressing constitutively active EGFR-VIII with or without PKM2 addition (Figure 1C,D).

Most labeling from [^{32}P]-PEP was eliminated by addition of excess cold ATP, suggesting that [γ-^{32}P]-ATP was either generated from [^{32}P]-PEP, or present as a contaminant in the reaction to serve as the phosphoryl group donor for most of the observed phosphorylation events. Indeed, [^{32}P]-PEP is synthesized from commercial [^{32}P]-ATP using pyruvate kinase (Mattoo and Waygood, 1983; Vander Heiden et al., 2010), and despite a step to enrich for [^{32}P]-PEP, these preparations are contaminated by small quantities of [γ-^{32}P]-ATP (Figure 2A). Preparative HPLC of [^{32}P]-PEP allowed for quantitative separation from the contaminating [γ-^{32}P]-ATP. To test the contribution of each phosphoryl donor to protein phosphorylation in a cell lysate, we incubated cells with crude [^{32}P]-PEP, HPLC purified [^{32}P]-PEP, and the HPLC fraction containing [^{32}P]-ATP present as a contaminant in crude [^{32}P]-PEP. Most proteins phosphorylated by the impure [^{32}P]-PEP were phosphorylated by the contaminating [γ-^{32}P]-ATP fraction but not the purified [^{32}P]-PEP fraction (Figure 2B). Consistent with competition by cold ATP and PEP allowing determination of direct phosphoryl donors, the ~45 kDa protein identified previously was labeled from purified [^{32}P]-PEP. Addition of ADP to purified [^{32}P]-PEP restored phosphorylation of many proteins, and the resulting phosphorylation events could be competed by both cold ATP and cold PEP. These data argue that pyruvate kinase activity present in these reactions is sufficient to allow [γ-^{32}P]-ATP synthesis from ADP and [^{32}P]-PEP (Figure 2B, lanes 10-12). Since [γ-^{32}P]-ATP is the phosphoryl donor for most protein kinase activity in cells, these data suggest that the known role of PKM2 as a glycolytic enzyme might explain PKM2-dependent phosphorylation whereby PKM2 transfers the phosphoryl group from [^{32}P]-PEP to ADP present in cell lysate to synthesize [γ-^{32}P]-ATP and result in phosphorylation seemingly dependent on PEP and the addition of PKM2. Consistent with this possibility, a hypotonic cell lysate contains sufficient ADP to enable synthesis of [γ-^{32}P]-ATP from [^{32}P]-PEP when added to the lysate, and this ability is diminished if size exclusion chromatography is used to deplete metabolites in the lysate (Figure S6).

We next considered the possibility that our failure to observe protein phosphorylation dependent on both [^{32}P]-PEP and PKM2 in hypotonic or nuclear lysates could have been due to the absence of relevant protein kinase substrates. For instance, histones, a putative target of PEP-dependent PKM2 protein kinase activity (Yang et al., 2012a), are not efficiently extracted by many protocols used to prepare nuclear extracts (Figure S4) (Shechter et al., 2007). To determine whether PKM2 can phosphorylate histones in our assay, we incubated WT- or R399E-rPKM2 and commercially prepared histones from calf thymus with impure [^{32}P]-PEP. Although we failed to observe any phosphorylation upon addition of either rPKM2 or PKM2 (R399E), a nuclear extract of H1299 cells incubated with impure [^{32}P]-PEP was able to phosphorylate proteins that run at the expected size of histones (Figure 3A), suggesting that the presence of PKM2 in a nuclear extract can enable indirect transfer a phosphoryl group from PEP to histones. The inability of PKM2 to do this directly confirms that any dependence on PKM2 is to transfer the phosphoryl group to generate ATP rather than PKM2 acting directly as a protein kinase.

Recent work has suggested that the purine precursor SAICAR is an activator of PKM2 protein kinase activity (Keller et al., 2014). In particular, it has been suggested that absence of SAICAR from *in vitro* phosphorylation reactions could account for an apparent disparity in protein kinase activity between rPKM2 produced in *E. coli* and PKM2 obtained from mammalian cell nuclear extracts. To determine if the absence of SAICAR explained why we failed to observe PKM2-mediated protein kinase activity in cell and nuclear extracts, we tested if addition of SAICAR to a reaction with rPKM2 and cell lysate, nuclear extract, or purified histones could reconstitute a PKM2-depedent protein kinase activity (Figure 3B). In no case was SAICAR addition sufficient to cause protein phosphorylation that was competed by PEP addition but not ATP addition, or that was dependent on addition of PKM2. These data suggest that any increase in PEP-dependent protein phosphorylation following SAICAR addition that involves PKM2 is likely

explained by the ability of SAICAR to activate the glycolytic enzyme function of PKM2 (Keller et al., 2012), and promote generation of ATP as a phosphoryl donor for other protein kinases.

To further search for PEP-dependent phosphorylation events that require PKM2 functions other than its known action in generating ATP, we tested HPLC purified [^{32}P]-PEP in a reaction with protein extracts that were first desalted to remove contaminating ADP, and with or without the addition of rPKM2 or rPKM2-R399E. These reactions were performed with whole cell hypotonic lysates and nuclear extracts prepared from PKM2-expressing H1299 cells and MEFs as well as PKM2-null MEFs (Figure 3C). Using this approach, we observed several phosphorylated species, including the ~45 kDa species noted previously (Figure 1A); however no events were dependent on the addition of WT- or R399E-rPKM2, including events in extracts prepared from PKM2-null MEFs. These data argue that a PKM2-dependent protein phosphorylation activity is not detectable in these cells.

Failure to observe PEP-dependent protein phosphorylation that is dependent on PKM2 does not rule out the possibility that PKM2 possesses an ATP-dependent protein kinase activity. Both PEP and ATP can act as phosphate donors for normal PKM2 enzymatic activity, so an alternative explanation for reports of PKM2 protein kinase activity might involve PKM2 as an ATP-dependent protein kinase. The ability to detect ATP-dependent phosphorylation events dependent on the addition of rPKM2 to a whole cell lysate is complicated by the fact that many proteins undergo ATP-dependent phosphorylation. To mitigate this complication, and to control for the presence or absence of PKM2 in the lysates, we fractionated hypotonic and nuclear extracts from H1299 cells and from PKM2-expressing and PKM2-null MEFs by anion exchange chromatography. We assayed each fraction for phosphorylation dependent on the addition of rPKM2 (Figure 4A-C). One phosphorylated species (Figure 4A, H1299 hypotonic lysate fractions 1-2, MW ~60 kDa) showed dependence on the addition of rPKM2. The rPKM2 added

also has a MW of ~60 kDa, raising the possibility that phosphorylation of rPKM2 by kinases present in the lysate, rather than production of a phosphorylated species by PKM2, explains this result. Prior work has suggested that PKM2 can be a substrate for phosphorylation (Hitosugi et al., 2009). In support of rPKM2 being phosphorylated by a kinase present in the lysate, we were able to purify this species by Ni-NTA affinity chromatography (Figure 4D), indicating that this band represents phosphorylated rPKM2, not a protein phosphorylated by PKM2. Taken together, these data argue against PKM2 having direct protein kinase activity.

Discussion

We were unable to find evidence for PKM2 activity as a protein kinase utilizing either [^{32}P]-PEP or [γ-^{32}P]-ATP as a substrate. While negative results cannot be definitive, sensitive ^{32}P-labeling failed to identify any proteins phosphorylated in a PKM2-dependent manner across multiple cell types. Our findings demonstrate the importance of depleting contaminating adenine nucleotides from cell lystates and HPLC purification of enzymatically synthesized [^{32}P]-PEP to reduce [γ-^{32}P]-ATP generation *in situ*, which might otherwise lead to ATP-dependent phosphorylation events being misinterpreted as PEP-dependent. The finding that omitting these steps can result in pyruvate kinase mediated regeneration of ATP and produce data that could be misconstrued as PEP-dependent phosphorylation events provides an explanation for past reports of PEP-dependent PKM2 protein kinase activity.

For PKM2 to have activity as a protein kinase would require the enzyme to adopt a conformation in which both PEP and its protein substrate are simultaneously bound. To allow phosphoryltransfer reactions water must be excluded from an enzyme active site or hydrolysis of phosphate esters would be favored over the phosphoryltransfer reaction. The active site of PKM2 for phosphoryltransfer between pyruvate and ADP is located within the core of the

protein, between its A and B domains (Stammers and Muirhead, 1977). Following binding of substrate, a lid closes over this site, excluding water and facilitating phosphoryltransfer (Larsen et al., 1998). To accommodate a large protein substrate in place of the much smaller ADP, the position of the B domain would need to be dramatically altered to exclude water and allow transfer of the phosphoryl group to a residue on the target protein. Alternatively, a mechanism for phosphoryltransfer could involve a covalent phospho-enzyme intermediate similar to the phosphoryltransferase enzymes in bacteria, which transfer a phosphoryl group from PEP between several proteins before phosphorylating hexoses (Deutscher et al., 2006). There is, however, no evidence for intermediate phosphorylation of PKM2, and we did not observe labeling of PKM2 from [^{32}P]-PEP alone. Furthermore, the known mechanism of pyruvate kinase as an enzyme involves direct phosphoryltransfer from PEP to ADP (Dombrauckas et al., 2005).

It has been suggested that protein substrates of PKM2 bind to the ADP binding site of this enzyme, supported by the apparent competitive inhibition of PKM2 protein kinase activity by ADP (Gao et al., 2012; Keller et al., 2014). This observation could also be explained by end-product inhibition of a contaminating ATP-dependent kinase by ADP. The ability of protein substrates to occupy the ADP-binding site of PKM2 is particularly surprising given the diversity of protein kinase substrates suggested to be PKM2 targets. PKM2 has been reported to phosphorylate 149 protein substrates lacking a clear phosphorylation motif, suggesting degenerate specificity of the active site (Keller et al., 2014). By contrast, nucleotide binding is highly specific as PKM2 is unable to efficiently phosphorylate diverse nucleotide substrates, instead showing strong selectivity for ADP (Mazurek et al., 1998). In addition, PKM1 has the same binding site for ADP as PKM2, and shows similar selectivity for ADP (Morgan et al., 2013; Plowman and Krall, 1965). In fact, PKM2 and PKM1 have identical active sites. These isoforms differ by the alternative inclusion of one exon, which encodes only regulatory components of the protein further arguing against a specific kinase function for PKM2. A more plausible

explanation is that PKM2 serves to regenerate ATP from PEP for other kinases as an explanation for past reports of PKM2 protein kinase activity.

Although we did not detect protein kinase activity by PKM2, several protein species were labeled by [^{32}P]-PEP independent of the presence of PKM2. PGAM and phosphoglucomutase were identified as targets of PEP-dependent phosphorylation in *Xenopus* lysates, and these studies concluded that the phosphorylations were dependent on the transformation of PEP into other glycolytic intermediates via reverse glycolysis (Dworkin and Dworkin-Rastl, 1989). It is unlikely that reverse glycolysis is operative in our assay beyond PEP conversion to 2-Phosphoglycerate (2-PG) via enolase, as continued reverse glycolysis would be dependent on PGAM, whose labeling from [^{32}P]-PEP we have shown to be inhibited by orthovanadate. In fact, orthovandate has been previously shown to inhibit PGAM by promoting dephosphorylation of the catalytic histidine residue required for PGAM enzymatic activity (Carreras et al., 1982). It is also important to note that PEP (or 2-PG) may be transferring more than just a phosphate to the unknown ~45 kDa protein. Interestingly, another glycolytic intermediate, 1,3-bisphosphoglycerate, has recently been shown to post-translationally modify proteins on lysine to produce 3-phosphoglyceryl-lysine via a non-enzymatic mechanism (Moellering and Cravatt, 2013). Depletion of enolase from the reaction would distinguish between PEP-dependent and 2-PG-dependent phosphorylation, and will help clarify whether PEP-dependent labeling of the ~45 kDa protein is mediated by PEP or an enzymatic product of PEP other than ATP. Nevertheless, it appears that PEP-dependent phosphorylation is rare in mammalian cells and that PKM2 is not required for any of the events observed in this study. The methods to separate PEP-dependent phosphorylation in mammalian cells from ATP-dependent events with high sensitivity will allow identification of both the targets and enzymes involved.

Materials and Methods

Cell Culture

H1299 cells, MEFs, U87 cells, and U87 EGFR-VIII cells were cultured in RPMI 1640 or DMEM, supplemented with 10% heat-inactivated fetal bovine serum, penicillin (100 U/mL), and streptomycin (100 µg/mL). MEFs expressing Cre-ER and homozygous for a PKM2 conditional allele were generated from mice as described previously (Lunt et al., 2015) and immortalized by knockdown of p53. To delete PKM2, the MEFs were treated with 1 µM 4-hydroxytamoxifen for at least 3 days.

Protein Extraction and Purification

To prepare hypotonic lysates and nuclear extracts, cells were washed with ice cold PBS, collected by centrifugation at 650 × g, and incubated in three volumes of hypotonic lysis buffer (10 mM HEPES/KOH pH 7.6, 10 mM KCl, 1.5 mM $MgCl_2$, 1 mM EDTA, 1 mM EGTA, .5 mM DTT, 1x cOmplete mini protease inhibitor (Roche)) for 10 min on ice. Lysis was accomplished by passing cells through a 22.5-gauge needle fifteen times. Nuclei were pelleted for 10 min at 855 × g, and washed five times with four volumes of hypotonic lysis buffer. They were next resuspended in one volume of nuclear extraction buffer (20 mM HEPES/KOH pH 7.6, 500 mM NaCl, 1.5 mM $MgCl_2$, 1 mM EDTA, 1 mM EGTA, .5 mM DTT, 25% (v/v) glycerol, 1x cOmplete mini protease inhibitor (Roche)) and incubated for 30 min on ice with occasional mixing. Lysates were clarified for 10 min at 20 000 × g, and a high-salt extraction was accomplished by incubating the resulting pellet in high-salt solubilization buffer (Shechter et al., 2007) for 30 min. Proteins were desalted into hypotonic lysis buffer by passing samples through a Sephadex G-25 Fine (GE Healthcare) gravity column. For Q-column fractionation, samples were first concentrated to 1 mL on Pierce Concentrators with a 9 kDa molecular weight cutoff (Thermo Scientific). Samples were then desalted into buffer A (20 mM bis-tris-propane-HCl pH 8.7, 5 mM

KCl, 1 mM $MgCl_2$) on a 5 mL HiTrap Desalting column (GE Healthcare) and then loaded onto a 1 mL HiTrap Q HP column (GE Healthcare). Proteins were eluted in a linear gradient from buffer A to buffer A with 1 M KCl, and 1 mL fractions were collected. Protein concentration was determined by standard Bradford assay.

Expression and Purification of Recombinant PKM2

N-terminally 6xHis-tagged recombinant PKM2 and PKM2-R399E were expressed from the pET28a(+) vector in *E. coli* and batch purified using Ni-NTA agarose beads (Qiagen) as described previously (Anastasiou et al., 2012). The R399E mutation was introduced using the QuikChange II XL Site Directed Mutagenesis Kit (Agilent Technologies) and the following primers: 5'- CAATTATTTGAGGAACTCGAGCGCCTGGCGCCCATTACC-3' and 5'-GGTAATGGGCGCCAGGCGCTCGAGTTCCTCAAATAATTG-3'.

[^{32}P]-PEP Synthesis and Purification

[^{32}P]-PEP was synthesized as described previously (Mattoo and Waygood, 1983; Vander Heiden et al., 2010). Briefly, commercial rabbit muscle pyruvate kinase (Sigma) catalyzed synthesis from pyruvate and [γ-^{32}P]-ATP (Perkin Elmer) at 37 ºC for 45-60 min, followed by crude separation of PEP from ATP using a Vivapure Q Mini H columns (Satorius) with sequential elution in 0.3 and 0.6 M triethylammonium bicarbonate pH 8.5 (Sigma). Further purification was accomplished by reverse-phase ion-pairing high performance liquid chromatography. [^{32}P]-PEP (containing contaminating [γ-^{32}P]-ATP) was mixed with 100 µM of each of cold PEP and ATP. This mixture was loaded on to a ZORBAX SB-C18 Analytical column (Agilent), and eluted in a linear gradient from 5% (v/v) methanol, 15 mM acetic acid, and 10 mM tributylamine to 100% methanol. 500 µL fractions were collected. Three fractions containing the highest amount of PEP or ATP (as determined by TLC and autoradiography)

were pooled and dried under nitrogen gas. Samples were resuspended in water for use in *in vitro* reactions.

SAICAR Synthesis and Purification

SAICAR was synthesized enzymatically using adenosuccinate lyase (ADSL) purified by a previously described approach (Lee and Colman, 2007). ADSL (50 µg/mL) catalyzed the reaction between 13.5 mg/mL AICAR (Toronto Research Chemicals) and 50 mM fumarate at 37°C overnight in a buffer containing 20 mM HEPES pH 7.4, 50 mM ammonium acetate, 50 mM KCl, 2 mM EDTA, and 1 mM DTT (Keller et al., 2012). The reaction was loaded on to a 5 mL HiTrap Q HP column and eluted in a linear gradient from water to 3 M ammonium acetate. Peak fractions were pooled and lyophilized. SAICAR was resuspended in 10 mM HEPES-KOH pH 7.5 prior to use in *in vitro* reactions.

***In Vitro* Phosphorylation Reactions**

Unless stated otherwise, reactions were carried out at 30 °C for 1 h in previously published buffer (50 mM Tris-HCl pH 7.5, 100 mM KCl, 50 mM $MgCl_2$, 1 mM DTT) with 1x PhosSTOP (Roche) (Gao et al., 2012; Yang et al., 2012a). Protein extracts prepared as described above or calf thymus histones (Worthington Biochemical) were included at 100 µg/mL. Recombinant PKM2 was included in the reaction at 10 µg/mL. Where indicated, 1 mM Na_3VO_4, 0.5 mM SAICAR, or 1 mM cold competitor ATP or PEP were included in the reaction. Radioactive phosphate group donor substrates were ~6 nM (~20 µCi/mL) [γ-^{32}P]-ATP (Perkin Elmer) or ~4.5 nM (~13 µCi/mL) impure [^{32}P]-PEP, or ~3.5 nM (~10 µCi/mL) pure [^{32}P]-PEP or ~.31 nM (~.9 µCi/mL) pure [γ-^{32}P]-ATP. Reactions were quenched with addition of Lamelli sample buffer, and phosphorylated proteins were analyzed by 10% SDS-PAGE followed by autoradiography. Nickel-affinity purification was accomplished by incubating phosphorylation reactions with Ni-

NTA Beads (Qiagen) for 30 min. Beads were then washed with reaction buffer supplemented with 30 mM imidazole, and proteins were eluted by boiling in Lamelli sample buffer.

Thin-Layer Chromatography

0.5 µL of each reaction or compound were spotted on to PEI-cellulose F (EMD Millipore), and metabolites were resolved with 0.25 M NH_4HCO_3. Plates were dried and then visualized by autoradiography.

Western Blotting

Total protein extracts were prepared by incubating cells for 15 min in ice-cold RIPA buffer followed by clarification for 10 min at 20 000 × g. To confirm absence of PKM2 in MEFs, 15 µg of protein were resolved by 8% SDS-PAGE. To determine contents of cell extracts, volumes proportionate to the extraction buffer volumes were resolved by 8 or 10% SDS-PAGE. Proteins were transferred to a PVDF membrane and, following immunoblotting, were visualized by ECL assay. Antibodies used: PKM2, histone 3, lamin A/C (Cell Signaling Technologies: 4053, 4499, 4777, respectively), β-tubulin (Abcam: 21058).

DNA Extraction and Genotyping

Genomic DNA was extracted using the PureLink Genomic DNA Mini Kit (Life Technologies). *PKM* exon 10 was amplified by polymerase chain reaction as described previously (Israelsen et al., 2013), and reaction products were resolved on a 2% agarose gel.

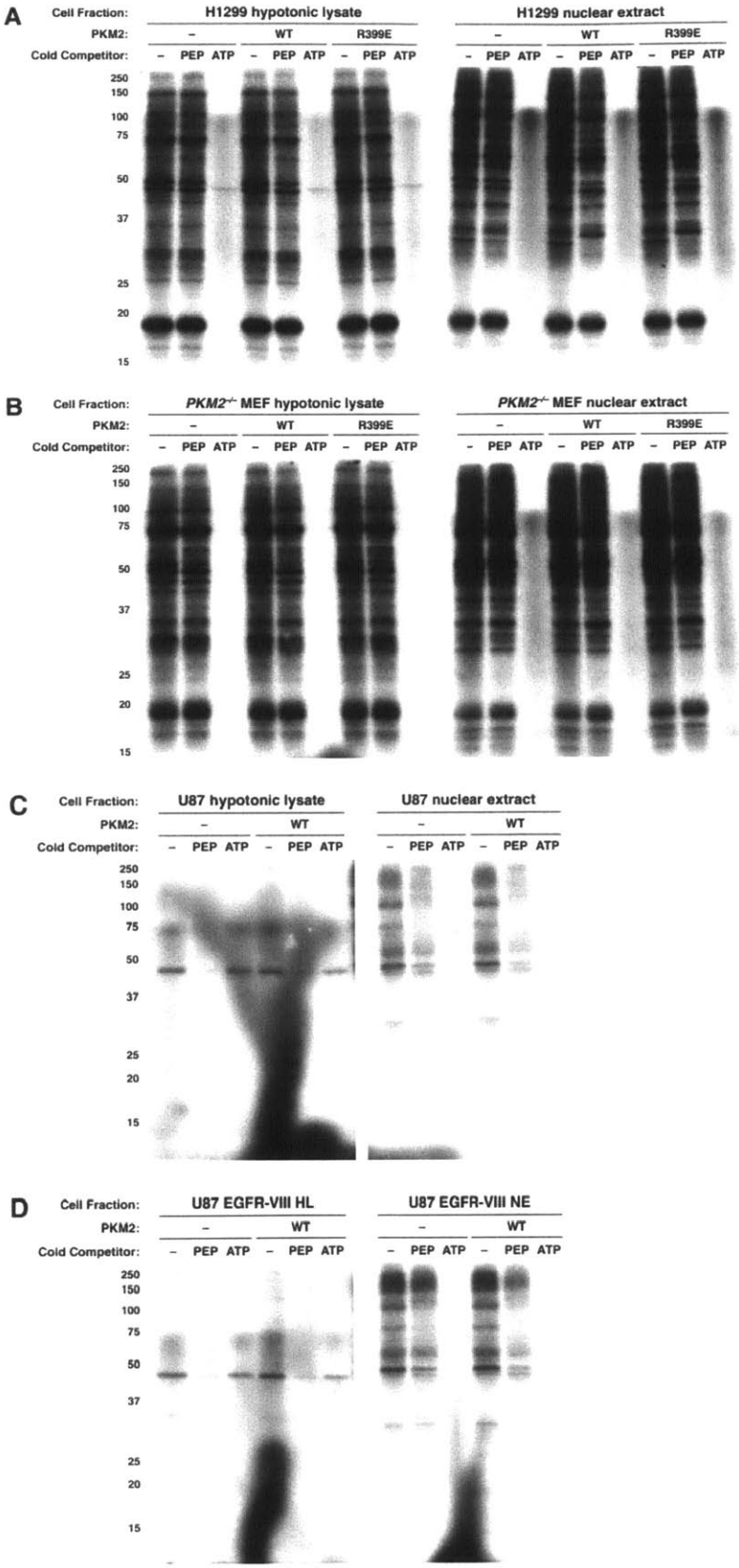
A
Cell Fraction:
H1299 hypotonic lysate
H1299 nuclear extract
PKM2:
–
WT
R399E
Cold Competitor:
– PEP ATP – PEP ATP – PEP ATP
– PEP ATP – PEP ATP – PEP ATP
250
150
100
75
50
37
25
20
15
B
Cell Fraction:
PKM2−/− MEF hypotonic lysate
PKM2−/− MEF nuclear extract
PKM2:
–
WT
R399E
Cold Competitor:
– PEP ATP – PEP ATP – PEP ATP
– PEP ATP – PEP ATP – PEP ATP
250
150
100
75
50
37
25
20
15
C
Cell Fraction:
U87 hypotonic lysate
U87 nuclear extract
PKM2:
–
WT
Cold Competitor:
– PEP ATP – PEP ATP
– PEP ATP – PEP ATP
250
150
100
75
50
37
25
20
15
D
Cell Fraction:
U87 EGFR-VIII HL
U87 EGFR-VIII NE
PKM2:
–
WT
Cold Competitor:
– PEP ATP – PEP ATP
– PEP ATP – PEP ATP
250
150
100
75
50
37
25
20
15

Figure 1 - Assessment of phosphoenolpyruvate (PEP) as a phosphoryl donor for protein phosphorylation. Hypotonic lysates and nuclear extracts from (*A*) H1299, (*B*) PKM2-null MEF, (*C*) U87, and (*D*) U87 EGFR-VIII cells were incubated for 1 h with impure [^{32}P]-PEP, and phosphorylated proteins analyzed by SDS-PAGE and autoradiography. Reactions were carried out with the addition of no enzyme, recombinant wild type (WT) or mutant (R399E) his-tagged PKM2 as indicated. In addition, no competitor or excess (1 mM) non-radioactive competitor PEP or ATP was also included where indicated.

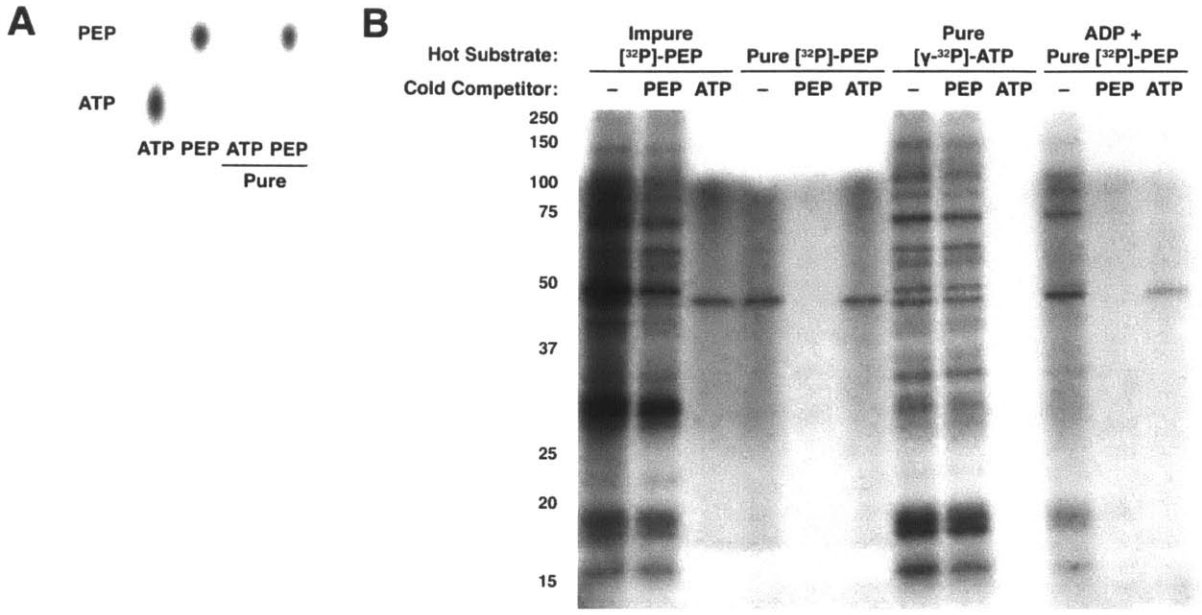

Figure 2 - Contaminating [γ-^{32}P]-ATP is the predominant phosphoryl donor when using crude [^{32}P]-PEP. (*A*) [^{32}P]-PEP synthesized from [γ-^{32}P]-ATP is contaminated by small amounts of [γ-^{32}P]-ATP, which can be separated by preparative HPLC. The purity of each fraction was analyzed by thin-layer chromatography and autoradiography. (*B*) The contaminating [γ-^{32}P]-ATP component of impure [^{32}P]-PEP is the phosphoryl donor for the majority of proteins phosphorylated by impure [^{32}P]-PEP. An H1299 hypotonic lysate was incubated for 1 h with recombinant PKM2 and different ^{32}P-containing metabolites as well as no competitor or excess (1 mM) non-radioactive competitor PEP or ATP as indicated. Phosphorylated proteins were analyzed by SDS-PAGE and autoradiography.

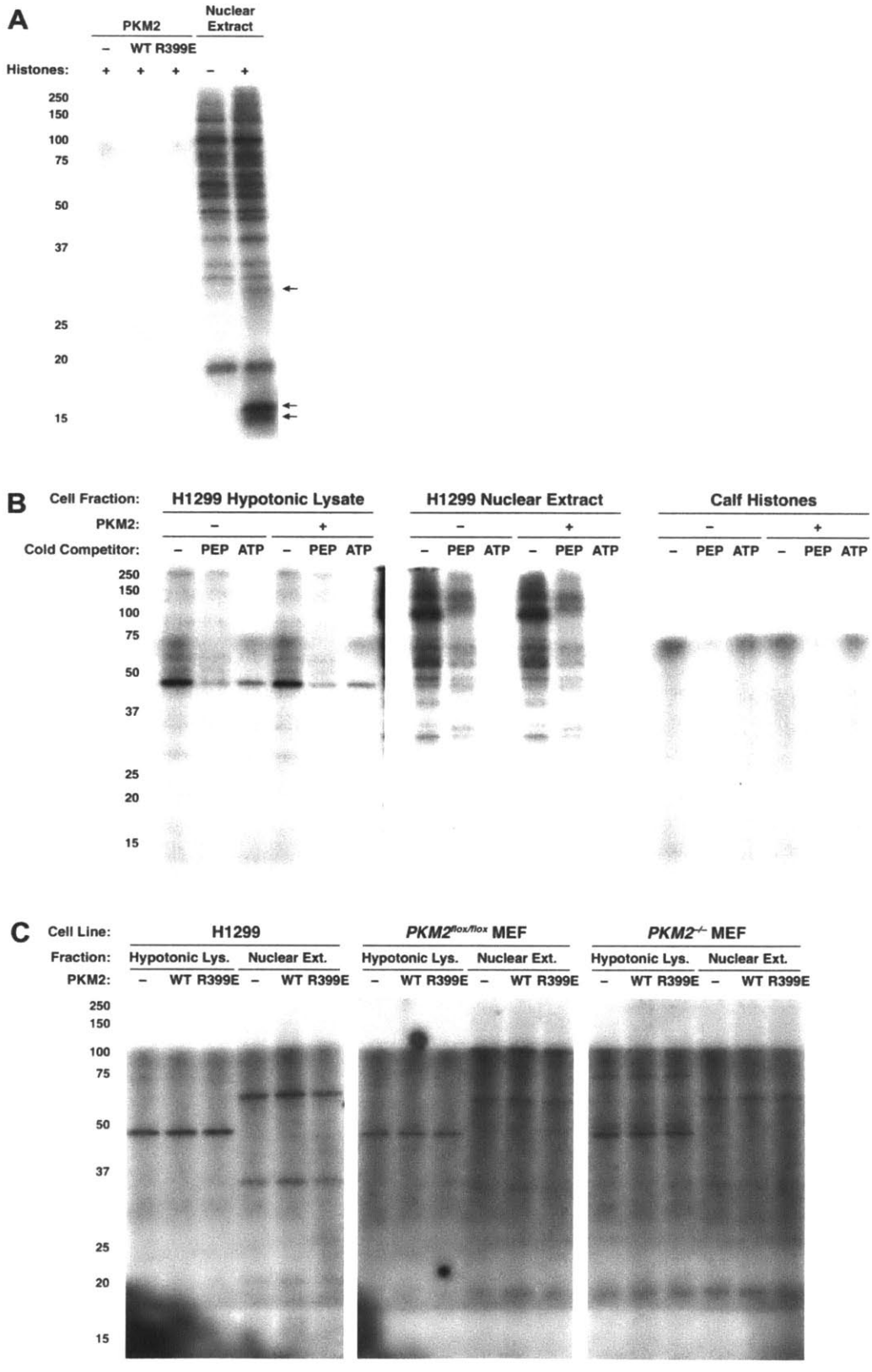
A
PKM2
Nuclear Extract
–
WT R399E
Histones: + + + – +
250
150
100
75
50
37
25
20
15
B
Cell Fraction:
H1299 Hypotonic Lysate
H1299 Nuclear Extract
Calf Histones
PKM2:
– +
Cold Competitor: – PEP ATP – PEP ATP – PEP ATP – PEP ATP – PEP ATP – PEP ATP
250
150
100
75
50
37
25
20
15
C
Cell Line:
H1299
PKM2flox/flox MEF
PKM2-/- MEF
Fraction:
Hypotonic Lys.
Nuclear Ext.
PKM2: – WT R399E – WT R399E – WT R399E – WT R399E – WT R399E – WT R399E
250
150
100
75
50
37
25
20
15

Figure 3. (*A*) Calf thymus histones were incubated for 1 h with impure [^{32}P]-PEP and no enzyme, recombinant wild type (WT) or mutant (R399E) PKM2 as indicated. An H1299 nuclear extract was also incubated with impure [^{32}P]-PEP with and without calf thymus histones added. Phosphorylated proteins were analyzed by SDS-PAGE and autoradiography. Arrows indicate phosphorylated proteins with apparent molecular weights similar to histones (core histones, 11-17 kDa, many histone H1 isoforms 25-35 kDa) (Shechter et al., 2007). (*B*) H1299 cell hypotonic lysates and nuclear extracts and calf thymus histones were incubated for 1 h with [^{32}P]-PEP and rPKM2 with or without 0.5 mM SAICAR as well as no competitor or excess (1 mM) cold competitor PEP or ATP. (*C*) Hypotonic lysates and nuclear extracts from H1299 cells and PKM2-expressing (flox/flox) or PKM2-null (-/-) MEFs were desalted and incubated for 1 h with HPLC-purified [^{32}P]-PEP with no additional enzymes or with added recombinant wild type or mutant (R399E) His-tagged PKM2.

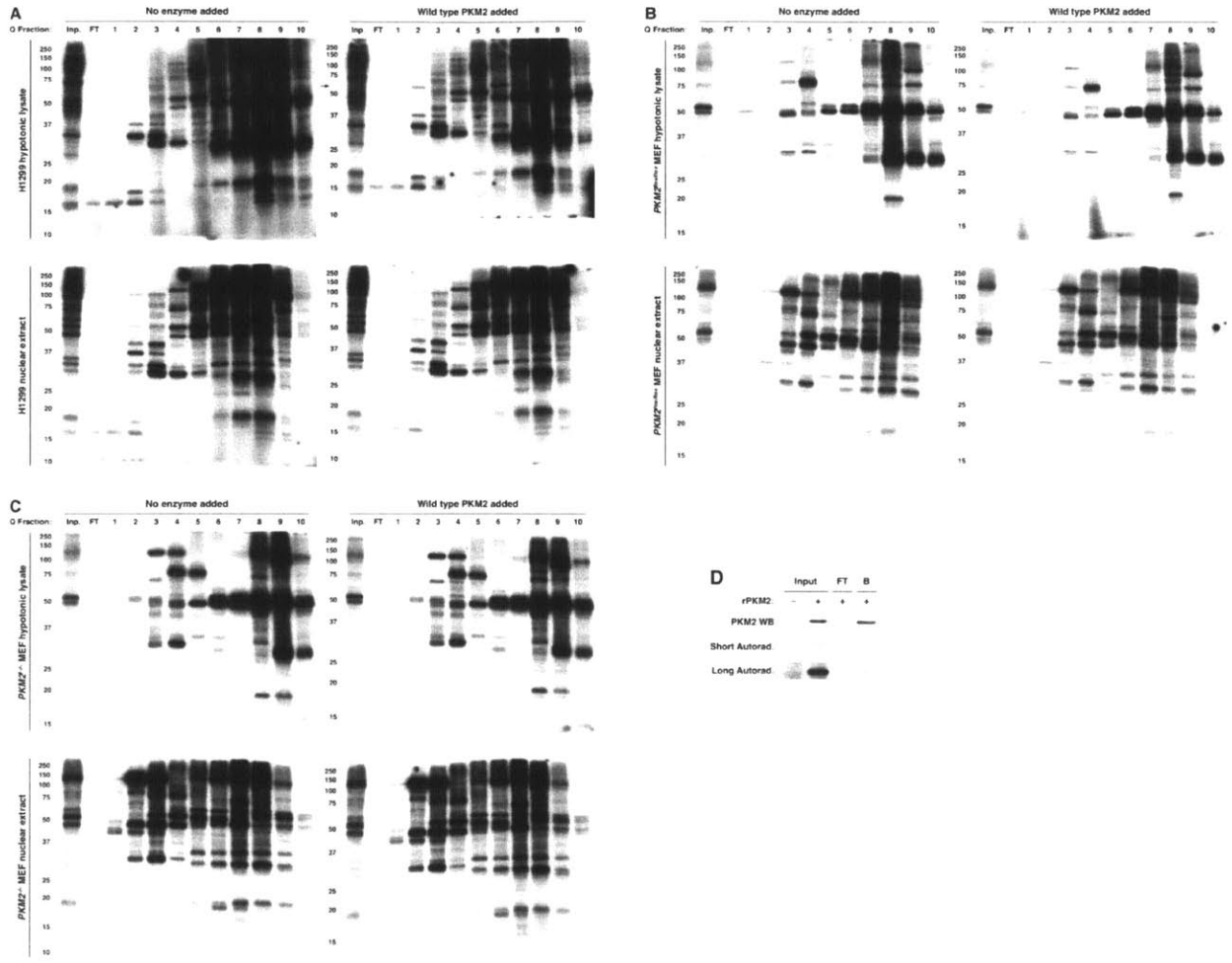

Figure 4 - Lack of evidence for an ATP-dependent protein kinase activity for PKM2. (*A*) H1299, (*B*) PKM2-expressing MEF, and (*C*) PKM2-null MEF hypotonic lysates and nuclear extracts were used to identify substrates for PKM2 kinase activity. Lysates were fractionated on a 1mL Q Sepharose HP column (Inp., 1:10 dilution of column input; FT, flow through; 1-10, fractions 1-10), and incubated for 1 h with [γ-^{32}P]-ATP with or without the addition of recombinant His-tagged PKM2. Phosphorylated proteins were analyzed by SDS-PAGE and autoradiography. (*D*) One protein (predominantly contained within H1299-hypotonic-lysate fractions 1 and 2) exhibited phosphorylation dependent on PKM2 addition. This phosphorylated protein co-purifies with PKM2 by nickel-affinity chromatography (Inp., Q column input; FT, nickel-affinity column flow through).

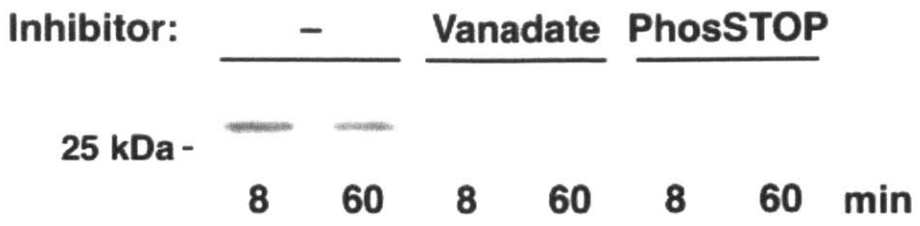

Figure S1 - Phosphoglycerate mutase 1 (PGAM1) labeling from [^{32}P]-PEP is inhibited by orthovanadate. H1299 hypotonic lysates were incubated for 8 min or 1 h with [^{32}P]-PEP and 1mM cold competitor ATP. The reaction was carried out without added phosphatase inhibitors or with the addition of 1 mM sodium orthovanadate (vanadate) or PhosSTOP (Roche), and proteins were resolved by SDS-PAGE and visualized by autoradiography.

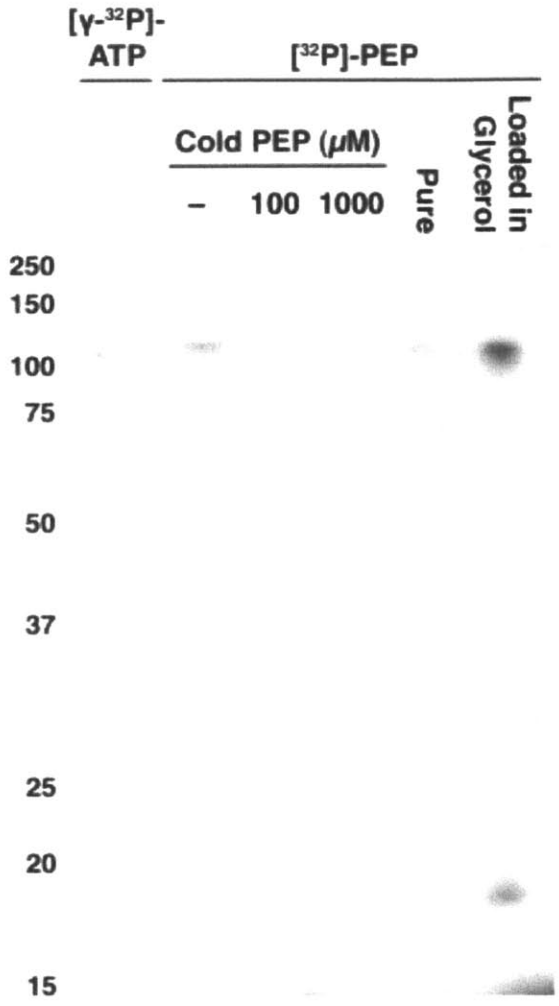

Figure S2 - [^{32}P]-PEP can label a polyacrylamide gel in the absence of added protein. [γ-^{32}P]-ATP (lane 1) and [^{32}P]-PEP (lanes 2-6) were analyzed by SDS-PAGE and autoradiography. These molecules migrate with the salt front of the gel as assessed by Geiger counting. This salt front is cut off before autoradiography, but [^{32}P]-PEP also labels what appears as two bands by autoradiography. Impure [^{32}P]-PEP was electrophoresed in the presence of no (lane 2), 100 μM (lane 3), or 1000 μM (lane 4) cold competitor PEP. HPLC-purified [^{32}P]-PEP (lane 5) and [^{32}P]-PEP loaded in ~7% (v/v) glycerol (as opposed to Lamelli sample buffer) (lane 6) produced a similar pattern.

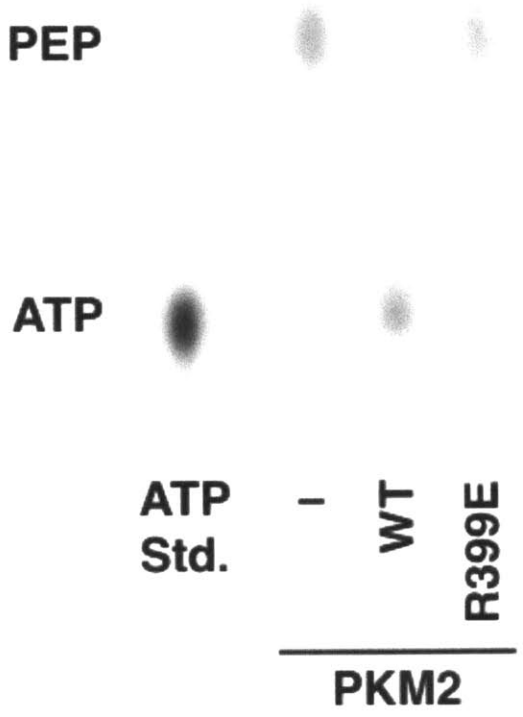

Figure S3 - Recombinant wild type and R399E mutant PKM2 display glycolytic pyruvate kinase activity. Lane 1: [γ-^{32}P]-ATP standard. Lanes 2-4: [^{32}P]-PEP and ADP were incubated for 45 min with no enzyme or 10 μg/mL recombinant wild type or mutant (R399E) PKM2. PEP and ATP were resolved by TLC and visualized by autoradiography.

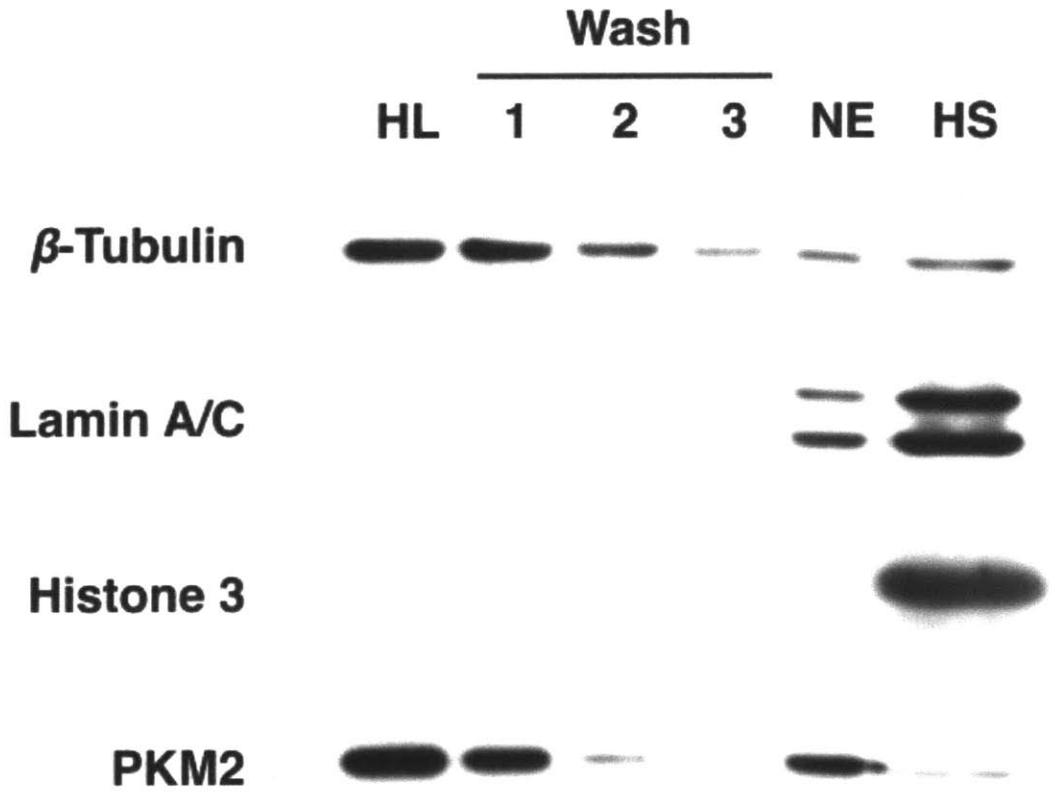

Figure S4. Protein levels of β-tubulin, lamin A/C, histone H3, and PKM2 were determined in cell extract fractions by western blotting. H1299 hypotonic lysate (HL) was prepared in buffer containing 10 mM KCl. The remaining material was washed three times with this buffer, and a nuclear extract (NE) was prepared from the resulting material using 500 mM NaCl. A high-salt (HS) extraction, containing histones, was then obtained by extraction with 2.5 M NaCl.

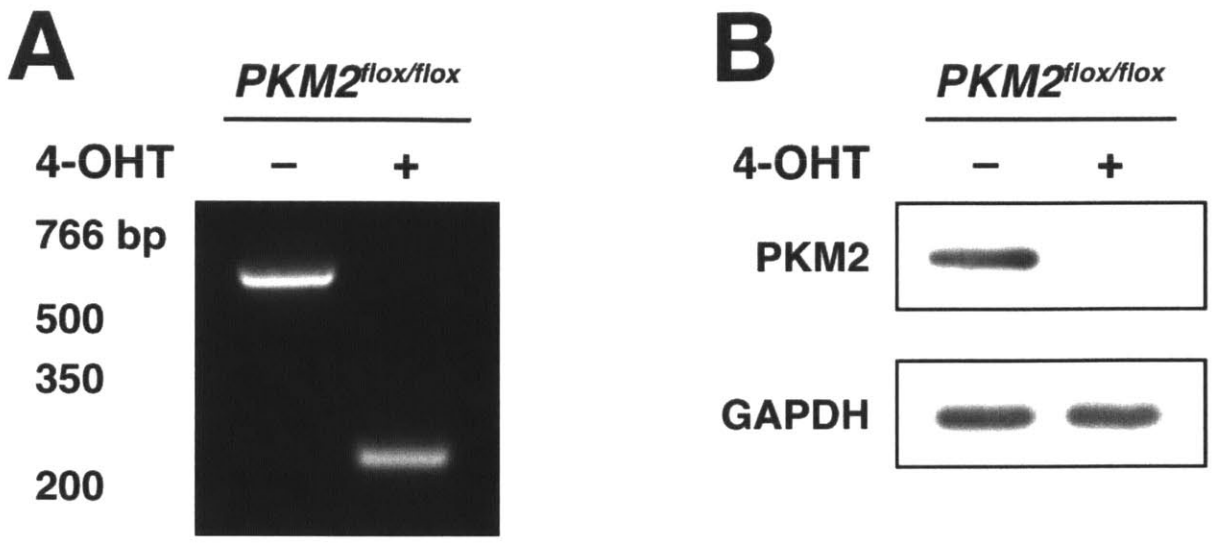

Figure S5 - PKM2 can be deleted from MEFs. Cre-ER expressing MEFs homozygous for a PKM allele where exon 10 (specific to PKM2) is flanked by two loxP sites (PKM2 flox/flox) were treated with .1% (v/v) ethanol or 500 nM 4-hydroxytamoxifen (4-OHT) and .1% ethanol. (A) Deletion of PKM exon 10 was confirmed by PCR using primers described previously (Israelsen et al., 2013). (B) PKM2 expression was analyzed by western blot analysis of cell lysates.

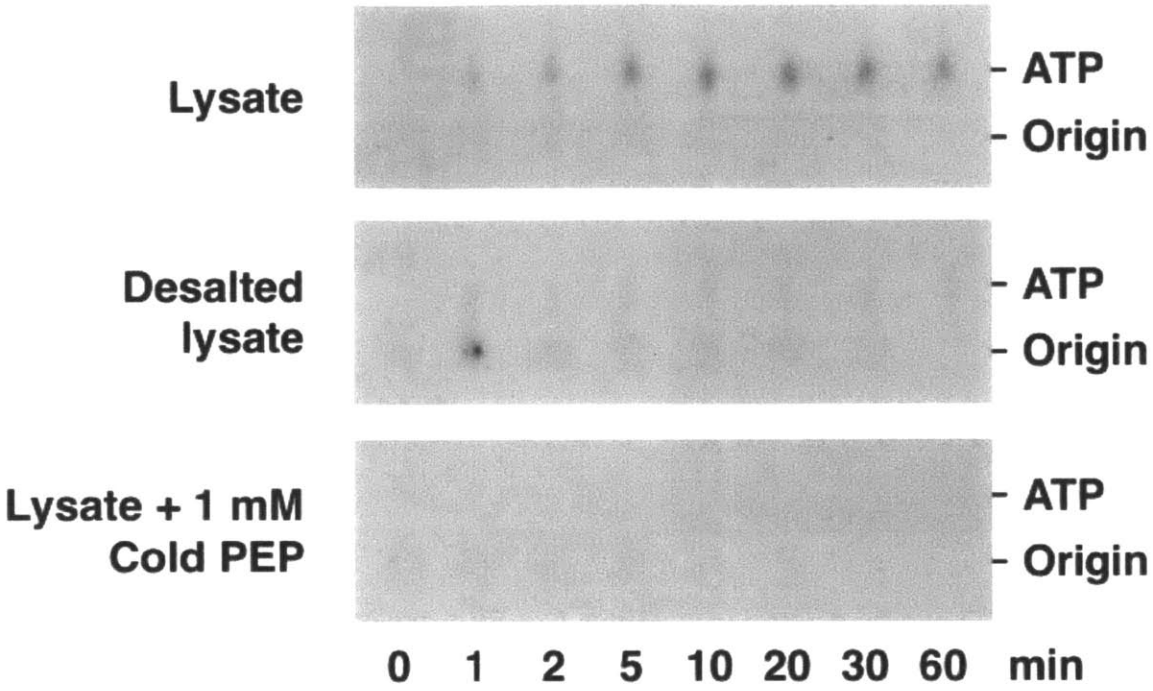

Figure S6 - A hypotonic lysate contains enough ADP to enable synthesis of [γ-^{32}P]-ATP. H1299 hypotonic lysates were incubated for the indicated times with rPKM2 and [^{32}P]-PEP. Labeled ATP produced by this reaction was measured by TLC and autoradiography.

References

Anastasiou, D., Yu, Y., Israelsen, W.J., Jiang, J.K., Boxer, M.B., Hong, B.S., Tempel, W., Dimov, S., Shen, M., Jha, A., *et al.* (2012). Pyruvate kinase M2 activators promote tetramer formation and suppress tumorigenesis. Nature chemical biology *8*, 839-847.

Beck, M., Schmidt, A., Malmstroem, J., Claassen, M., Ori, A., Szymborska, A., Herzog, F., Rinner, O., Ellenberg, J., and Aebersold, R. (2011). The quantitative proteome of a human cell line. Molecular systems biology *7*, 549.

Carreras, J., Climent, F., Bartrons, R., and Pons, G. (1982). Effect of vanadate on the formation and stability of the phosphoenzyme forms of 2,3-bisphosphoglycerate-dependent phosphoglycerate mutase and of phosphoglucomutase. Biochimica et biophysica acta *705*, 238-242.

Chaneton, B., Hillmann, P., Zheng, L., Martin, A.C., Maddocks, O.D., Chokkathukalam, A., Coyle, J.E., Jankevics, A., Holding, F.P., Vousden, K.H., *et al.* (2012). Serine is a natural ligand and allosteric activator of pyruvate kinase M2. Nature *491*, 458-462.

Christofk, H.R., Vander Heiden, M.G., Wu, N., Asara, J.M., and Cantley, L.C. (2008). Pyruvate kinase M2 is a phosphotyrosine-binding protein. Nature *452*, 181-186.

Cortes-Cros, M., Hemmerlin, C., Ferretti, S., Zhang, J., Gounarides, J.S., Yin, H., Muller, A., Haberkorn, A., Chene, P., Sellers, W.R., *et al.* (2013). M2 isoform of pyruvate kinase is dispensable for tumor maintenance and growth. Proceedings of the National Academy of Sciences of the United States of America *110*, 489-494.

Deutscher, J., Francke, C., and Postma, P.W. (2006). How phosphotransferase system-related protein phosphorylation regulates carbohydrate metabolism in bacteria. Microbiology and molecular biology reviews : MMBR *70*, 939-1031.

Dombrauckas, J.D., Santarsiero, B.D., and Mesecar, A.D. (2005). Structural basis for tumor pyruvate kinase M2 allosteric regulation and catalysis. Biochemistry *44*, 9417-9429.

Dworkin, M.B., and Dworkin-Rastl, E. (1989). Metabolic regulation during early frog development: glycogenic flux in Xenopus oocytes, eggs, and embryos. Developmental biology *132*, 512-523.

Gao, X., Wang, H., Yang, J.J., Liu, X., and Liu, Z.R. (2012). Pyruvate kinase M2 regulates gene transcription by acting as a protein kinase. Mol Cell *45*, 598-609.

Hitosugi, T., Kang, S., Vander Heiden, M.G., Chung, T.W., Elf, S., Lythgoe, K., Dong, S., Lonial, S., Wang, X., Chen, G.Z., *et al.* (2009). Tyrosine phosphorylation inhibits PKM2 to promote the Warburg effect and tumor growth. Science signaling *2*, ra73.

Israelsen, W.J., Dayton, T.L., Davidson, S.M., Fiske, B.P., Hosios, A.M., Bellinger, G., Li, J., Yu, Y., Sasaki, M., Horner, J.W., *et al.* (2013). PKM2 isoform-specific deletion reveals a differential requirement for pyruvate kinase in tumor cells. Cell *155*, 397-409.

Jiang, Y., Li, X., Yang, W., Hawke, D.H., Zheng, Y., Xia, Y., Aldape, K., Wei, C., Guo, F., Chen, Y., *et al.* (2014). PKM2 regulates chromosome segregation and mitosis progression of tumor cells. Mol Cell *53*, 75-87.

Keller, K.E., Doctor, Z.M., Dwyer, Z.W., and Lee, Y.S. (2014). SAICAR induces protein kinase activity of PKM2 that is necessary for sustained proliferative signaling of cancer cells. Mol Cell *53*, 700-709.

Keller, K.E., Tan, I.S., and Lee, Y.S. (2012). SAICAR stimulates pyruvate kinase isoform M2 and promotes cancer cell survival in glucose-limited conditions. Science *338*, 1069-1072.

Kung, C., Hixon, J., Choe, S., Marks, K., Gross, S., Murphy, E., DeLaBarre, B., Cianchetta, G., Sethumadhavan, S., Wang, X., *et al.* (2012). Small molecule activation of PKM2 in cancer cells induces serine auxotrophy. Chemistry & biology *19*, 1187-1198.

Larsen, T.M., Benning, M.M., Rayment, I., and Reed, G.H. (1998). Structure of the bis(Mg2+)-ATP-oxalate complex of the rabbit muscle pyruvate kinase at 2.1 A resolution: ATP binding over a barrel. Biochemistry *37*, 6247-6255.

Lee, P., and Colman, R.F. (2007). Expression, purification, and characterization of stable, recombinant human adenylosuccinate lyase. Protein expression and purification *51*, 227-234.

Lunt, Sophia Y., Muralidhar, V., Hosios, Aaron M., Israelsen, William J., Gui, Dan Y., Newhouse, L., Ogrodzinski, M., Hecht, V., Xu, K., Acevedo, Paula N.M., *et al.* (2015). Pyruvate Kinase Isoform Expression Alters Nucleotide Synthesis to Impact Cell Proliferation. Molecular Cell.

Mattoo, R.L., and Waygood, E.B. (1983). An enzymatic method for [32P]phosphoenolpyruvate synthesis. Analytical biochemistry *128*, 245-249.

Mazurek, S., Grimm, H., Wilker, S., Leib, S., and Eigenbrodt, E. (1998). Metabolic characteristics of different malignant cancer cell lines. Anticancer research *18*, 3275-3282.

McKnight, S.L. (2014). Please keep me 2uned to PKM2. Mol Cell *53*, 683-684.

Moellering, R.E., and Cravatt, B.F. (2013). Functional lysine modification by an intrinsically reactive primary glycolytic metabolite. Science *341*, 549-553.

Morgan, H.P., O'Reilly, F.J., Wear, M.A., O'Neill, J.R., Fothergill-Gilmore, L.A., Hupp, T., and Walkinshaw, M.D. (2013). M2 pyruvate kinase provides a mechanism for nutrient sensing and regulation of cell proliferation. Proceedings of the National Academy of Sciences of the United States of America *110*, 5881-5886.

Parnell, K.M., Foulks, J.M., Nix, R.N., Clifford, A., Bullough, J., Luo, B., Senina, A., Vollmer, D., Liu, J., McCarthy, V., *et al.* (2013). Pharmacologic activation of PKM2 slows lung tumor xenograft growth. Molecular cancer therapeutics *12*, 1453-1460.

Plowman, K.M., and Krall, A.R. (1965). A kinetic study of nucleotide interactions with pyruvate kinase. Biochemistry *4*, 2809-2814.

Shechter, D., Dormann, H.L., Allis, C.D., and Hake, S.B. (2007). Extraction, purification and analysis of histones. Nature protocols *2*, 1445-1457.

Stammers, D.K., and Muirhead, H. (1977). Three-dimensional structure of cat muscle pyruvate kinase at 3-1 A resolution. Journal of molecular biology *112*, 309-316.

Vander Heiden, M.G., Locasale, J.W., Swanson, K.D., Sharfi, H., Heffron, G.J., Amador-Noguez, D., Christofk, H.R., Wagner, G., Rabinowitz, J.D., Asara, J.M., *et al.* (2010). Evidence for an alternative glycolytic pathway in rapidly proliferating cells. Science *329*, 1492-1499.

Wang, Y.H., Israelsen, W.J., Lee, D., Yu, V.W., Jeanson, N.T., Clish, C.B., Cantley, L.C., Vander Heiden, M.G., and Scadden, D.T. (2014). Cell-state-specific metabolic dependency in hematopoiesis and leukemogenesis. Cell *158*, 1309-1323.

Yang, W., Xia, Y., Hawke, D., Li, X., Liang, J., Xing, D., Aldape, K., Hunter, T., Alfred Yung, W.K., and Lu, Z. (2012a). PKM2 phosphorylates histone H3 and promotes gene transcription and tumorigenesis. Cell *150*, 685-696.

Yang, W., Zheng, Y., Xia, Y., Ji, H., Chen, X., Guo, F., Lyssiotis, C.A., Aldape, K., Cantley, L.C., and Lu, Z. (2012b). ERK1/2-dependent phosphorylation and nuclear translocation of PKM2 promotes the Warburg effect. Nature cell biology *14*, 1295-1304.

Notes

U87 and U87 EGFR-VII cells were generously provided by the White Lab at MIT.